Integrin β1 cluster stability in the context of cellular mechanosensing and radiosensitivity

Stabilität von Integrin β1 Clustern im Kontext der zellulären Mechanoperzeption und Radiosensitivität

Vom Fachbereich Biologie der Technischen Universität Darmstadt
zur Erlangung des Grades eines Doktor rerum naturalium (Dr. rer. nat.)
genehmigte Dissertation von Laura Babel (M. Sc.) aus Frankfurt am Main
Tag der Einreichung: 25.08.2017
Tag der mündlichen Prüfung: 15.11.2017
Darmstadt 2017 — D 17

1. Gutachten: PD Dr. Tobias Meckel
2. Gutachten: Prof. Dr. Gerhard Thiel

TECHNISCHE
UNIVERSITÄT
DARMSTADT

Integrin β1 cluster stability in the context of cellular mechanosensing and radiosensitivity
Stabilität von Integrin β1 Clustern im Kontext der zellulären Mechanoperzeption und Radiosensitivität

Genehmigte Dissertation von Laura Babel (M. Sc.) aus Frankfurt am Main

1. Gutachten: PD Dr. Tobias Meckel
2. Gutachten: Prof. Dr. Gerhard Thiel

Tag der Einreichung: 25.08.2017
Tag der Prüfung: 15.11.2017

Darmstadt — D 17

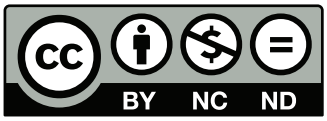

Ehrenwörtliche Erklärung

Ich erkläre hiermit ehrenwörtlich, dass ich die vorliegende Arbeit entsprechend den Regeln guter wissenschaftlicher Praxis selbstständig und ohne unzulässige Hilfe Dritter angefertigt habe. Sämtliche aus fremden Quellen direkt oder indirekt übernommenen Gedanken sowie sämtliche von Anderen direkt oder indirekt übernommenen Daten, Techniken und Materialien sind als solche kenntlich gemacht. Die Arbeit wurde bisher bei keiner anderen Hochschule zu Prüfungszwecken eingereicht.

Darmstadt, den 25.08.2017

_____

(Laura Babel)

Summary

Cell-based high-content-screenings (HCS) use monolayer-based 2D cell cultures [1] with a highly artificial environment as these cells lack three important aspects: (i) They lack dimensionality since these cells are not allowed to adhere to extracellular supports, (ii) provide a highly polarized mechanical environment and (iii) lack the ability to maintain local concentration heterogeneities. In contrast, 3D cell cultures, such as spheroid or ECM-based (extracellular matrix) cultures, mimic the *in vivo* conditions by providing physical, (bio)chemical and mechanical properties as well as soluble factors [2, 3, 4]. Thus, it comes to no surprise that the use of 2D cell cultures in industrial and preclinical screenings leads to limited predictive values for clinical efficacy of compounds.

Cells cultured in a 3D cell culture system, show in comparison to 2D cultured cells, a different gene expression, morphology, cytoskeletal organization, migration and proliferation rates as well as a different distribution in cell cycle phases [5, 6, 7]. All these phenotypes differ if compared to 2D cultured cells due to a different expression of proteins with huge effects on e.g. the effectiveness of cancer inhibitors [8, 9, 10].

In contrast to 2D cultured cells, 3D cultured cells are allowed to interact with the ECM. Key mediators for this cell-ECM interaction are heterodimeric transmembrane proteins called integrins. The interaction with the ECM modulates many processes, such as proliferation, gene expression, cellular survival and cell migration [11, 12, 13]. The cell's interaction with the ECM is highly interesting as integrins containing the $\beta 1$ subunit contribute to a process called cell-adhesion-mediated radioresistance (CAM-RR). In comparison to 3D cultured cells, 2D cells are significantly more sensitive towards ionizing radiation [14, 15, 16].

Until the begin of this thesis, CAM-RR was linked to the chromatin structure that differs between cells cultured in 2D and 3D conditions. Namely, the presence of a higher fraction of heterochromatin in 3D cultured cells was shown to correspond to a decreased amount of residual DNA double strand breaks after X-irradiation [16, 17]. Integrins as the key mediators of a cell's interaction with the ECM are clearly involved in this culture-condition dependent effect, mainly the players acting downstream of integrin signaling have bee thoroughly investigated (ILK, FAK, JNK1, Akt1, PINCH, HDAC) [18, 19, 20, 21].

Chapter I of this thesis aims to capture the plasma membrane (PM) located effects of ionizing radiation (IR) on $\beta 1$ integrins. Therefore, 2D and 3D cultured cells were irradiated with different doses of x-rays. The effects of IR on the nanoscale localization and organization of integrin $\beta 1$ clusters were measured with single molecule localization microscopy (SMLM) and subsequent quantitative data analysis. It was shown that the radioresistance of 3D culture cells relies on stable and intact integrin $\beta 1$ clusters, which are hard to disrupt even with high doses of IR. In contrast, 2D cultured cells are not able to organize integrins into stable clusters and display a rather loose and heterogeneous organization. Upon irradiation this unstable condition is disrupted by low doses of IR. Therefore, the radioresistance of 3D cultured cells relies on a stable organization of integrin $\beta 1$ clusters, whereas the radiosensitivity emerges from the 2D cells inability to properly organize these proteins in the nanoscale.

In **Chapter II** of this thesis the well-known radiosensitizer and integrin $\beta 1$ inhibitor AIIB2 is used to actively disrupt the integrin clusters of 3D cultured cells and, in combination with IR, to induce radiosensitivity. Integrins not only link the cell with the ECM, they also originate the mechanosensing system of cells by physically linking the ECM (via integrins - actin - nesprin - SUN proteins - lamin) with the nucleus. A combined treatment with AIIB2 and IR leads to an integrin cluster break-down and to an interruption of this mechanosensing machinery if 2D and 3D cultured cells. By following

the mechanosensing system it became clear that CAM-RR of 3D cultured cells is not only based on a stable integrin $\beta 1$ clustering but also on a balanced mechanobiological system. In contrast, the 2D cell culture system is highly artificial and does not provide the means to investigate mechanobiological aspects.

The ability of integrin clustering to be a target for induced radiosensitivity proves that beside DNA damage and its subsequent repair, PM located effects of IR are a powerful tool in radiotherapy. **Chapter III** of this thesis aims to answer the question, whether the effects of IR on the integrin $\beta 1$ clustering are lipid-raft dependent. It could be shown that integrin clusters colocalize with cholesterol lipid-rafts. However, upon irradiation integrins are separated from their raft localization - integrin clusters are disrupted while cholesterol microdomains are not effected by high doses of IR. This proves, that (i) the effects of IR on integrin clustering are lipid-raft independent and (ii) it implies the possibility of an independent coclustering of both. These results challenge the generalized assumption that protein clustering is governed by lipid-rafts.

In closing, the integrin involvement in tumorgenesis (metastasis, angiogenesis) and cellular reactions towards anti-cancer treatment (drug- and radioresistance) makes them an important target in current tumor studies [22, 23]. The results summarized in chapter I and II of this thesis demonstrate that a combined approach of 3D cell cultures and SMLM should become a integral part of preclinical screenings. With this, it would be possible to combine the virtues of super resolution microscopy with the capability of 3D cultured cells to enhance the predictive value of HCS. SMLM as part of preclinical screenings would extend the molecular phenotype to the molecular dimension, i.e. the nanoscale localization and organization of molecules or proteins. 3D cell cultures as part of such a screening would provide the correct physiological environment.

Still, the vast majority of cell-based HCS use (i) monolayer-based 2D cell cultures [24] and (ii) simple microscopical methods (wide-field or confocal microscopy) [25], neglecting to target the nanoscale molecular phenotype of e.g. PM located proteins .

Zusammenfassung

Zell-basierte High-Content-Screenings (HCS) verwenden zumeist als Monolayer kultivierte 2D Zellen [1]. Dieses Zellkultursystem ist hoch artifiziell, da es mehrere wichtige Aspekte nicht ausreichend nachstellt: (i) 2D kultivierten Zellen fehlt es an Dimensionalität, (ii) es ist ein stark polarisiertes, mechanobiologisches System und (iii) lokale Konzentrationsunterschiede molekularer Gradienten existieren nicht.

Im Gegensatz zu dieser klassischen Zellkulturtechnik ahmen sogenannte 3D Zellkultursysteme die *in vivo* Eigenschaften der natürlichen extrazellulären Matrix (ECM) in Form von z.B. Hydrogelen oder Sphäroidkulturen nach [2]. Hierbei werden physikalische, (bio)chemische und mechanische Eigenschaften berücksichtigt [3, 4]. Zellen, die in einem 3D Zellkultursystem kultiviert werden, weisen im Vergleich zu 2D kultivierten Zellen, unter Anderem eine unterschiedliche Morphologie, Proliferations- und Migrationsrate auf [5, 6, 7]. Auch die Übertragbarkeit der Ergebnisse von 3D Zellkultur basierten Versuchen auf z.B. exprimierte Tumormarker oder medikamentöse Behandlungen, ist deutlich erhöht [9, 8, 10].

Im Gegensatz zu der Standard 2D Zellkultur haben 3D kultivierte Zellen die Möglichkeit mit der ECM zu interagieren [26]. Diese Interaktionen finden durch Signalprozesse an der Plasmamembran statt, wodurch viele Prozesse wie Migration, Proliferation, Differenzierung und Zellüberleben reguliert werden [11, 12, 13]. Integrine sind hierbei die Hauptvermittler der Zell-ECM Interaktion. Dieser Prozess ist besonders interessant, da er im direkten Zusammenhang mit der cell-adhesion-mediated-radio-reistance (CAM-RR) steht, die nur für Zellen beobachtet werden kann, die in 3D kultiviert werden [27].

Bis zu Beginn dieser Thesis wurde die CAM-RR mit Chromatinstrukturen, die sich zwischen 2D und 3D kultivierten Zellen unterschieden, in Zusammenhang gebracht. Hierbei führt ein erhöter Anteil an Heterochromatin von 3D kultivierten Zellen zu einer geringeren Menge an Doppelstrangbrüchen nach einer Bestrahlung mit Röntgenstrahlen. Zum Anderem wurde dieser Prozess mit ECM-bindenden Integrinen, welche eine $\beta 1$ Untereinheit besitzen, in Verbindung gesetzt [14].

Ziel des **ersten Kapitels** dieser Arbeit war es, die an der Plasmamembran lokalisierten Effekte ionisierter Strahlung auf $\beta 1$ Integrine zu untersuchen. Hierfür wurden 3D kultivierte Zellen mit Röntgenstrahlen bestrahlt und die nanoskalige Verteilung der Integrincluster mittels Einzelmolekülmikroskopie untersucht und anschließend quantifiziert. Durch Vergleichsexperimente mit 2D kultivierten Zellen konnte gezeigt werden, dass die Strahlenresistenz der 3D kultivierten Zellen auf ihrer Fähigkeit beruht, Integrincluster besser zu organisieren. Im Gegensatz zu 3D Zellen, weisen 2D kultivierte Zellen eine dynamische und instabile Clusterung der Integrine auf. Zudem konnte nachgewiesen werden, dass die Signalweiterleitung mittels Integrinen in 2D kultivierten Zellen fehlerhaft ist. Demnach konnte gezeigt werden, dass stabile Integrincluster 3D kultivierter Zellen zu einer Strahlenresistenz, dynamische und instabile Cluster 2D kultivierter Zellen hingegen zu einer Strahlensensitivität führen.

Im **zweiten Kapitel** dieser Arbeit wurde der Integrininhibitor AIIB2 verwendet um die Integrincluster 3D kultivierter Zellen zu destabilisieren und so, in einem kombinierten Ansatz aus Inhibitor und Bestrahlung, eine Strahlensensitiviät zu induzieren. Integrine sind nicht nur für die Zell-ECM Interaktion verantwortlich. Durch eine physikalische Verbindung (u.A. Aktin, die Kernmembranproteine Nesprin und SUN) sind sie mit der nuklearen Lamina verbunden und können so die Chromatinverteilung beeinflussen. Durch das Folgen der mechanobiologischen Verbindung zwischen Integrinen und Nukleus konnte nachgewiesen werden, dass die CAM-RR 3D kultivierter Zellen auf ein funktionierendes, ausbalanciertes Mechanoperzeptions-System mit seinem Ursprung in einer korrekten Integrinclusterung beruht. Hingegen besitzen 2D kultivierte Zellen ein nicht funktionsfähiges, artifiziell versteiftes mechanobiologisches System.

Das **dritte Kapitel** dieser Dissertation beantwortet die Frage, ob die membranlokalisierten Effekte der Röntgenstrahlung auf das Integrinclustering Lipid-raft abhängig sind. Hierbei wird zudem die generalisierte Abhängigkeit zwischen Raft- und gleichzeitiger Proteinlokalisierung hinterfragt. Integrine und Cholesterolmikrodomänen kolokalisieren, eine Bestrahlung mit einer hohen Dosis ionisierender Strahlung ist jedoch in der Lage Integrine aus diesem System herrauszulösen, während Cholesterolrafts durch die Bestrahlung nicht beeinflusst werden. Dies zeigt, dass (i) die Effekt der ionisierenden Strahlung auf Integrine Lipid-raft unabhängig sind, aber auch, dass (ii) die Kolokalisierung beider Mikrodomänen womöglich voneinander unabhängig sind.

Schlussendlich, nur durch einen kombinierten, methodischen Ansatz aus 3D Zellkultur und Einzelmolekülmikroskopie war es möglich das Integrinclustering als Target für die Induzierung der Strahlensensitivität zu identifizieren. Hierbei ist das durch Einzelmolekülmikroskopie bestimmte Proteinclustering eine erweiterte Form des molekularen Phenotyps, welcher sonst z.B. Proteinaktivitäten beschreibt. Durch die Implementierung der Einzelmolekülmikroskopie und der 3D Zellkultur in ein Phenotyp-basiertes HCS könnten die Vorteile beider Methoden die Aussagekraft solch eines Screnning bereichern: (i) 3D Zellkulturen spiegeln den *in-vivo* exprimierten Phenotyp wieder und (ii) Einzelmolekülmikroskopie würde es ermöglich den molekularen Phenotyp zu bestimmen und den Einfluss möglicher Leitstrukturen auf die nanoskalige Verteilung eines Targets zu quantifizieren.

Trotz dieser Vorteile basieren vorklinische Screenings zumeist auf artifiziellen 2D Zellkulturen und auf mikroskopischen Methoden, die eine deutlich geringere Auflösung aufweisen.

Contents

1 Abstract

The cellular interaction with the extracellular matrix (ECM) modulates many key processes such as proliferation, migration, differentiation and survival. In addition, resistance to ionizing radiation has been found to be higher in cells cultured in presence of a 3D matrix, a process, which has been termed cell-adhesion mediated radio-resistance (CAM-RR). These cells are able to properly organize ECM-binding (extracellular matrix) integrins containing a $\beta 1$ subunit into firm and stable clusters. Upon irradiation, these clusters are hard to break. On the contrary, cells cultured under standard, monolayer-based conditions are unable to keep this clustered status and are therefore radiosensitive. Radioresistance is thus linked to the ability to maintain a well defined organization of integrins in clusters, making integrin distribution a potential drug target for radiosensitization.

With the use of the integrin $\beta 1$ inhibitory antibody AIIB2, a well-known radiosensitizer, it is possible to induce radiosensitivity and in combination with ionizing radiation (IR) to break integrin $\beta 1$ clusters of 3D cultured cells. In 2D cultured cells the treatment with AIIB2 completely abolished integrin clustering. As integrins are the key mediators of cell adhesion and mechanosensing, they originate the molecular signaling towards chromatin remodeling in response to a cell's microenvironment. By following the physical link from integrins up to the nucleus with single molecule localization microscopy, it was found that the disintegration of integrin clusters has a direct impact on this nuclear mechanosensor. Collectively, these results show that, in addition to biochemical also mechanobiological cues and in particular nuclear mechanosensing have to be considered as relevant to uncover the molecular events behind adhesion related radiosensitivity. Therein, 2D cultured cells are highly artificial and do not provide the means to investigate mechanobiological aspects.

Not only the involvement of ECM-binding integrins in radioresistance of various tumor types makes them an important target in actual cancer studies, they also contribute to drugresistance, metastasis and angiogenesis. So far, the vast majority of high-content screenings (HCS) use flat cultured, highly artificial monolayer-based 2D cells and standard microscopy techniques. The here achieved results prove that 3D cell cultures and single molecule microscopy are powerful tools for preclinical screenings. It would be possible to combine the virtues of microscopy of the nanoscale with the capability of 3D cultured cells to enhance the predictive value of high-content-screenings (HCS).

2 General Introduction

2.1 Single molecule microscopy in preclinical screenings

Light microscopy has come a long way from its scientific introduction in the 17th century by Robert Hooke and Antonie van Leeuwenhoek until today.

The invention of superior optics, fluorescence microscopy and its adaptive development towards confocal microscopy (CLSM) made microscopy into a method that has a huge impact on answering biological enigmas. Until 1981 microscopy was bound by its diffraction limit rendering its application on analyzing processes smaller than 200 nm [28]. The development of super resolution imaging by overcoming the diffraction barrier gave a powerful boost for observations on the nano scale. Methods, such as SIM (structured illumination microscopy), STED (stimulated emission depletion), PALM (photoactivated localization microscopy) and STORM (stochastic optical reconstruction microscopy) allow researchers to observe details down to assemblies of just a few labeled biomolecules. These advancements in optical microscopy techniques were honored in 2014 with the Nobel prize [29].

Surprisingly, microscopical methods applied in preclinical screenings are still stuck in the techniques of the 80s. Mainly simple imaging techniques such as wide field fluorescence microscopy or confocal microscopy are used, neglecting the huge advantages of super-resolution microscopy to image processes at the nano scale [25].

2.1.1 Preclinical screenings

Preclinical drug development is characterized by a frequent cycle between compound synthesis and optimization, each of which are followed by a screening step. From a screening point of view, the goal is to rapidly identify compounds that have a desirable profile and to eliminate those that do not. These screenings can either be high-throughput (HTS) or high-content screenings (HCS) [30].

In their simplest form, HTS are used to answer well defined questions. Hundreds of thousands of experimental samples are simultaneously tested under defined conditions. The read-out is an average over an ensemble of proteins present per well, carried out in multi-well-plates of different formats (from 96 well up to 6144 well) disregarding differences that might exist between molecules (e.g. active and inactive fraction) and ignoring cellular context altogether[31]. These techniques fail to provide temporal and spatial resolution and they do not directly show whether the identified molecule has a functional role in the cellular process of interest or not [32]. High-content screenings (HCS) overcome these limitations by combining modern cell biology methods with automated high resolution microscopy in form of targeted or phenotypic screenings.

Targeted- vs. phenotype-based screening

Modern drug development for a specific disease either begins with the so called target- or with a phenotypic-based screening of a compound library.

In phenotypic screenings (forward pharmacology) compound libraries are screened against cells or animals with the goal to identify phenotypic deviations from the unchallenged physiological state. Here, the molecular mechanism and protein target can remain unknown as lead molecules are obtained first. In the targeted screening approach (reverse pharmacology), compound libraries are screened against

identified and isolated biological targets [33, 34]. Initially, phenotypic screens used to be the sole application in drug development. But, molecular target-based drug screenings became the main approach in pharmaceutical and academic research centers in the past 25 years. However, since the 1980s, the interest in phenotypic screenings is renewed, leading to an increased number of approved drugs discovered by phenotypic screens exceeding those obtained through the molecular target-based approach [35].

The cellular phenotype is complex as it is the summation of the activity state of many pathways [36]. There are many different approaches to identify changes in the phenotype, such as cell morphology, migration and differentiation [35]. Assays targeting cell growth, cell death, intracellular signaling and protein transcription are widely used. They range from cell cycle analysis over protein expression, localization and degradation to gene expression analysis. In contrast to the targeted-based screening approaches, phenotypic assays achieve a higher biological relevance due to the use of small animal- and cell-based screens. For many diseases small-animal models (zebrafish, *Drosophila melanogaster, Xenopus laevis*) exist. Phenotypic screenings that use *in vivo* models can provide rich information about compound distribution, metabolism and toxicity but due to species differences, some of these animal models have a poor relevance for human diseases. Cell-based phenotypic screenings overcome this disadvantage for primary compound screens as they use human cell lines. The most commonly used assays for cell based screens are (i) cell viability, (ii) signal pathway and (iii) disease-related phenotypic assays [35].
With the use of phenotypic screens on the level of HCS a highly detailed, multi-parameter profile can be acquired, which include transcriptional, proteomic and imaging-based measurements. Each method can quantify changes in several cellular processes that may be amenable for targetings with small-molecule drugs. The most powerful tool in multi-parameter profiling are DNA and protein arrays. With them it is possible to survey thousands of genes, mRNAs and proteins at once [37].

2.1.2 Imaging the phenotype

Image-based screenings are a powerful tool to gain systematic insights into biological processes as they can directly show if the identified molecule has a functional role in the cellular process that is under investigation - or not [38]. With the use of automated microscopy and image processing it is possible to screen and quantify changes in the visual phenotype in cells and organism. Under the use of imaging techniques in the screening pipeline, the phenotypes of each cell in a well can be recorded, leading to very detailed datasets for every single cell [39]. By measuring multiple cellular phenotypes and subsequent quantitative data analysis, samples can be sorted in distinct subtypes. This application is, for example, applied for systematic genome-wide RNA-interference screens for dozens of phenotypes. In addition, image-based screenings can be used for (i) fluorescent reporter gene screens, (ii) for measurements that assess changes in sub-cellular localizations and, obviously, (iii) for assays were complex changes of the morphology are of interest [31, 32].

For all these applications mainly three imaging techniques are used: wide field fluorescence microscopy, confocal microscopy (CLSM) and flow cytometry. The critical disadvantage of all these techniques will be the focus of this chapter: They all lack spatial resolution thereby averaging fluorescent signals of several molecules into a mean intensity value, neglecting the possibility of advanced microscopy techniques to provide information about the nanoscale distribution and organization of single molecules or proteins of interest (Figure 2.1 A).

SMD for molecular phenotype screening

Super-resolution techniques provide novel insights into sub-cellular processes and structures as they are able to resolve features beneath the diffraction limit. Due to the wavelength character of diffracted light, objects smaller than 200 nm in the lateral dimensions (and approximately 500 nm in the axial dimension) are visualized as a blur. But most of the subcellular structures are of smaller size (e.g. membrane proteins,

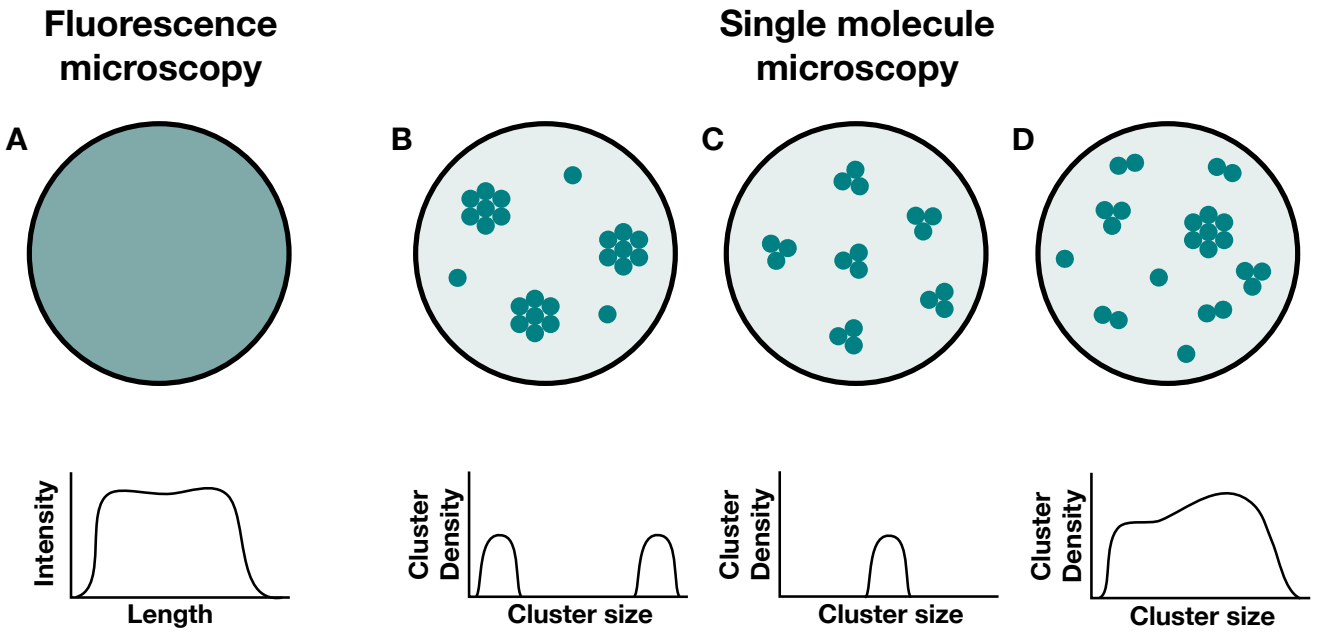

Figure 2.1: Single molecule microscopy provides profound information about the molecular phenotype. A - D: Obtained signals of fluorescently labeled molecules, the number of fluorophores is constant. A: Fluorescence microscopy is unable to identify single molecules and only a simple intensity profile is obtained. B - D: Single molecule localization microscopy is able to provide information about different molecule distributions, localizations and organizations. This figure is adapted from Lauer et al. [42]

ribosomes, vesicles) and can only be resolved with the use of super-resolution microscopy techniques. STED (stimulated emission depletion) or SIM (structured illumination microscopy) are techniques that modify the extrication light pattern through controlled engineering of the point-spread function (PSF). With this, a smaller spot size is achieved leading to a resolution of up to 20 nm.

Another method to overcome the diffraction limit employs photoswitchable fluorophores and their ability to be stochastically activated. With this, very closely located molecules that reside in the same diffraction-limited volume can be detected by merging all detected localizations obtained with a repeated cycle of activation and detection. There are various implementations of this single molecule localization microscopy (SMLM) with the result that this technique is known under different names. This includes PALM (photoactivated localization microscopy) and STORM (single molecule localization microscopy). By breaking the diffraction limit up to 25 nm this technique allows for protein co-localization, single molecule tracking and localization studies on the nano scale.

SMLM as part of preclinical screening would extend the assessment of a cellular phenotype to the molecular dimension, i.e. the nanoscale localization and organization of molecules or proteins of interest. While traditional fluorescence microscopy can only give basic information about protein localization and its local concentration, SMLM can differentiate between different protein organizations and localizations (Figure 2.1 B - D). With this it would be possible to screen for compounds that have a direct effect on the nanoscale organization and localization of proteins, which in turn directly effects protein activity [40], signaling [41] and therefore cell fate.

2.2 *In vivo*-like cell cultures for cell-based screenings

Not only advanced microscopy techniques are unconsidered in preclinical screenings, even worse, the industry is only slowly moving towards advanced cell culture techniques which better mimic *in vivo* conditions. Most assays use monolayer-based cell cultures that present a highly artificial environment to the cells. The use of such cell culture systems, termed 2D cell cultures, has a limited predictive value for clinical efficacy of compounds as these cells lack three important aspects: (i) They lack dimensionality as these cells are not allowed to adhere to extracellular supports or adjacent cells with their entire surface, (ii) provide a highly polarized rather than homogeneous mechanical environment and (iii) lack the ability to maintain local concentration heterogeneities, e.g. gradients of soluble compounds (see Figure 2.2 A and B).

To successfully screen for compounds a cell culture system does not only have to mimic *in vivo* conditions, but it should also enhance the predictive value of HCSs [1].

2.2.1 3D cell cultures and their advantage towards 2D cells

In recent years, many methods were introduced to fill the gap between monolayer-cultured 2D cells and animal models. All these cell culture techniques mimic the *in vivo* conditions by providing physical, (bio)chemical and mechanical properties of tissues in respect to cell-cell and cell-extracellular matrix (ECM) interactions as well as soluble factors [3, 4]. The most commonly used - so called 3D cell culture systems - are based on multi-cellular spheroids or on ECM materials that surround the cells.

Cellular spheroids are cell aggregates generated within a hanging drop or in rotating-wall vessels. In both cases, the natural tendency of a variety of cell types is used to form tissue-like aggregates [2] (see Figure 2.2 E and F). Spheroid cell cultures are usually used to mimic chemical gradients (e.g. oxygen, drug delivery, metabolites and nutrients) and tumor tissue. With this technique it is possible to easily generate co-aggregates of different cell types and with this, to better analyze complex intra-and inter-cellular signaling circuits [43].

On the other hand, *in vivo* properties can be imitated by culturing cells embedded in an ECM (see Figure 2.2 C and D). The extracellular matrix provides an adequate distribution and density of adhesion sites, mechanical resilience and local concentrations of solutes. Cells interact through ECM receptors (e.g. integrins) with binding motifs of ECM molecules and migrate by using ECM-cleaving proteins (metalloproteinases, MPPs). For an ECM-based 3D cell culture system, natural ECM sources such as collagen (e.g. types I, III, V and XI) [44], elastin, laminin, fibronectin [45] or complex protein mixtures such as Matrigel [46] can be used as a scaffold for cells. Hereby, collagen I is the main component of the ECM in interstitial tissues determining the spatial organization and stability of connective tissue. These natural ECM sources provide the needed presentation of recognition motives (e.g. RGD) as well as cleavage sites for cell-induced remodeling of the ECM [47, 48]. ECM-based 3D cell cultures are used in the form of hydrogels with a water content of up to 99% (w/w) and with similar viscoelastic and diffusive transport characteristics as the natural ECM [3].

Besides the use of natural ECM scaffolds, also synthetic forms of ECMs are commonly used, typically in the form of nontoxic PEG (polyethylene glycol) hydrogels or semi-synthetic gels such as GelMA (gelatin methacryloyl). Especially for manipulations of the scaffold itself such ECM variants are prone, as physical properties are controllable [49, 50].

Cells cultured in a 3D cell culture system show, in comparison to 2D cultured cells, not only a different gene expression [6, 51, 52], morphology [53], cytoskeletal organization [54], migration [5] and proliferation rate [6, 7] but also a different distribution in cell cycle phases [55]. All these phenotypes differ if compared to 2D cultured cells due to a different expression pattern of proteins with a huge impact on the effectiveness of cancer inhibitors [9, 8, 10]. With this it is obvious that the standard monolayer 2D cell culture is not suitable as a cell culture system in preclinical screenings as it is irrelevant for the identification of new drugs. Additionally, while it is well accepted that the micro environment has a

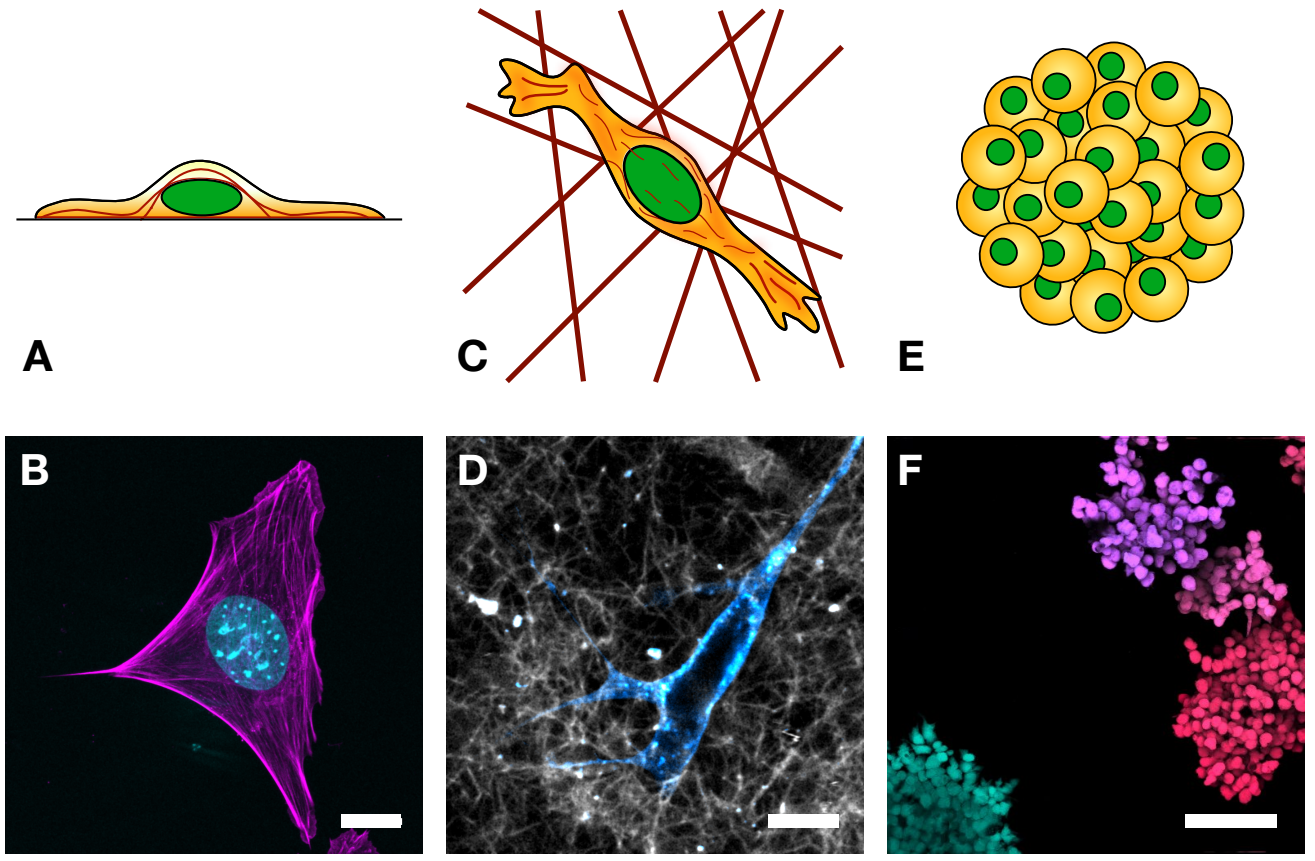

Figure 2.2: 3D cell culture system has a strong impact on the cells A: Flat cultured 2D cells. B: Actin (magenta) and DNA (cyan) staining of a 2D cultured MEF cell. Scale bar is 5 μm. C: ECM-based 3D cell culture. D: MEF cell (PM staining with cell mask orange, blue) cultured in a collagen hydrogel (gray). Scale bar is 10 μm. E: Spheroid 3D cell culture. F: HeLa spheroids, PM staining with cell mask orange. Scale bar is 100 μm.

profound impact on cell physiology, the vast majority of experiments in cancer and biological research are still done with artificial, 2D cultured cells [56].

In addition, it is possible to use whole animals or organs as *in vivo* imitating models. Organotypic slices preserve the cytoarchitecture and the cellular differentiation of the original tissue. Small animals (e.g. zebrafish) or mammalian embryos (e.g. mice) provide data on the behavior of cells in their original physiology with the opportunity for time-lapse imaging. But these two techniques are highly demanding in their standards, as tightly controlled temperature and oxygeneration are needed, thus rendering them impracticable for HCS applications [2].

2.3 Integrins in cancer research

The vast majority of *in vitro* cancer studies are still performed with the use of 2D cultured monolayer cells, even trough these artificial culture conditions result in misleading research observations and hypotheses [56]. To enhance the predictive value of cell culture systems in tumor studies, the advances in 3D cell culture engineering need to become an integrative part of cancer research.

Cancer is a disease involving changes in the genome that produce oncogenes with gain of function and tumor suppressor genes with loss of function. These changes are acquired during a multi step development of tumors leading to the following capabilities of cancer cells:

(i) Cancer cells are able to avoid apoptosis, they (ii) sustain their proliferative signaling, (iii) evade growth suppressors, (iv) activate invasion and metastasis, (v) are immortal, (vi) induce angiogenesis, (vii) reprogram the energy metabolism and (viii) evade immune destruction [57, 58].

In cancer treatment, ionizing radiation (IR) and anti-cancer drugs are used to cause DNA damage or to inhibit signaling pathways that lead to cell death. One of the major problems in cancer therapy is the resistance of cancer cells against chemotherapeutics and radiation, limiting the effectiveness of current cancer therapies. Screening approaches have the power to identify novel mechanism of these two resistances as well as their molecular signatures and genotypes that predict tumor response if (i) the correct cell culture system (ii) and the proper screening method is used [59].

One important group of proteins contributing to drug- and radioresistance are the extracellular matrix receptors integrins. In addition, integrins are known to be responsible for tumor metastasis and angiogenesis as well as cancer progression and cell survival, which makes them an important target for tumor therapy [22, 23]. Further more, integrins are also found in tumor-associated cells, such as the vascular endothelium or fibroblasts, regulating the contribution of such cells to cancer progression. Never the less, integrins itself are not oncogenes. Rather, some oncogenes require integrin signaling. In addition, some growth or cytokine receptors in cancer and host cells crosstalk with integrins, affecting expression, ligand affinity, and signaling of these receptors. Integrin expression in different cancer types is associated with diverse phenotypes. For example, in melanoma cells lymph mode metastasis is promoted by integrins, in colon cancer integrin expression is associated with a reduced patient survival [60].

2.3.1 Integrins

One of the key mediators for the cell's interaction with the ECM are integrins, which are noncovalently linked, heterodimeric type I transmembrane proteins consisting of an α and β subunit [26]. In total, there are 18 α and 8 β subunits, which assemble to 24 known integrin heterodimers [61]. Upon a successful interaction of integrins with the ECM, many integrins as well as membrane associated and intracellular proteins cluster into large assemblies known as focal adhesions (FAs) [62]. The extracellular domain of ECM-binding integrins recognizes the conserved tripeptide Arg-Gly-Asp (RGD) of ECM proteins such as collagen, laminin or fibronectin [26, 63]. RGD is bound at the interface between the α and β subunit [64, 65] of integrins containing e.g. the αV, β1 or β3 subunit.

The binding between integrins and ECM leads to the so called outside in activation, triggering changes of the cytoskeleton or gene expression, cell migration, proliferation as well as cellular survival [11, 12, 13]. These processes are transduced by the recruitment of FAK (focal adhesion kinase), the recruitment and activation of SFKs (Src-family kinases) and by the activation of PI3K (Phosphoinositide 3-kinase). Integrin-ECM communication is tightly involved in tumorgenesis and cellular reactions to anti-cancer treatment. ECM-binding integrins are known to contribute to tumor progression and they are overexpressed in many tumors and malignant cell lines [66, 67].

While the outside in activation is an example for the activation of traditional receptors, integrins can be additionally activated by the inside-out mechanism. Here, an intracellular activator (e.g. talin, kindlin) binds to the β tail leading to a conformational change in the integrin dimer and its subsequent activation and its increased affinity towards extracellular ligands [68, 69].

2.3.2 Integrins and their role in CAM-RR

One powerful example for the false use of 2D cells in anti-cancer research concerns integrin adhesion receptors. 2D cells are not only differently affected by anti-cancer drugs [9, 8, 10], in comparison to 3D cultured cells they are significantly more sensitive towards ionizing radiation. The radiosensitivity of 2D cells has its origin in a disturbed distribution and organization of integrins containing a $\beta 1$ subunit [41]. In contrast, the ability of 3D cells to better organize $\beta 1$ integrins contribute to the ability of 3D cells to be radioresistant. This effect is also known as cell-adhesion-mediated-radio-resistance (CAM-RR) [27, 14].

So far, CAM-RR was linked to the chromatin structure that differs between cells cultured under 2D and 3D conditions [70]. Namely, the presence of a higher fraction of heterochromatin in 3D cultured cells was shown to correspond to a decreased amount of residual DNA double strand breaks (DSB) after X-ray irradiation [17]. While integrins as the key mediators of a cells interaction with the ECM, are clearly involved in this culture-condition dependent effect, mainly the players acting downstream of integrin signaling have been thoroughly investigated (ILK, FAK, JNK1, Akt1, PINCH1, HDAC) [18, 19, 20, 21].

Focal adhesions

Focal adhesions are multi functional organelles that mediate many cellular processes, such as cell-ECM adhesion, force transmission, cytoskeletal regulation, cell mobility and signaling [62]. Focal adhesions are multi protein arrays that link ECM-binding integrins with the actin cytoskeleton (see Figure 2.3). This integrin-adhesome consist of more than 150 distinct components [71], whereas the main proteins that form the link between integrins and the cytoskeleton are: talin, vinculin, paxilin and FAK (focal adhesion kinase) [72]. Integrins reside in focal adhesions through free-diffusion and immobilization cycles, whereas integrin activation promotes immobilization stabilized by actin and ECM binding [73].

Not only the proteins inside the focal adhesion are highly dynamic, also the whole multi-protein complex is always in a process of adhesion turnover and maturation. Focal adhesions are cellular structures with a size of 200 nm and below [74], whereas most of the knowledge about them was obtained from 2D-based cell cultures [75]. At first is was proposed, that focal adhesions are an artifact of 2D cultured cells but, by reducing the background-fluorescence in 3D cultured cells, adhesion complexes were also revealed in ECM-based cell cultures [76]. Still, it was also discovered that FAK signaling is fundamentally different if 2D and 3D cultured cells are compared - 2D cells express twice as much active FAK (phosphorylated focal adhesion kinase) as 3D cultured cells implying that the focal adhesion signaling, with its origin in the interaction of integrins with the ECM, is by its very nature different [41].

2.3.3 Protein and lipid clustering

The term clustering is generally associated with the interaction of different subunits of proteins to form dimers or heterodimers. For integrins, the combination of α and β subunits causing the recruitment of multivalent protein complexes to the cytoplasmic domain is meant in this context.

For this thesis the term clustering is defined as the association of many integrin subunits within a zone of about 200 nm where the mobility is confined [73]. These regions are multiprotein complexes known as focal adhesions. Still, whether clustering triggers outside-in signaling to facilitate integrin activation, or whether clustering occurs after integrin activation has yet to be fully understood. There are many other known protein clusters present in the PM including the synaptic protein syntaxin, [77], signaling protein Lat [78], GPI anchored proteins [79] and cytoskeleton components such as actin [73].

The term clustering is not only used for protein assemblies. One of its prominent forms is used in the context of lipid microdomains - known as lipid rafts. Physical differences in lipids such as chain length, chain geometry and head group cause different membrane components of the plasma membrane (PM) not to be homogeneously distributed on the cell surface but rather to aggregate in domains. Specifically,

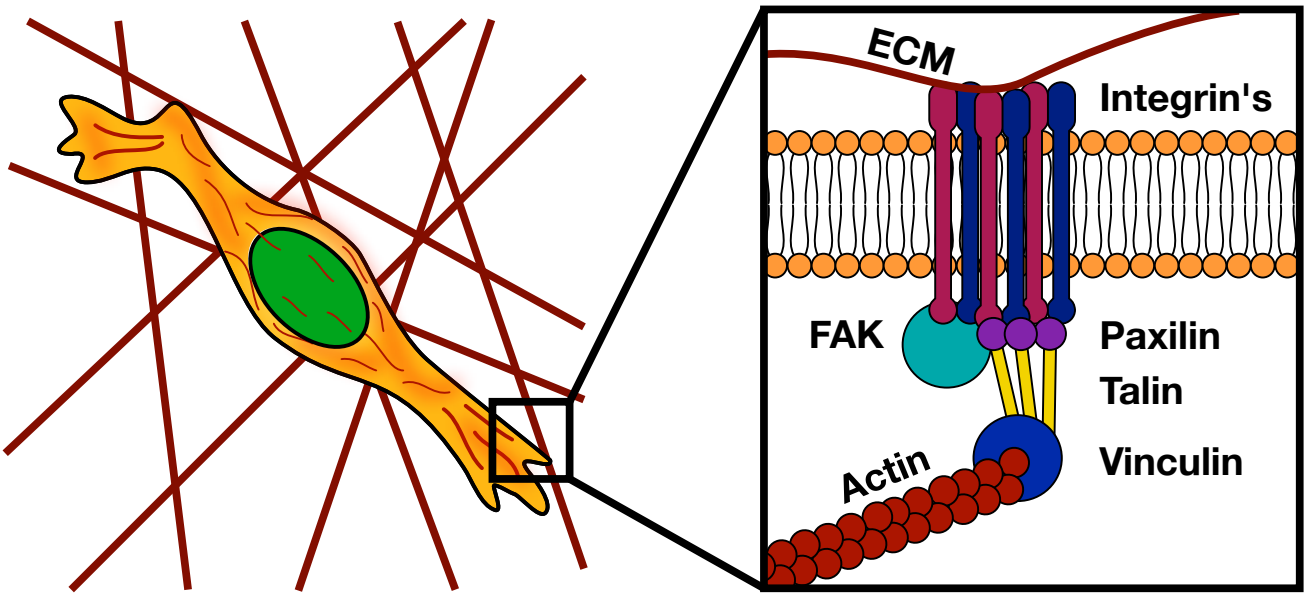

Figure 2.3: Focal adhesions connect ECM-binding integrins with the cytoskeleton. Main components are: FAK (focal adhesion kinase), paxilin, talin, vincluin and actin. Focal adhesions are known to comprise of more than 150 distinct components including structural proteins that mediate the physical link to actin (e.g. paxilin, vincluin) and regulatory proteins (e.g. FAK).

sphingolipids and cholesterol aggregate in microdomains known as lipid rafts [80, 81]. Lipid rafts are highly dynamic structures (10 - 200 nm) that limit the free diffusive properties of biomembranes as proposed by Singer and Nicolson in their fluid mosaic model [82]. These micro structures are known to function as parts of signaling cascades or as platforms for membrane protein clustering and therefore for protein activity [40]. Proteins localize in lipid rafts either due to a direct interaction with the lipid head group or due to physical forces such as lateral pressure, charge interactions or the local curvature of the membrane [83].

Still, the generalized view of lipid rafts as an organizing platform is highly questionable as reported for the case of integrin and cholesterol. Integrins are known to reside in cholesterol lipid rafts [84], but it was found that integrin and cholesterol clustering is lipid-raft independent.

2.3.4 Imaging and quantification of clustering

To image the effects of drug treatment or ionizing radiation on the nanoscale distribution of integrins and other molecular phenotypes, SMLM is used. This method is not only compatible with 2D cultured cells, but also with 3D cell cultures [41]. For cells cultured on a coverslip TIRF microscopy can be used to image protein distributions. This method uses the total reflection of the incoming LASER (light amplification by stimulated emission of radiation) at the glass-water interface to generate an evanescent field. Total internal reflection can only be observed if the light travels from a medium with a higher refractive index (e.g. glass dish, n = 1.5) to a medium with a lower refractive index (e.g. water phase (cytosol) n = 1.3). During this process, a portion of the energy of the reflected light forms the so called evanescent wave originating at the class-water interface, whereas the evanescent field has the same frequency as the incident light. Fluorophores within this field are not excited by the absorption of photons but by getting in resonance with the electromagnetic field. The penetration depth, which is the distance at which the intensity exponentially falls to half of the value at the glass-water interface, of this field is typically in the range of 100 nm making it is possible to exicate fluorophores with a dramatically reduced background fluorescence and in consequence a contrast unmatched in fluorescence microscopy [42].

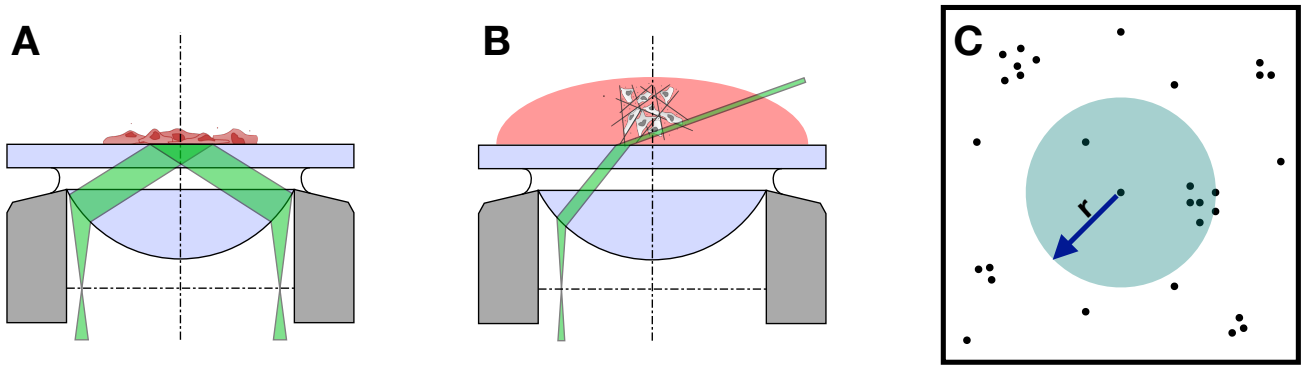

Figure 2.4: Single molecule microscopy of 3D cells and its data analysis A: Illumination scheme for TIRF microscopy. B: Illumination scheme for HILO microscopy. C: Analysis of single molecule data with the Ripley's K function. Shown is a scatter plot where every point is a detected molecule. The Ripley's K function computes every signal that falls within the marked radius for every detected signal. A and B were prepared by PD Dr. T. Meckel, TU Darmstadt.

3D cell cultures are not amenable to this method as these cells are not in the range of the evanescent field. To measure single molecules in 3D cells it is possible to combine STORM with HILO (Highly inclined laminated optical) sheet based microscopy [85]. Here, an axially confined illumination is achieved by focusing the excitation LASER off-center into the the back focal plane of a high NA objective. The beam refracts at the coverslip-water-interface and propagates into the 3D cell culture at a shallow angle to the coverslip, while also crossing the focal plane of the objective. The result is an axially confined illumination zone and an axially and laterally confined detection zone. With this, only a subfraction of STORM capable dyes (e.g. Alexa-488 or Alexa-633) linked to antibodies can be activated, excited, and detected allowing for a contrast sufficient to robustly detect individual antibodies and localize their signal with a precision of typically 30 nm [41].

With this it is possible, to image single molecules of cells cultured in 2D and 3D under life-cell or fixed conditions and to quantify the obtained data. Rapid and complete immobilization fixation protocols [86] make it possible to get snapshots of the highly dynamic clustering process of proteins. To quantify these snapshots the Ripley's K function is used. This method computes the average number of signals that fall within defined radii of each detected single molecule. With this it is possible to obtain (i) a value that describes the clustering of the analyzed dataset and (ii) the mean radius of the analyzed clusters [87, 88, 89]. A detailed description can be found in the supplementary of Babel et al. (Section 6.1).

Based on this method it is possible to further quantify the data, parameter such as: number of clusters, signals per cluster, cluster density or the ratio of clustered vs unclustered signals can be determined [90].

2.4 Mechanobiology and its impact on CAM-RR

Integrins are front and center in the cellular processes that belong to the emerging field of mechanobiology. Integrins link the extracellular matrix with the intracellular cytoskeleton directly enabling cells to sense and produce mechanical forces [91]. As CAM-RR has its origin in a proper nanoscale distribution of $\beta 1$ integrins, the involvement of mechanobiological cues come more and more into focus.

Mechanotransduction is defined as the process by which cells translate mechanical stimuli into biochemical signals, enabling cells to sense changes in the physical environment and adjust their structure and function accordingly [92]. One classical and powerful process, were mechanobiological signaling is crucial, is migration. Cell migration through 3D tissue or confined microenvironments is highly dependent on the cells ability to alter physical tissue constrains and cell deformability [93]. The cells ability to be deformable relies on cytoskeleton and nuclear shape reorganization [94]. The nucleus is thereby mechanically linked with the ECM via multiple proteins that transmit forces to the nuclear envelope and into the nuclear interior, converging the main structural protein of the nucleus - the nuclear lamina [95].

2.4.1 3D cell culture sensed by integrins - Integrins and their impact in mechanobiology

Integrins, as the key mediators of cell adhesion not only facilitate the mechanical anchoring of cells to extracellular supports but also originate the ability of cells to sense the mechanical properties of their surrounding. Intriguingly, the mechanical information is not transmitted via signaling cascades, but a direct continuous connection between the ECM and chromatin is responsible for signal transmission [96, 97]. Changes in the microenvironment are detected and transferred via actin and nuclear envelope proteins (nesprin-1 and 2, SUN1 and 2) into the nucleus, leading to a reorganization of the nuclear lamina [91, 98]. With this connection, 3D cultured cells are able to mirror changes in the ECM directly in the nucleus [99, 100], as the nuclear lamina is reorganized and transcription factors are activated [101]. The nucleoskeleton lamin forms a network of intermediate filaments on the nucleoplasmic surface of the inner nuclear membrane and is mechanically interconnected with chromosomes which are positioned in distinct locations [102, 103]. Lamin associated proteins (e.g. lamin B receptor, emerin) anchor the lamin network with chromatin structures and enable lamins to regulate DNA synthesis, chromatin organization and gene transcription [104, 105]. In particular lamins A and C provide structural support to the nucleus and define, together with the ECM, the final ends of the mechanotransduction system.

Hence, integrins act as a mechano-sensor and bring the culture conditions and chromatin organization into a direct molecular connection. On the other hand, the so called LINC (linker of the nucleoskeleton and cytoskeleton) complex, composed of KASH (nesprin) and SUN domain proteins, located at the outer and inner nuclear membrane, is the second mechano-sensor (see Figure 2.5). Much like integrins bridge the plasma membrane to couple the ECM with the cytoskeleton, the LINC complex bridges both nuclear membranes to physically link actin, microtubules, or intermediate filaments to lamins turning the nuclear envelope into a force-sensitive interface between the cytoplasm and the chromatin [95].

The advantage in the use of this mechanical link instead of soluble signaling factors lies in its speed. Mechanical force propagation from the ECM to the nucleus is nearly immediate ($\sim$1 ms). In comparison, small molecules, such as calcium, take about 25 s, a motor-protein based translocation even up to 50 s. This makes the mechanical link between integrins and the nucleus the fastest way to transport information [91].

Integrin clustering and nuclear lamin distribution as a read out for force transmission

Both, the clustering of integrins and the lamin distribution at the inner nuclear membrane are markers for a correct force transmission and nuclear mechano sensing. A combined approach of super- and high resolution microscopy reveals significant differences between the two mechano-sensors, making (i)

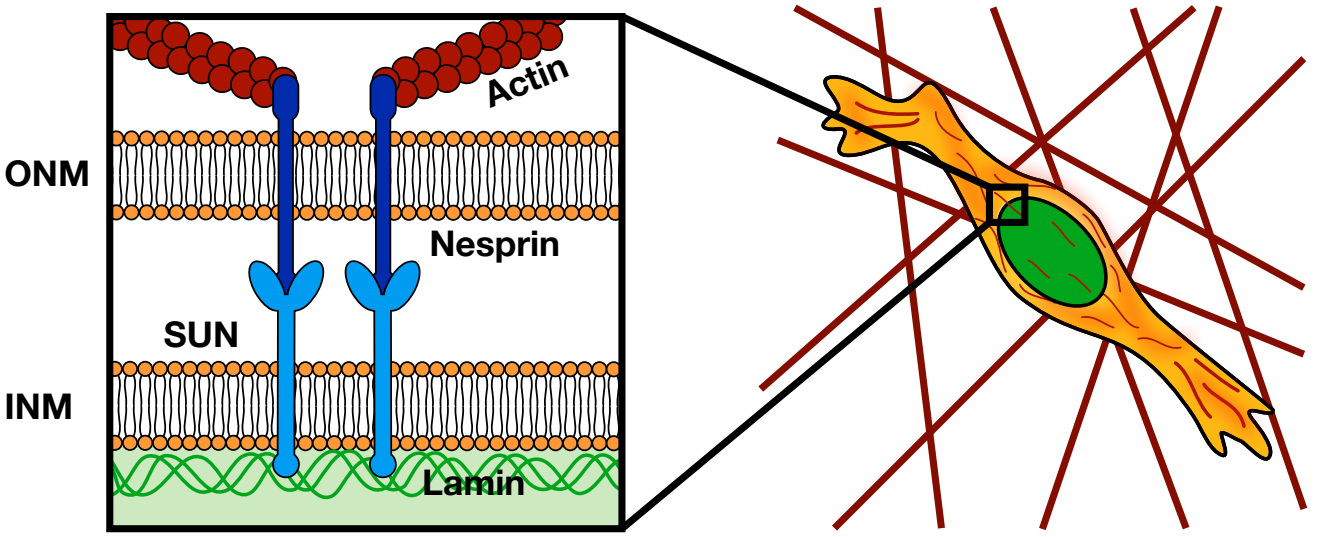

Figure 2.5: LINC (linker of nukleoskeleton and cytoskeleton) complex turns the nuclear envelope into a mechano-sensor. LINC complex components are: actin, nesprin and SUN proteins. Nesprins, a member of KASH proteins, reside in the outer nuclear membrane (ONM) and interact towards the cytoplasm with actin and, towards the inner nuclear membrane (INM), with SUN proteins. SUN proteins reside in INM and are linked inside the nucleus to the nuclear lamina (Lamin). The nuclear lamina interacts with chromosomes and contributes to spatial genome organizations.

integrin clustering and (ii) the nuclear lamin distribution and organization to a read out for a correct force transmission between ECM and nucleus (see Figure 2.6).

Integrin clustering is a mechano sensor

Integrins are the key proteins that connect the cell with the ECM. It comes to no surprise, that the nanoscale distribution and localization of ECM-binding integrins differ if 2D and 3D cultured cells are compared. With the use of SMLM it was detected that 3D cultured cells keep nearly all integrins in a clustered organization. Only about 10% of all detected integrins are not part of a cluster. Further more, these cells contain more $\beta 1$ integrins per cluster and even keep different integrins within the same clusters ($\alpha v\beta 1$, $\alpha v\beta 3$ and $\beta 1\beta 3$), if compared to 2D cultured cells. 3D cells are therefore able to combine integrin heterodimers with similar functions (to bind ECM) within the same cluster. 2D cultured cells are unable to maintain this level of organization. A significant portion of $\beta 1$ integrins freely diffuse (about 25%) in the plasma membrane, rendering them unable to take part in signaling. In addition, integrin subtypes were found to segregate into separate clusters rather than colocalize within the same clusters as in the 3D case. With this, it is obvious that the cell culture condition, and therefore the given mechanical stimuli, alone cause a marked difference in the ability of cells to maintain well organized integrin clusters (see Figure 2.6 and [41]).

Nuclear lamin organization is a mechano sensor

With integrins as the originator of the cells ability to sense mechanical properties, it comes to no surprise, that the nuclear envelope located marker for force transmission, the interface between actin - nesprin - lamin, differs greatly if 2D and 3D cultured cells are compared. With the use of confocal microscopy it was identified that the network of lamin intermediate filaments on the nucleoplasmic surface of the inner nuclear membrane is highly ECM dependent. 2D and 3D cultured cells differ in their distribution of lamin A/C beneath the inner nuclear membrane vs intranuclear signals. Intensity values of inner nuclear signal are significantly higher in 3D cultured cells. The soft environment made up of ECM yields in a reduced cytoskeletal tension and into higher levels of lamin A/C phosphorylations [100], which in turn,

yields a more soluble and mechanically weaker lamin network [92]. In other words, the softer the cellular environment, the more flexible and mobile the nuclear space. The mechano-balance, with its origin in a proper localization of integrins in clusters, is responsible for the 3D cells ability to reorganize its nuclear lamina in response changes in the ECM.

With the speed-advantage of the mechanical link between ECM and nucleus, force propagation along the cytoskeleton component actin is used to transport mechanical signals. Actin and lamin colocalize in form of strong, fibrous colocalizations between both filamentous proteins in 2D cultured cells. On the contrary, prominent f-actin bundles are more or less absent in 3D cultured cells leading to a far less intense colocalization and organization of lamin into fibers under 3D conditions, revealing that the force propagation between ECM and nucleus is by it's very nature incomparable.

With this it can be concluded, that the two cell culture conditions alone cause a marked difference (i) in the ability of cells to maintain well organized integrin clusters (ii) and to distribute lamin between the nuclear lamina and the intranuclear space.

The integrin - actin - LINC - lamin connection is able to mirror the mechanical properties of the ECM in the nucleus. Inside the nucleus the nucleoskeleton lamin is connected with chromosomes - so that any treatment of cells with the nucleus as the prime target needs to take this connection into account. With this connection in mind, the 3D environment was identified as a strong contributor to cell survival and numerous signaling pathways like Akt (Park et al. 2008), or NF-κB [106] were found to be involved. Recently, the inhibition of β1 integrin was also shown to reduce the expression of proteins involved in DNA repair, mainly those involved in non-homologous end joining (NHEJ) (Dickreuter et al. 2016), providing direct evidence for the reason behind CAM-RR.

Integrin clustering is the first sensor for radioresistance

Focal adhesions containing the β1 integrin subunit are a fast and sensitive compounds to react on ionizing radiation and are therefore the prime read out for radioresistance. 2D cells are unable to organize β1 integrins into firm and stable clusters but instead display a rather loose and heterogeneous organization. Upon irradiation this unstable condition is severely disrupted by low doses of IR and upon an irradiation with a high dose it completely breaks apart (see Figure 2.6 K). On the other hand, 3D cells are not affected by low doses of IR and only slightly upon irradiation with high doses of IR. Compared to 2D cultured cells, 3D cells are able to strictly organize integrins in stable clusters (see Figure 2.6 D). Hence, the ability of 3D cells to form stable integrin clusters contributes to their radioresistance.

2D and 3D cells differ not only in their ability to organize integrins into firm clusters and in their organization of the mechanical link involving actin - LINC and lamin. Also the immediate downstream partner, the FAK (focal adhesion kinase) differs if (i) 2D and 3D cultured cells are compared and (ii) its reaction towards IR is cell culture dependent. The number of activated FAK, its phospohorylated form pFAK, is in 2D cultured cells twice as high as in 3D cultured cells. The amount of pFAK is reduced upon treatment with IR only in 2D cells, whereas 3D cells are, again, not affected by this treatment.

The mechano-system is the second sensor for radioresistance

Through the SMLM of integrins and subsequent cluster analysis the nanoscale distribution and organization and its changes in response to IR are clear. However, for these differences to have an effect on cellular reactions, survival and CAM-RR, signaling from the organized and - upon IR - disintegrated integrin clusters have to change as well. It comes to no surprise, that with integrins as the originator of mechanotransduction, effects on their cluster status also changes the force transmission along the integrin - actin - LINC - lamin connection which makes the whole mechano system of a cell a read-out for radioresistance.

Along this connection, the distribution of NE located and inner-nuclear located lamin as well as the interface actin - lamin, located at the NE, are markers for a correct mechano-force transmission and consistently for radioresistance.

The ability of lamin to form a thin layer beneath the NE (NE-Lamin) versus a dispersed intranuclear localization (IN-Lamin) is a useful indicator of the forces that are transferred from the stiffness of the culture environment to the NE via actin and nesprin. In 3D cultured cells, the fraction of IN-lamin is 1.5x higher if compared to 2D cultured cells. In response to IR, 3D cultured cells with their intact mechanosensing, reorganize their laminar. On the contrary, 2D cells with their impaired mechanosensing, are unable to do this (see Figure 2.6 E and L).

For 2D cells, the entire mechanosensing chain is affected by IR: (i) complete integrin cluster break-down, (ii) actin cytoskeleton is fragmented and (iii) the actin - nesprin - lamin interface is lost. With the loss of the mechanosensing system, NE located lamin can not redistribute towards the nucleus center. In contrast to 3D cultured cells, here (i) integrin clusters only slightly shifted, (ii) actin is not fragmented upon irradiation and (iii) the actin - LINC complex is intact and is still part of the mechanosensing. The less rigidly connection between actin and lamin seems to be responsible for the lamin reorganization and redistributions to intranuclear regions in 3D cultured cells, which is part of the 3D cells ability to be radioresistant.

2.4.2 Targeting of integrins - turning 3D cells into 2D cells?

Stable integrin clusters contribute to the radioresistance of 3D cultured cells. With this, it is reasonable to assume that if radioresistance relies on intact integrin clusters an active disintegration of integrin clusters may in turn induce radiosensitivity. In short, the firm clustering of 3D cells needs to be transformed into the unorganized integrin distribution of 2D cultured cells. For this, an antagonist against the ability to form clusters, rather than antagonist that target the ligand-binding side, has to be used.

Integrin antagonists Cilengitide

Cilengitide is a selective $\alpha v\beta 3$ and $\alpha v\beta 5$ integrin inhibitor made up of a cyclic RGD pentapeptide (cyclo(RGDfV-)). This inhibitor uses the cell attachment site of various ECM molecules - the RGD motif [63]. Both integrins, $\alpha v\beta 3$ and $\alpha v\beta 5$, are upregulated in endothelial and endothelium cells undergoing angiogenesis - which makes Cilengitide an inhibitor for angiogenesis [107]. Cilengitide has anti tumor activity in recurrent glioblastomas, where it inhibits angiogensesis, tumor invasion and proliferation. These positive anti-angiogenesis can be further increased by a combination with classical anti-cancer drugs. Still, the addition of Cilengitide to temozolomide chemotherapy did not improve therapy outcomes (phase III trial) so that Cilengitide will not be further developed as an anti-cancer drug at Merck KGaA, Darmstadt [108].

Integrin inhibitor AIIB2 targets clustering and induces radiosensitivity

While Cilengitide is a classical small-molecule antagonist, AIIB2 is a monoclonal antibody against integrin $\beta 1$. By binding integrin $\beta 1$ it inhibits the integrins ability to attach the cell with the ECM. This antibody is well known to enhance the radiosensitivity towards IR of 3D cultured cells and mice xenografts [18, 109, 110]. So far, mainly the effects of AIIB2 induced integrin inhibition on diffusion based signaling involving Akt [109] or NF-κB [106] were analyzed.

With its ability to induce radiosensitivity in 3D cultured cells it is righteous to ask if this is connected to the potential ability of this inhibitor to destabilize integrin cluster and therefore to shift mechanobalance.

And indeed, 3D cultured cells treated with the AIIB2 integrin $\beta 1$ inhibitor exhibit an impaired cluster status by still remaining a mechanical link between integrins and the nucleus. Only a combined treatment of IR and AIIB2 leads to an interruption of the mechanobiological balance with clear effects at both ends of the mechanobiological system: On one end, integrins decluster as the tension feedback is lacking, and on the other end, lamin redistribution, as a tension signal, is lost (see Figure 2.6 F and G). This radiosensitive mechanobiological system is not at all comparable with the radiosensitiviy of 2D cultured cells. The pre-tension of the mechanosensing machinery of 2D cultured cells is on a high level that does not allow for an adaptive response upon any treatment including AIIB2 or IR treatment. The 2D culture condition itself can be viewed as a stress factor, so that it comes to no surprise, that cell cultured under 2D and 3D conditions show a different response to any additional treatment (see Figure 2.6 M and N). It became evident, that the 2D cell culture system is highly artificial and does not provide the means to investigate mechanobiological aspects.

With this it is possible to draw a connection between radiosensitivity and mechanobiological cues. The target is hereby the clustering of integrins itself. However, microscopy capable to monitor the nanoscale distribution in cells cultured in meaningful 3D environments would need to become an integral part of the preclinical screening process.

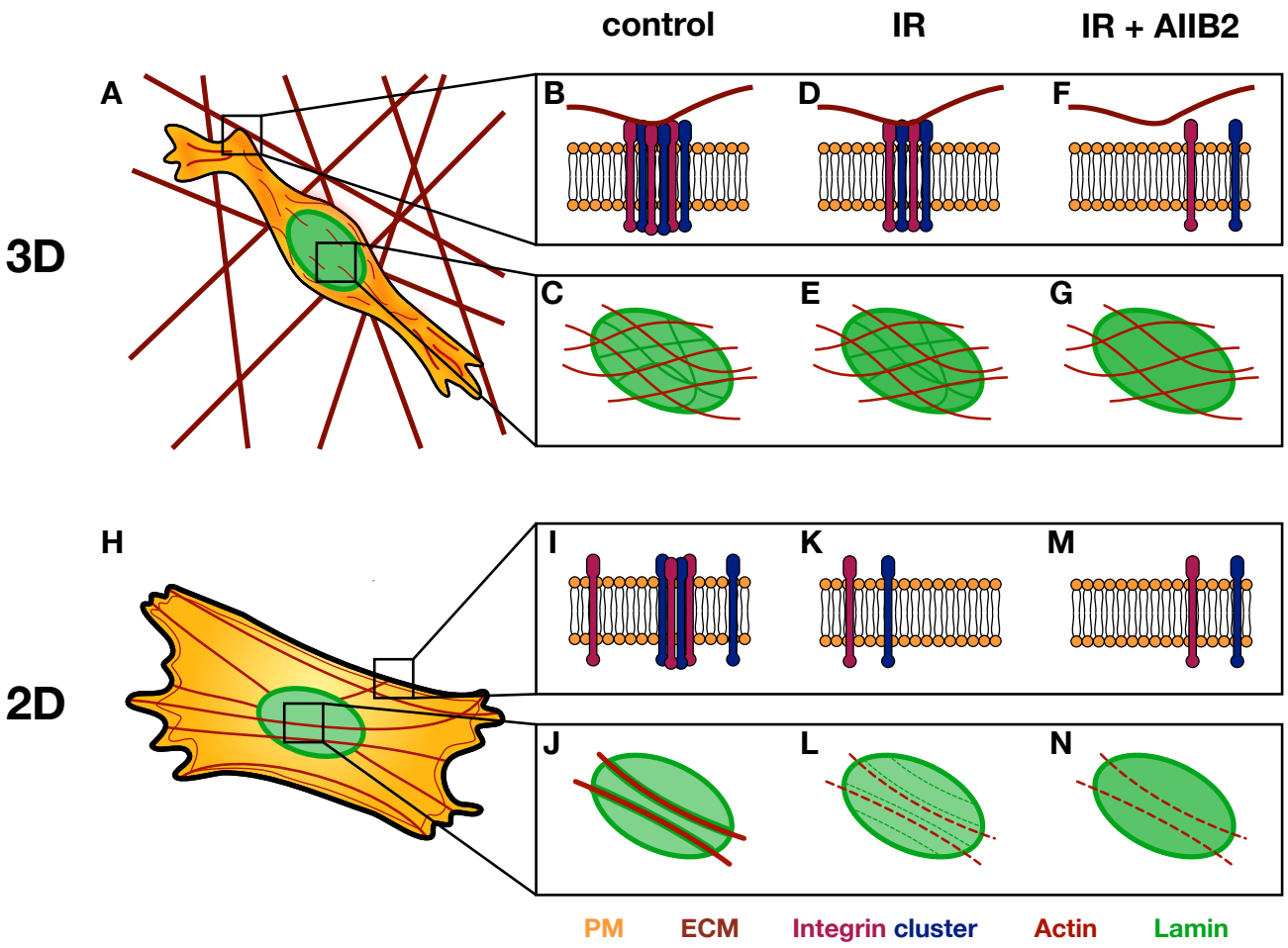

Figure 2.6: Integrin clustering and lamin organization as (i) a mechano sensor and a marker for radioresistance (ii) as well as a target for radiosensitization. (A) 3D cultured cells exhibit (B) stable and firm integrin clusters and (C) only partly colocalizing meshworks of lamin and non dominantly f-actin, which surround the nucleus. (D) Upon high doses of IR integrin clustering is only slightly affect, leading to a shift in the mechano-homeostasis resulting in (E) a higher intranuclear signal of Lamin. The apical actin - lamin connection and therefore the transmission of mechanical cues is not affected. (F) Only a combined treatment with high doses of ionizing radiation and integrin $\beta 1$ inhibitor AIIB2 lead to (F) a integrin cluster break-down and subsequent loss of nuclear mechanosensing (G) as also the actin - lamin connection is lost. (H) 2D cells exhibit (I) a loose and dynamic organized integrin clustering and (J) a strong, fibrous colocalization of actin and lamin resulting in an impaired mechanosensing. (K) Upon low and high doses of IR integrin clusters fall apart and (K) the overstressed interaction between actin and lamin is lost. With the loss of mechanosensing, the nuclear lamina can not be reorganized. (M) Combined treatment of IR and AIIB2 can not further stress the integrin clustering (N) but also leads to actin fragmentation and to the loss of apical lamin.

2.5 Are the PM located effects on integrin clustering lipid raft mediated?

The ability of integrin clustering to be a target for induced radio sensitivity proves that beside DNA damage and its subsequent repair, plasma membrane (PM) located events are a powerful tool in radiotherapy. It is well accepted that IR has profound affects on the PM, mainly lipid peroxidation, generation of ceramides and its organization in ceramide lipid rafts are well studied. Thereby, the generation of reactive oxygens (ROS) damages and modifies lipids directly and activates sphingomyelinaes (SMase) that in turn transform sphingomyeline into ceramide. Ceramide rafts are known to spatially reorganize receptors (e.g. cytokine receptors, death receptors and toll-like receptors) and intracellular signaling molecules contributing to apoptosis [111, 112, 113]. With ceramide being pro-apoptotic, inhibitors of SMase may be a useful tool in radiation therapy, as radiation induced-apoptosis of non-tumor tissue may be attenuated [114, 115, 116].

Nevertheless, PM located signaling also includes lipid organization and dynamics. As the impaired integrin signaling of 2D cultured cells already suggests, also the membrane dynamics itself and the organization of lipids in its rafts differ significantly if 2D and 3D cultured cells are compared. While 3D cultured cells exhibit a higher membrane mobility, 2D cell possess higher clustered lipid rafts (cholesterol microdomains) with a smaller radius if compared to 3D cultured cells.

2.5.1 Effects of IR in the PM located integrin β1 clustering are lipid raft independent

With the use of ionizing radiation as a strong extrinsic manipulator of integrin clustering it is possible to interfere with the coclustering of cholesterol containing lipid rafts and $\beta 1$ integrins. Integrins decluster in response to high doses of X-rays [41], while cholesterol rafts are surprisingly stable - even after a sudden and complete disappearance of proteins they colocalize with. With this it became clear, that the membrane located effects of IR on $\beta 1$ integrin clustering are lipid raft independent.

Integrin clusters colocoalize with cholesterol rafts, implying that the integrin activation and its ability to bind ECM molecules is raft dependent. This generalized view, that only because a protein is part of a lipid raft its activity depends on this localization, is challenged when the reaction of both, integrin and lipid clustering, is analyzed upon irradiation with high doses of IR. If lipid rafts are responsible for the protein cluster stabilization, it was expected that IR breaks cholesterol raft organization in concert with integrin cluster break down. Still, integrins disintegrate in a lipid raft independent manner. Even high doses of IR could not break the cholesterol raft organization. This effect is prominent in 2D cultured cells, here a high dose of IR leads to a complete integrin cluster break down and integrin - lipid raft separation, whereas cholesterol rafts stay clustered (see Figure 2.7 C and D). In 3D cultured cells, high doses of IR lead to a slight decrease in integrin clustering, but still, some integrin cluster remain intact. These integrin clusters still colocalize with cholesterol microdomains (see Figure 2.7 A and B). This small experiment shows, that it is possible to separate proteins from their lipid raft localization by an extracellular stressor and that cholesterol rafts are a far more stable system than expected. But this experiment also indicates that neither, the integrin nor the cholesterol clusters are responsible for the organization of the other, questioning the generalized view that lipid rafts are organizing platforms.

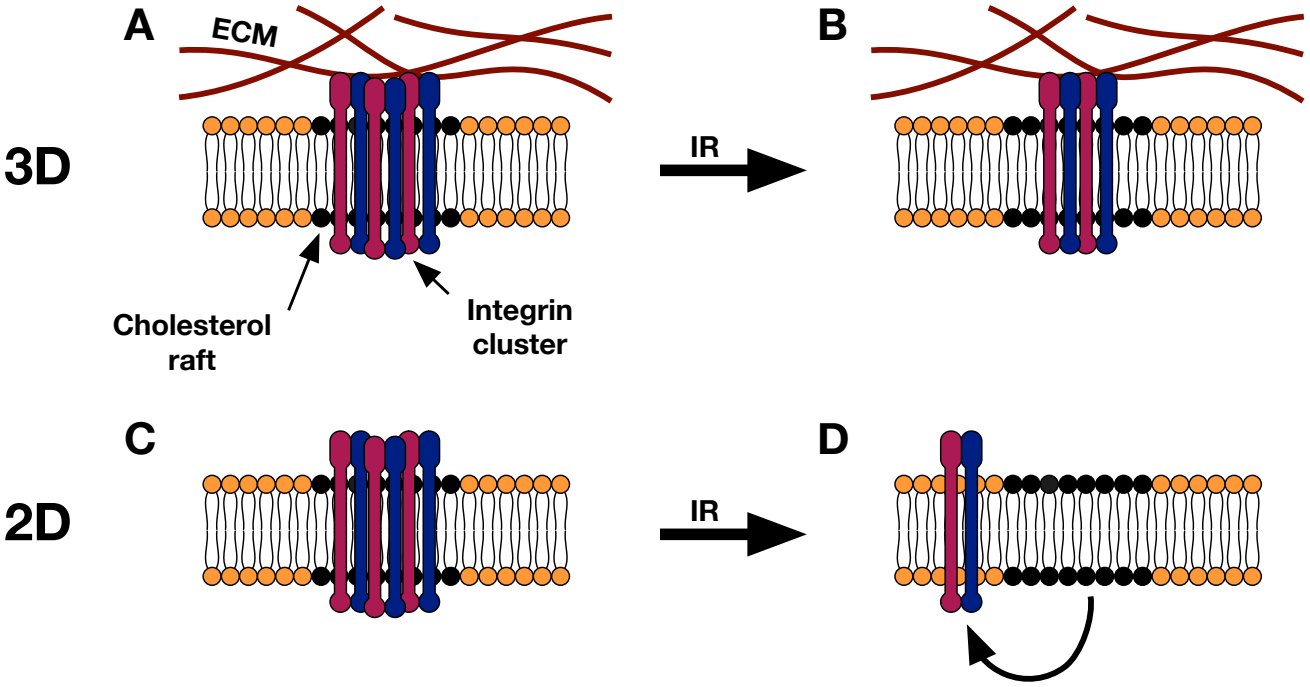

Figure 2.7: Effects of IR in the PM located integrin β1 clustering are lipid raft independent. Integrin clusters colocalize in cholesterol microdomains. (A) Stable and firm organized integrin clusters of 3D cultured cells interact with binding motifs (e.g. RGD) of the ECM. (B) Upon irradiation integrin clustering is slightly reduced but integrin clusters remain in cholesterol rafts. Binding to the ECM is still possible. (C) Mobile and dynamic integrin cluster of 2D cultured cells also localize in cholesterol rafts. (D) Upon irradiation integrins decluster and separate from their cholesterol raft localization. Cholesterol rafts are not affected by IR.

2.6 Aim of this thesis

In cancer treatment, ionizing radiation (IR) and anti-cancer drugs are used to cause DNA damage or to inhibit signaling pathways that lead to cell death. One of the major problems in cancer therapy is the resistance of cancer cells against chemotherapeutics and radiation, limiting the effectiveness of current cancer therapies. One important group of proteins contributing to drug- and radioresistance, are the extracellular matrix receptors and key mediators for cell adhesion - integrins [22, 23].

The cellular interaction with the extracellular matrix (ECM) modulates many key processes such as proliferation, migration, differentiation and survival [11, 12, 13]. In addition, cells cultured under 3D conditions in presence of an ECM display a marked radioresistance towards ionizing radiation (IR) in comparison to conventionally 2D cultured cells. This process, also known as cell-adhesion-mediated-radio-resistance (CAM-RR) and is linked (i) to ECM-binding integrins containing the $\beta 1$ subunit and (ii) to the chromatin distribution that differs between cells cultured on stiff surfaces versus cell grown on soft planar supports or under 3D culture conditions [15, 14, 16]. Integrins not only facilitate the mechanical anchoring of cells to the ECM but also originate the important ability of cells to sense the mechanical properties of their surrounding. Therefore, integrins bring the cell culture condition and chromatin organization into a direct molecular connection [96]. On the basis of this knowledge, the aim of this thesis was to (i) capture the plasma membrane located effects of IR on $\beta 1$ integrins, (ii) induce radiosensitivity by integrin $\beta 1$ inhibition (iii) and to follow the mechanical link with its origin in a proper integrin clustering up to the nuclear lamina. For this a combined methodical approach of single molecule microscopy and 3D cell culture was chosen.

The approach of this aim and its outcome is summarized in the following layout and in Figure 2.8:

Chapter I: „Direct Evidence for Cell Adhesion-Mediated Radioresistance (CAM-RR) on the Level of Individual Integrin $\beta 1$ Clusters“

I Integrin mobility, clustering and localization differ if 2D and 3D cultured cells are compared

II Integrin $\beta 1$ signaling of 2D cultured cells is impaired

III Radioresistance relies on intact integrin $\beta 1$ clustering of 3D cultured cells

Chapter II: „Radiosensitization by α-integrin $\beta 1$ (AIIB2) is based on integrin cluster breakdown and loss of nuclear mechanosensing“

I It is possible to induce radiosensitivity in 3D cultured cells by targeting integrin $\beta 1$ clusters

II CAM-RR is based on intact integrin clustering and subsequent balanced mechanosensing system

III 2D cell culture system is highly artificial and does not provide the means to investigate mechanobiological aspects

Chapter III: „Lipid-rafts remain stable even after ionizing radiation induced disintegration of $\beta 1$ integrin containing focal adhesions“

I $\beta 1$ integrins can be separated from their lipid raft localization by IR as an extracellular stressor

II Cholesterol rafts are not affected by high doses of IR

III Integrin $\beta 1$ clustering could be independent of its localization in cholesterol lipid-rafts

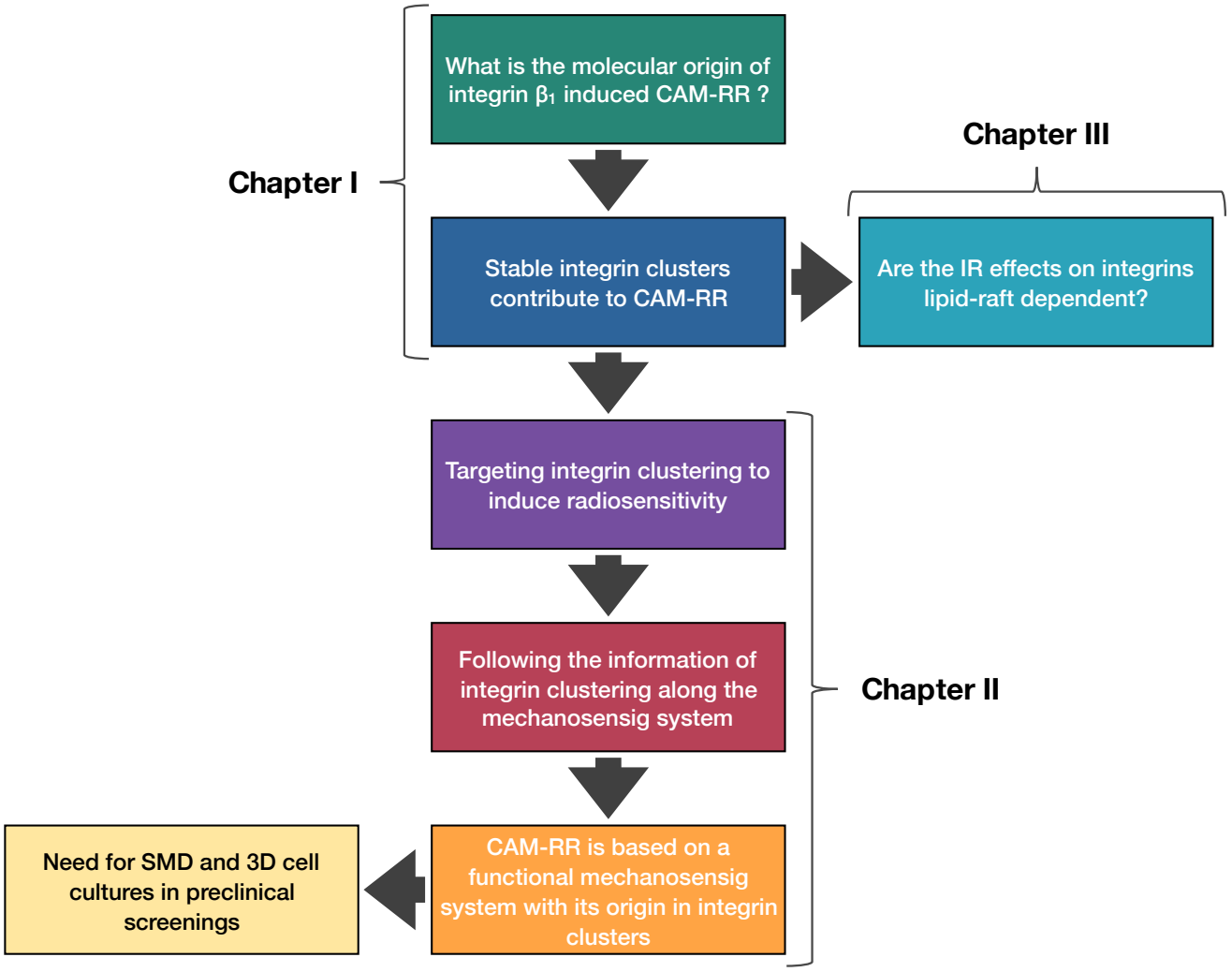

Figure 2.8: Aim of this thesis. The aim of this thesis was to clarify the membrane located events behind CAM-RR (cell adhesion mediated radioresistance) with its origin in integrins containing the $\beta 1$ subunit. In chapter I it was discovered that the stable integrin clustering of 3D cultured cells contributes to their radioresistance. In chapter II, integrin clustering was successfully targeted by AIIB2 induced integrin $\beta 1$ inhibition and with a combined treatment of IR and AIIB2 radiosensitivity was induced in 3D cultured cells. By following the mechanosensing system (integrin - actin - nesprin - lamin) it was discovered that radioresistance does not only relay on an intact integrin clustering but also on a balanced mechanosensing system. This proves that it is possible to target the clustering of proteins in the PM, but only if SMD and 3D cell cultured are used in preclinical screenings. Chapter III answers the question, whether the PM located effects of IR on integrin clustering are lipid-raft dependent.

3 Publications

Chapter I is based on the following publication:

Babel, Laura, Miriam Grunewald, Robert Lehn, Markus Langhans, and Tobias Meckel. 2017. „Direct Evidence for Cell Adhesion-Mediated Radioresistance (CAM-RR) on the Level of Individual Integrin $\beta 1$ Clusters“ Scientific Reports 7 (1): 3393.

Publications not included in this thesis:

Langhans, Markus, Wadim Weber, **Laura Babel**, Miriam Grunewald, and Tobias Meckel. 2017. „The Right Motifs for Plant Cell Adhesion: What Makes an Adhesive Site?“ Protoplasma 254 (1): 95 to 108.

Janko, Marek, Michael Jocher, Alexander Boehm, **Laura Babel**, Steven Bump, Markus Biesalski, Tobias Meckel, and Robert W. Stark. 2015. „Cross-Linking Cellulosic Fibers with Photoreactive Polymers: Visualization with Confocal Raman and Fluorescence Microscopy“ Biomacromolecules 16 (7): 2179 to 87.

Bump, Steven, Alexander Boehm, **Laura Babel**, Sonja Wendenburg, Franz Carstens, Samuel Schabel, Markus Biesalski, and Tobias Meckel. 2014. „Spatial, Spectral, Radiometric, and Temporal Analysis of Polymer-Modified Paper Substrates Using Fluorescence Microscopy“ Cellulose 22 (1). Springer Netherlands: 73 to 88.

Chapter I

Direct evidence for cell adhesion-mediated radioresistance (CAM-RR) on the level of individual integrin β1 clusters

SCIENTIFIC REPORTS

OPEN

Direct evidence for cell adhesion-mediated radioresistance (CAM-RR) on the level of individual integrin β1 clusters

Received: 22 January 2017
Accepted: 13 April 2017
Published online: 13 June 2017

Laura Babel[1,2], Miriam Grunewald[1,2], Robert Lehn[1], Markus Langhans[1] & Tobias Meckel[1,2]

The cellular interaction with the extracellular matrix (ECM) modulates many key processes such as proliferation, migration, differentiation and survival. In addition, cells cultured under 3D conditions in presence of an ECM display a marked radioresistance towards ionizing radiation (IR) in comparison to conventionally 2D cultured cells. This process, also known as "cell-adhesion-mediated-radio-resistance" (CAM-RR), has been linked to the chromatin structure that differs between cells cultured on stiff surfaces versus cell grown on soft planar supports or in 3D environments. As integrins are the key mediators of cell adhesion and mechanosensing, they originate the molecular signalling towards chromatin remodelling in response to a cell's microenvironment. We aimed to investigate this molecular origin that leads to CAM-RR by investigating the distribution of integrins at the single molecule level and show that cells cultured in 2D keep a lower fraction of integrin β1 in clusters and maintain a less defined cluster status than 3D cultured cells. Upon X-irradiation this nanoscale distribution of integrin β1 is disturbed at much lower dosages in 2D versus 3D cultured cells. Radioresistance is thus linked to the ability to maintain a well defined organization of integrins in clusters, making integrin distribution a potential drug target for radiosensitization.

It is now well accepted that the microenvironment of cells has a profound impact on their physiology, which traditional two dimensional cell cultures are unable to provide[1–7]. In particular, cells cultured on a flat and rigid support lack three important aspects, which are key parameters for the physiological communication of cells with their environment[8,9]. First, they lack dimensionality in that they do not allow cells to adhere to extracellular supports or adjacent cells with their entire surface, second, they provide a highly polarized rather than homogeneous mechanical environment and third, they lack the ability to maintain local concentration heterogeneities, e.g. gradients of soluble compounds. All mentioned parameters, namely (i) the distribution and density of adhesion sites on the extracellular matrix (ECM) or receptors on neighbouring cells, (ii) their mechanical resilience and (iii) local concentrations of solutes are processed by many signalling processes at the plasma membrane (PM), thereby modulating key processes such as proliferation[10], migration, differentiation and survival[11,12].

Integrins, as the key mediators of cell adhesion, not only facilitate the mechanical anchoring of cells to extracellular supports but also originate the important ability of cells to sense the mechanical properties of their surrounding. Intriguingly, this mechanical information is directly transmitted via a continuous molecular connections between focal adhesions and chromatin rather than a signalling cascade of soluble messengers[13,14]. In more detail, changes in the microenvironment are detected and transferred via actin and nuclear envelope proteins (nesprin-1 and 2, SUN 1 and 2) into the nucleus, leading to a reorganization of the nuclear lamina[15,16], the activation of transcription factors[17] and to a change in the mechanical properties of the nucleus itself[18]. With Lamin as an indicator of stiffness perception and signalling to the nucleus it was shown that a cellular environment with a low stiffness leads to a soft nucleus, whereas the stiffer supports yields a stiff nucleus[18,19]. Hence, integrins bring the culture conditions and chromatin organization into a direct molecular connection, with the result that the mechanical properties of the ECM are mirrored by the nucleus with the result of a mechanically balanced ECM-nucleus connection[15].

[1]Membrane Dynamics, Department of Biology, Technische Universität Darmstadt, Darmstadt, Germany. [2]GRK 1657, Molecular and cellular responses to ionizing radiation, Technische Universität Darmstadt, Darmstadt, Germany. Correspondence and requests for materials should be addressed to T.M. (email: tobias.meckel@me.com)

With this connection in mind, it becomes apparent that any treatment of cells with the nucleus as the prime target needs to take this delicate balance into account. One such example is found in the treatment of cells, predominantly tumors, with ionizing radiation. While the prime reason of using radiation is to cause levels of DNA damage that ultimately lead to cell death, it was found that cells embedded in an ECM show a marked radioresistance towards ionizing radiation (IR) in comparison to conventionally 2D cultured cells[20]. This effect, also known as "cell-adhesion-mediated-radio-resistance" (CAM-RR), tellingly shows that the true impact of radiation on cell survival has to be understood as a combination of the radiation's damaging effect on DNA as well as its disturbing effect on the balanced ECM-nucleous connection. Along those lines, CAM-RR was linked (i) to ECM-binding integrins containing the β1 subunit and (ii) to the chromatin structure that differs between cells cultured on stiff surfaces versus cells grown on soft planar supports or under 3D culture conditions[21]. Namely, the presence of a higher fraction of heterochromatin in 3D cultured cells was shown to correspond to a decreased amount of residual DNA double strand breaks (DSB) after X-ray irradiation[22]. As (i) a higher amount of heterochromatin protects the DNA against DSB induction and (ii) a forced enrichment of euchromatin leads to hypersensitive DNA-damaging not only residual but also prompt DSBs may be reduced in 3D cells[21,23,24]. While integrins as the key mediators of a cell's interaction with the ECM are clearly involved in this culture-condition dependent effect, mainly the players acting downstream of integrin signalling have been thoroughly investigated (ILK, FAK, JNK1, Akt1, PINCH1, HDAC)[25–28]. The membrane located effects of ionizing radiation on β1 integrins, involving the formation, dynamics and maintenance of integrin clusters to form focal adhesions (FAs) at the plasma membrane (PM), have so far not been in the focus of a detailed study, neglecting the possibility of the integrin distribution itself as a potential drug target for radiosensitization.

We therefore aimed to catch the very origin of the signalling that eventually leads to the changes that make cells radio-resistant in 3D environments, by following the plasma membrane located nanoscale organization of β1 integrins in response to both X-irradiation and culture conditions. For this, we optimized a collagen I based 3D cell culture system to be compatible with single molecule microscopy[29] and used nuclear lamin organization to select for cells with a balanced ECM-nucleus connection.

To investigate the effects of IR on the integrin signalling we focused on the integrin clustering as well as on quantifiable parameters such as cluster density or number of integrins per cluster of 2D and 3D cultured cells. Our results show that (i) physiologically conditions lead to a different organization of β1 integrins and important downstream partner per se and (ii) X-ray irradiation leads to a nanoscale distribution of integrin β1 of 2D cultured cells at much lower dosages, as compared to cells cultured in our 3D cell culture system. We also show that integrins containing the β3 or αv subunit are affected differently by IR in dependence of the cell culture conditions. These results serve as an important entry point to characterize the membrane located events behind CAM-RR and may lead to the use of the integrin distribution as a potential drug target for radiosensitization.

Results

A 3D cell culture system tailored for single molecule microscopy and X-irradiation. To investigate the effects of IR on the nanoscale organization of integrins with single molecule precision, we first had to optimize and characterize our approach to culture and image cells in a 3D collagen I based hydrogel, in order to meet the requirements set by the cells, the irradiation protocol, and the microscopy method. To achieve meaningful single molecule recordings and X-irradiation treatments, only cells within a distance of 20–50 μm to the coverslip were chosen for measurements. Within this range, reasonable contrast and image quality was achieved to detect single molecule signals with a localization precision of around 30 nm[29]. Also, at this distance, the glass doubling effect for radiation experiments[30] still applies, allowing us to apply the same irradiation doses to cells cultured under 2D and 3D conditions for our comparative analysis (Fig. 1A).

In addition, cells within this range were completely surrounded by the collagen matrix[31]. More important from a mechanobiological point of view and the main rationale behind culturing cells in 3D hydrogels is, however, to provide cells an environment of low and isometric stiffness. As we were not able to measure the elastic modulus within a collagen hydrogel at the required position, we made use of the cells mechanosensing capabilities. For that we measured the nuclear distribution of lamin A/C in 2D and 3D cultured mouse embryonal fibroblast (MEF) cells, as this protein is known to change with the stiffness of the extracellular environment[18]. As expected, the distribution of lamin A/C to the nuclear envelope versus an intranuclear location was found to be much stronger in 2D than 3D cultured cells (Fig. 1B and C). Line profiles (see Supplementary Figure 1) reveal a higher level of non-nuclear envelope lamin A/C in cell cultured in 2D (~37%) versus 3D (~58%).

Hence, with lamin A/C as a read-out for nuclear stiffness perception, we can show that cells grown under our 3D conditions perceive a stiffness environment, that is markedly different from the planar rigid environment of a 2D culture, despite the low proximity to the coverslip of only 20–50 μm.

Furthermore, the drastically different morphology of MEF cells, as used throughout this study, was greatly affected by the 3D culture conditions (Fig. 1), both on the level of individual cells and multicellular arrangements. While 2D cultured MEF cells show the familiar flat morphology, MEF cells cultured in our 3D collagen system spread in all spatial directions (Fig. 1D–G). After a week-long culture a well ordered multicellular organization developed (Fig. 1F and G). Next to the results for intranuclear lamin A/C distribution, these morphological differences are an additional indication that our 3D culture system provides a microenvironment properties that are markedly different to the culture of MEF cells on planar rigid surfaces.

The culture condition has a strong impact on the nanoscale distribution of integrins. While individual membrane proteins of cells cultured on coverslips can be imaged using TIRF microscopy[32], 3D cultured cells are not amenable to this method[29]. To record and detect the location of single proteins in cells cultured in 3D collagen I hydrogels, we combined HILO illumination[33] with STORM measurements[34]. With this approach, an axially confined illumination of cells distant to the coverslip is achieved by focusing the excitation laser

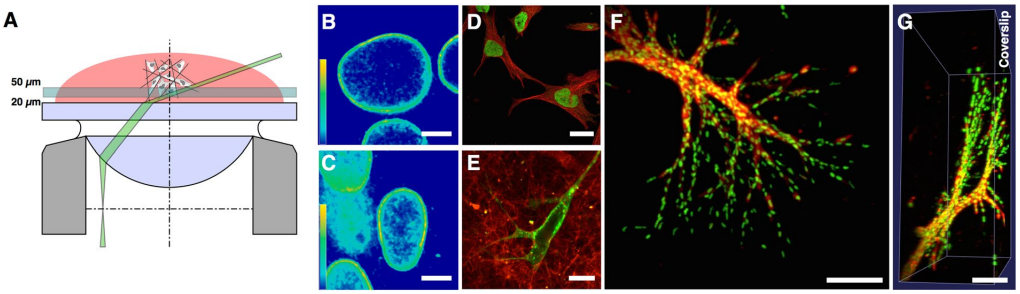

Figure 1. 3D cell culture conditions have a strong impact on intranuclear lamin distribution and overall morphology of MEF cells. (**A**) 3D cell culture system for single molecule microscopy and irradiation experiments: Cells embedded in the collagen-hydrogel are placed on a coverslip. A thin, highly inclined laminar optical sheet (HILO) is used to illuminate a subfraction of fluorescently labeled primary integrin antibodies of cells cultured in 3D in a distance of of 20–50 µm to the coverslip. By combining STORM and HILO a sufficient imaging contrast is obtained to detect single molecule signals in 3D cultured cells. (**B**) Heat map of a Lamin A/C immunostaining of 2D versus (**C**) 3D cultured cells. Scale bar is 5 µm, respectively. (**D**) A β-Tubulin (red) and H2A (green) immunostaining visualize the cytoskeleton and the nucleus of 2D cultured MEF cells. Scale bar is 25 µm. (**E**) CMO (green) staining of the PM of a 3D cultured MEF cell cultured in a collagen hydrogel (red). Scale bar is 10 µm. (**F**) MEF cells after a week-long 3D culture (maximum projection of a 3D confocal stack). (**G**) 3D volume rendering of (**F**).

off-center into the the back focal plane of a high NA objective. The beam refracts at the coverslip-water-interface and propagates into the 3D cell culture at a shallow angle to the coverslip, while also crossing the focal plane of the objective. The result is an axially confined illumination zone and axially and laterally confined detection zone with - in our case - a lateral diameter of typically 30 µm and a thickness (i.e. axial extension) of 1.2 µm. With this illumination scheme only a subfraction of STORM capable Alexa dyes (Alexa-488) linked to the respective antibody were activated, excited and detected allowing for a contrast sufficient to robustly detect individual antibodies and localize their signal with a precision of typically 30 nm. Single proteins in 3D cultured cells could thus be localized with a similar precision as in 2D cultured cells in our comparative analysis.

With this technique we observed clear differences in the nanoscale distribution and mobility of β1 integrins in living cells (Fig. 2A–D). A live cell antibody staining revealed (by simple visual inspection of live recordings; data not shown) for 2D as well as 3D cultured cells that integrins are predominantly localized in non-mobile clusters (green arrowheads), a finding also reported by Rossier *et al.*[35] for 2D cells. In addition, a significant fraction of β1 integrins was found to be unclustered and highly mobile in 2D but not in 3D cultured cells. This mobile fraction is best visualized in a scatterplot of all localization for the 2D culture (Fig. 2B) and 3D culture case (Fig. 2D), in which the single and separated pixels (green arrows) represent the mobile integrins. While in 2D around 25% of all detected integrins fall in this mobile category, in 3D, only very few integrins are not part of a cluster (10%). Single molecule tracking of live cell antibody stained β1 integrins confirms this visual observation. Whereas the mean square displacement plot of β1 integrin mobility measured in 3D cultured cells shows a strong confinement (fast saturation of the curve) and low mobility (low slope, Fig. 2E, red), β1 integrins in 2D culture cells are, on average, much faster and far less confined in their mobility (Fig. 2E, blue). Fitting both plots to a model for confined diffusion reveals that β1 integrins in 2D and 3D cultured cells are confined in their mobility to an area of $1.2 \pm 0{,}045$ and $0.33 \pm 0{,}005\,\mu m^2$ and display a mean mobility with diffusion coefficients of $0{,}02 \pm 0{,}0005$ and $0{,}002 \pm 0{,}0001\,\mu m^2/s$, respectively.

Our live cell single molecule measurements show that cells cultured in 3D achieve a much more defined organization of integrins in clusters. In addition, they also reveal a much lower separation of integrin subtypes into separate clusters (Figs 2F, G and S2). By staining different ECM-binding integrin combinations, namely αvβ1, αvβ3, and β1β3, we assessed the colocalization of integrins on cells fixed with a protocol optimized for membranes to avoid antibody-induced clustering of incompletely immobilized membrane proteins[36]. Not only the colocalization of the integrin subunits αv with β1 and αv with β3 was increased if cells are surrounded by the ECM (S2A,B), but even the integrins β1 and β3 were found to co-cluster in the PM of 3D (Fig. 2F) but not 2D cultured cells (Fig. 2G).

Taken together, 3D cultured cells showed a far lower distribution of integrins into separate clusters, but rather combine integrin heterodimers with similar function - here to bind the ECM - within the same clusters, i.e. focal adhesions. Virtually none of the integrins in 3D cultured cells were not organized in clusters. Thus, integrin clusters of 3D cultured cells were clearly found to be more defined and to contain more integrin subtypes.

IR differently affects the nanoscale distribution and organization of β1 integrins in dependence of the culture conditions. To investigate the membrane-located events in response to IR, 2D and 3D cultured cells were X-irradiated with different doses, fixed at specific time points after the irradiation, and stained for endogenous β1 integrins. Due to the rapid and complete immobilization of the fixation protocol[36], the following results represent snapshots of the dynamic and continuous process of protein cluster formation and degradation and thus show the current balance between these competing processes for the respective time point of fixation.

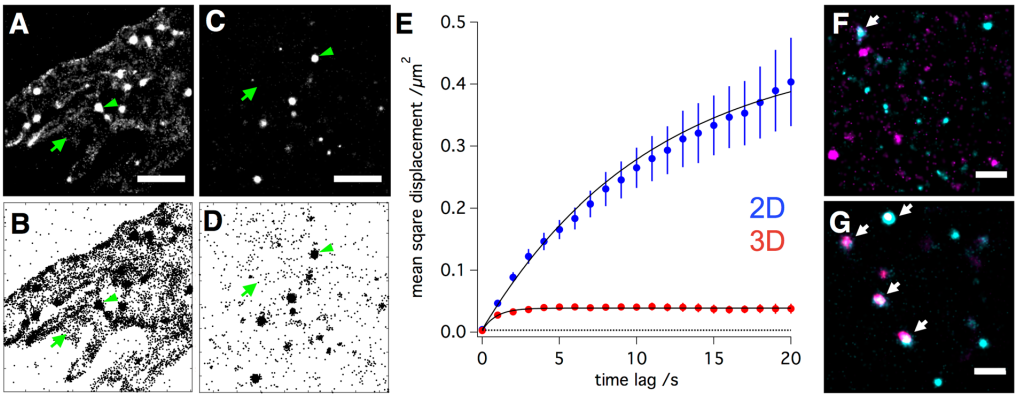

Figure 2. 2D versus 3D cell culture conditions have a strong impact on the nanoscale distribution of integrins. (**A**) Normalised gaussian and (**B**) Scatter plot visualization of single molecule localization data obtained through a live-cell immunostaining of 2D cultured cells with a directly labeled integrin β1 antibody. Scale bar is 2 µm. (**C** and **D**) Corresponding data of a live-cell integrin β1 immunostaining of 3D cultured cells. A much higher fraction of integrins in 2D cultured cell is not part of a cluster as compared to 3D cultured cells (immobile integrin clusters = green arrowheads, individual mobile integrins = green arrows). Single molecule tracking of live cell antibody stained β1 integrins confirms this visual observation. Whereas the mean square displacement plot of β1 integrin mobility measured in 3D cultured cells shows a strong confinement (fast saturation of the curve) and low mobility (low slope, Fig. 2E, red), β1 integrins in 2D culture cells are, on average, much faster and far less confined in their mobility (Fig. 2E, blue). Fitting both plots to a model for confined diffusion reveals that β1 integrins in 2D and 3D cultured cells are confined in their mobility to an area of $1.2 \pm 0{,}045$ and $0.33 \pm 0{,}005\,\mu m^2$ with diffusion coefficients of $0{,}02 \pm 0{,}0005$ and $0{,}002 \pm 0{,}0001\,\mu m^2/s$, respectively. The dotted line represents the lower limit of the detectable square displacement (in our case $4\times (28\,nm)^2 = 0{,}003136\,\mu m^2$). (**F**) Colocalization of β1 (cyan) and β3 (magenta) integrins in 2D and (G) 3D cultured cells. Scale bar is 1 µm. Arrows indicate integrin-subunit colocalization (white) of β1 (cyan) and β3 (magenta) integrin subunits.

The effects of IR on the distribution and organization of β1 integrins can directly be recognized by a visual inspection of the single molecule localization results, where each dot represents an individual detection (Fig. 3A and I). Measurements on untreated 2D and 3D cultured cells reveal that β1 integrins are organized as clusters with a radius of ~200 nm and show a comparable degree of clustering under both 2D and 3D culture conditions (see S3). Upon IR, however, this picture changes in clear dependence on said culture conditions (Fig. 3C,F and K,N).

Following visual inspection, a cluster analysis using Ripley's K function helps to put the visual impression on quantitative grounds. In brief, the function computes the average number of signals that fall within defined radii of each detected signal. Plotting this number (L(r)−r)) versus the respective radii yields a distribution (H-plot) whose maximum represents the most prominent cluster formation in the dataset. The height of the first local maximum (H(r)max) gives a measure of the degree of clustering and its position the radius of the most frequent clusters[37–39] (For further informations see S4). In addition, 2D plots of the L(r)−r values are represented as heat-maps to visualize clustered regions. Taken together, clusters, i.e. regions with a higher density of signals, are visualized as yellow regions in the heat maps (Figs 3B,D,G,J,L,O and S5 and S6) and the degree of clustering shows as the peak height in Fig. 3E,H and M,P. A summary of all maximum values for the degree of clustering (H(r)max) and the corresponding values for the cluster radii is shown in Fig. 4 for all X-irradiation doses, time points after irradiation and culture conditions.

2D cultured cells were irradiated with 0.5, 2, 6 and 15 Gy. While an irradiation with 0.5 Gy does not affect integrin clusters we could show that a dose of 2 Gy is sufficient to break the clustering of integrins directly after radiation (2 min) and that an irradiation with 6 and 15 Gy leads to an identical decrease in clustering (****$p \leq 0.0001$ for 2, 6 and 15 Gy) (Figs 3D,G and S5). The kinetics of cluster regeneration was found to strongly depend on the initial dose, as clusters of cells irradiated with 2 Gy regenerate faster as clusters of cells irradiated with 6 or 15 Gy. Corresponding H-plots of Ripley's K function and summarized bar plots of the degree of clustering reveal that the clustering of integrins of 2D cultured cells irradiated with 2 Gy starts to regenerate 1 h after IR and nearly returns to full recovery 6 h after IR (Figs 3E and 4A). After an irradiation with 15 Gy clusters also start to regenerate 1 h after IR, but even 24 h after IR recovery remains incomplete (Figs 3H and 4A). As H max and the cluster radius r max correlate, the same effects were expected and detected. While an irradiation leads to a significant decrease (****$p \leq 0.0001$) of cluster radii, 2 Gy irradiated cells regenerated completely, whereas 6 and 15 Gy irradiated cells do not (Fig. 4C). An irradiation with 0.5 Gy did not show a significant effect on the cluster radius.

For cells cultured in 3D, the effects of ionizing radiation differ greatly. In contrast to 2D cultured cells, irradiation doses of 2 and 6 Gy had no discernible effect on the organization of β1 integrins in clusters. Only at a dosage level of 15 Gy slight, but significant changes in the clustering (*$p \leq 0.05$) and their radii became apparent

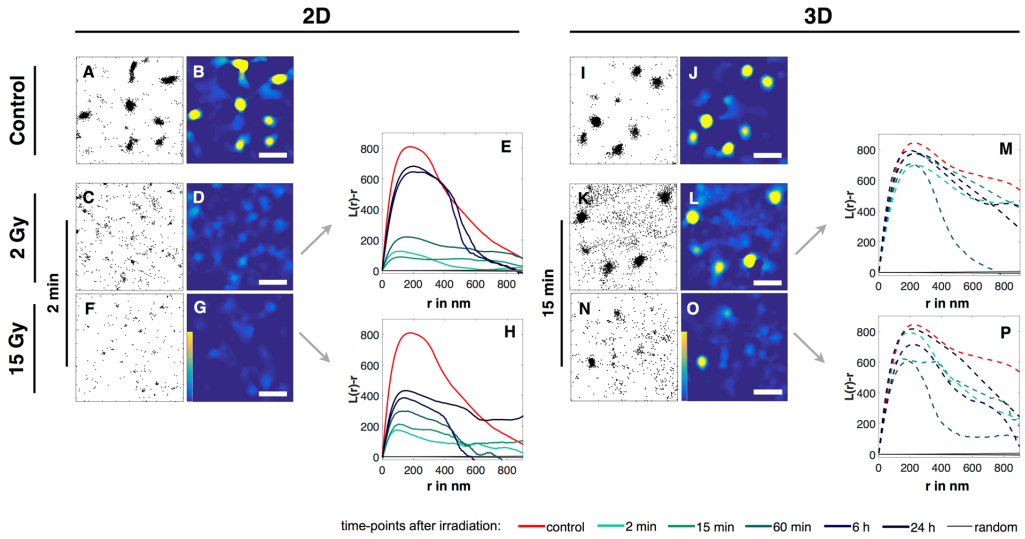

Figure 3. Effects of IR on the nanoscale distribution and organization of β1 integrins of 2D and 3D cultured MEF cells. Single molecule localization data of integrin β1 immunostainings obtained from fixed cells 2 min (2D) and 15 min (3D) after IR, as well as unirradiated controls are shown. Scatter plots show all detected β1 integrin localizations (**A**,**C**,**F** and **I**,**K**,**N**), while the corresponding heat maps (**B**,**D**,**G** and **J**,**L**,**O**) visualize unclustered (dark blue) and clustered (yellow) regions; scale bas are 1 µm. (**G**,**H** and **O**,**P**) Statistical analyses of all β1 integrin localizations found in all recorded cells of a given culture condition and irradiation dose are shown as H-Plots of Ripley's K function, in which the peak heights (L(r)−r) represent the degree of clustering and its position the most frequent cluster size (r (in nm)). Shown are the distributions of β1 integrins as found for non irradiated, 2D cultured cells (**A**,**B**) for 2D cultured cells irradiated with 2 Gy (**C**,**D**,**E**), and for 2D cultured cells irradiated with 15 Gy, fixed 2 min after IR (**F**,**G**,**H**), respectively. The corresponding H-Plots (**E** and **H**) show results for control (red) and cells irradiated with 2 Gy fixed 2 min (turquoise), 15 min (light green), 1 h (green), 6 h (blue) and 24 h (dark blue) after IR. In addition, the analysis of a random distribution of localizations containing the same number of signals as the control is shown in black. (**I**–**P**) Corresponding data of 3D cultured cells, but fixed 15 min after IR. Heat maps of all remaining conditions (IR dose and time points after IR) are summarized in Figs S5 and S6.

(Figs 3L,O and 4B,D and S7). Moreover, not only the dosages required to affect the clustering of β1 integrins are significantly higher in 3D cultured cells, also the kinetics of the process differ. In contrast to 2D cultured cells, an effect on β1 clustering started to become discernible only 15 min after an IR of 15 Gy with an almost complete recovery after 6 h and a full recovery after 24 h (Fig. 3P).

Taken together, these results clearly reveal a strong dependance of the nanoscale organization of β1 integrins on the culture conditions with 3D cultured cells being far more resistant to IR in maintaining the clustered organization of the adhesion receptor and showing a much faster recovery to do so after high IR doses.

The distinct and, at the same time, rapid effects of IR on membrane organization suggest that rather than DNA damage, more immediate effectors are responsible for the swift response. X-irradiation is always accompanied by the generation of reactive oxygen species (ROS) which leads to the damage of many structural and functional molecules[40]. Hence, to examine the role of ROS, 2D cultured cells were treated with 100 µM H_2O_2 and 3D cultured cells were treated with 500 mM H_2O_2 prior to fixation and integrin β1 staining. In response to the treatment, the degree of clustering as well as cluster radii significantly decreased 2 min for 2D and 15 min for 3D cells after the treatment (Fig. S8) reaching the same level as irradiated cells. Thus, as the kind, extent and timing of H_2O_2 are similar to those observed after IR, radiation produced ROS are likely the main, if not the sole cause for the disintegration of integrin clusters.

While we are aware that 500 mM is an unnaturally high concentration of H_2O_2, lower concentrations did not cause an discernible effect on the clustering of integrins in 3D cultured cells. Of note, however, the all 3D cultured cells did survive this treatment without major changes in morphology (data not shown).

Detailed cluster analysis reveals distinct differences in the effects of IR on the clustering and the cluster size of β1 integrins. To gain further insight into the membrane located events in response to ionizing radiation and in dependence of the culture conditions, we sought to extract more quantitative values from the cluster analysis of our single molecule localization data. For that, we defined a common threshold value that defines a cluster to have a higher signal density than the mean of all untreated cells.

Using this value, heat maps were converted into binary cluster maps, from which parameters like cluster area and number of clusters per µm² were directly obtained. Masking the original localization data with these

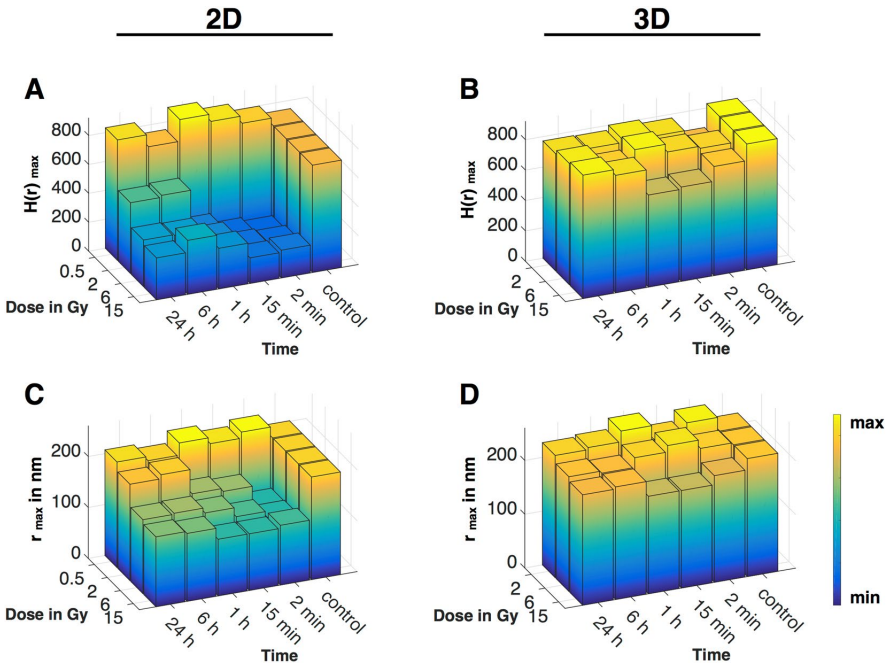

Figure 4. Effects of IR on the cluster density (H (r) max) and the cluster radius (r max in nm) of β1 integrins of 2D and 3D cultured MEF cells. Bar plots of medians of H (r) max and r max obtained from H-Plots of Ripley's K function analysed datasets (S6), visualised as a combination of bar plot and heat map (low value in blue, high value in yellow). For 2D cells N = 2 and n = 20, for 3D cells N = 2 and n = 10. Controls were pooled, therefore for 2D cells N = 8, n = 80 and for 3D cells N = 6, n = 30. 2D cells were irradiated with 0.5, 2, 6 and 15 Gy, 3D cells were irradiated with 2, 6 and 15 Gy. Cells were fixed and stained as controls, 2 min, 15 min, 1 h, 6 h and 24 h after IR. (**A**) Plot of H max of 2D cultured cells. (**B**) Plot of r max of 2D cultured cells. (**C**) Plot of H max of 3D cultured cells. (**D**) Plot of r max of 3D cultured cells. For a better visualisation significances are displayed in S6.

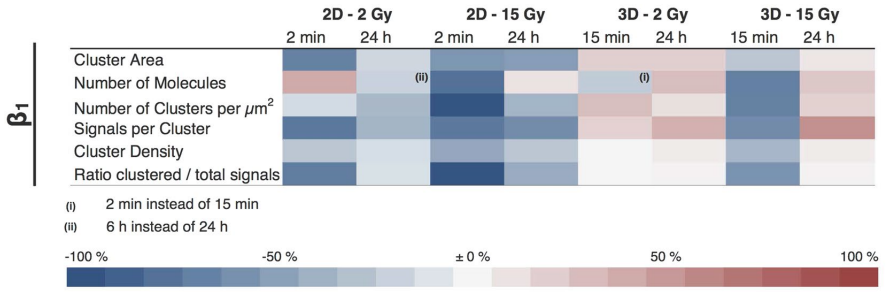

Figure 5. Percentual change of various parameter after IR of β1 integrins of 2D and 3D cultured MEF cells.

binary maps yielded additional values like signals per cluster, signals per cluster area (i.e. cluster density) as well as total number of signals and the ratio of clustered vs total number of molecules. To simplify inspection of the results, we summarized them in a heat map table (Fig. 5), where negative changes are assigned to a blue and positive to a red colour intensity. Changes were determined 2 min and 24 h for 2D, and 15 min and 24 h after irradiation for 3D cultured cells.

In detail, cells cultured in 2D irradiated with 2 Gy showed a significant decrease in the cluster area, the signals of molecules per cluster and in the ratio of clustered versus total number of molecules. The total number of molecules increased, while the number of clusters and the cluster density were only slightly affected. 24 h post-irradiation, almost all parameters returned to their pre-irradiation values. At 15 Gy, except for the total number of signals, a similar trend but more drastic changes were found. The most significant decreases are seen

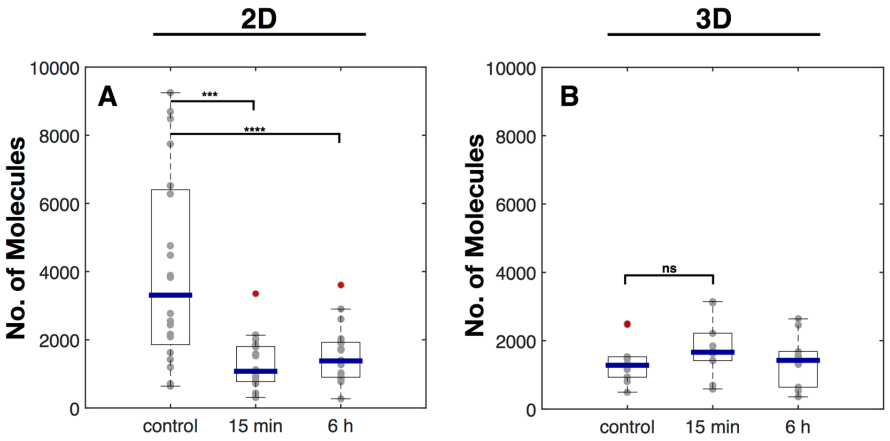

Figure 6. Effects of IR on pFAK of 2D and 3D cultured MEF cells. Box plots of the number of molecules per $4 \times 4\,\mu m$ ROI of cells cultured in 2D (**A**) and 3D (**B**). Cells were irradiated with 6 Gy and were fixed 15 min and 6 h after irradiation. For 2D cells N = 2 and n = 20, for 3D cells N = 2 and n = 10. Statistical analysis was performed with an ordinary one-way ANOVA. ***$p \leq 0.001$ and ****$p \leq 0.0001$. NS, not significantly different. If not further noted no significance was detected.

for the the number of clusters and the ratio of clustered vs unclustered molecules. While the number of molecules exceed the initial value, most parameters did recover but failed to completely return to the initial values. Only the cluster area did not show any recovery.

In contrast, cells cultured in 3D irradiated with 2 Gy showed an entirely different reaction towards IR. Except for the number of molecules, where only a slight decrease was detected, all other parameter showed none or slight, but never significant increases. 3D cells irradiated with 15 Gy showed a decrease in all parameters 15 min after IR, but all of them returned to or exceeded their initial value. Details for all values and test for significance are summarized in S9–11

β3 and αv integrins are differently affected by IR than β1 integrins. To investigate whether IR has an effect on integrins containing αv or β3 the same set of comparative experiments were performed and summarized in S12–18, as well as in Supplementary Table 1. Both integrin subunits showed, in comparison to β1, an entirely different reaction towards IR, which, on its own, strengthens the significance of our findings for the latter. While integrin heterodimers containing the β3 subunit barely show any changes to the various treatments and culture conditions, integrins containing a αv subunit revealed intermediate results. As αv dimerizes with both β subunits and the resulting integrin heterodimers have different cellular functions[41], namely cell adhesion (αvβ1) and migration (αvβ3)[42], this comes as no surprise. It does, however, nicely demonstrate the capabilities of single molecule over ensemble measurements. As the behaviour of all integrin subunits are recorded individually and all interactions with their partners are recognized individually, the behaviour of αv, which is here presented as an average, could as well be dissected into to its interaction with only β1 or β3. A more detailed presentation and discussion of the αv and β3 data can be found in the Supplementary.

FAK phosphorylation status markedly differs before and after irradiation in dependence of the culture conditions. Through our detailed analysis on integrins, we have clearly shown how their nanoscale distribution and organization changes in response to IR and culture conditions. However, for these differences to have an effect on cellular reactions, survival and ultimately CAM-RR, signalling from the differently organized and - upon IR - disintegrated integrin clusters need to change as well. We therefore assessed the IR and cell culture dependence of the integrin's immediate downstream partner, the focal adhesion kinase (FAK), and quantified the amount of its phosphorylated, i.e. activated from, pFAK (Fig. 6). While the number of pFAK in untreated cells was found to be about twice as high in 2D versus 3D cultured cells, the amount after an irradiation with 6 Gy was nearly identical for both culture conditions and did not recover within 6 h. pFAK levels of 3D cultured cells were not affected by an irradiation with 6 Gy.

These findings are in line with our observation that 2D cultured cells are unable to maintain integrins in well defined clusters and tend to separate different heterodimers into distinct clusters rather than combining them as the 3D cultured cells. Hence, a possible interpretation for the pFAK results is, that integrin signalling in 2D cultured cells is able to initiate the signalling cascade, but may be ineffective further downstream. In consequence, a higher pool of pFAK builds up, but is likely to be ineffective to properly propagate the signal in 2D cultured cells, whereas this is not the case in 3D cultured cells.

Discussion

Studies on the cellular effects of IR are generally focused on DNA damage, its subsequent repair, checkpoint activities and, ultimately, cell survival[43]. With this focus, it was identified that cell adhesion and, in particular,

cellular growth within the 3D environment of extracellular matrix proteins renders cells resistant to higher doses of ionizing radiation than cells grown on planar rigid supports. This resistance was reflected in a lower number of residual DNA double strand breaks (DSBs) and a higher survival rate and was termed cell adhesion mediated radioresistance (CAM-RR)[20,23]. While the origin of this culture-condition dependent resistance is clearly located at the integrins as the key proteins that sense and report the properties of the extracellular environment, so far mainly the players acting downstream of integrin signalling have been thoroughly investigated (ILK, FAK, JNK1, Akt1, PINCH1, HDAC)[25–28]. To fill this gap, we focused in our study on the immediate and rapid effects of IR on the nanoscale organization of the plasma membrane of cells grown under classical 2D as well as 3D culture conditions. To that end, we characterized the impact of IR on the formation, dynamics and maintenance of integrin clusters to form focal adhesions (FAs) at the plasma membrane (PM) using single molecule localization microscopy (SMLM). Our achievement to apply the virtues of SMLM to investigations on nanoscale changes of membrane protein distributions in cells grown under both conditions with comparable accuracy, allows us to draw detailed comparative conclusions regarding the influence of a cell's environment on the membrane located events behind CAM-RR.

We found that already the culture conditions in absence of any irradiation cause a marked difference in the ability of cells to maintain a well organized membrane. While 3D cultured cells keep nearly all integrins in a clustered organization, contain more β1 integrins per cluster and even keep different integrins within the same clusters (αvβ1, αvβ3 and β1β3), 2D cultured cells are unable to maintain this level of organization for these aspects. A significant portion of β1 integrins was found to freely diffuse in the membrane, rendering them unable to take part in signalling. In addition, integrin subtypes were found to segregate into separate clusters rather than colocalize within the same clusters as in the 3D case. Intriguingly, this less defined clustering was accompanied by a significantly higher number of phosphorylated FAK (pFAK) in 2D versus 3D cells, indicating an overall impaired signalling efficiency at planar culture conditions. Taken together, mechanisms to keep a well defined integrin cluster organization are acting efficiently in 3D but not 2D cultured cells.

This inability of cells to maintain a well defined cluster status for integrins and an effective integrin signalling already points to a lower tolerance for additional stressors. In fact, we found that even low doses of IR are sufficient in 2D to completely abolish the cells ability to maintain integrins clustered, while 3D cultured cells were not only able to maintain the clustered organization against much higher doses of X-irradiation but also showed a faster recovery for doses that actually did induce a mild effect (15 Gy).

In detail, already a 2 Gy dose caused the number of signals per cluster to decrease and the number of unclustered molecules to increase (i.e. the ratio of clustered to total signals to decrease). In other words, an irradiation with 2 Gy caused β1 integrins to leave the clusters but stay in the PM by lateral diffusion. An irradiation with 15 Gy, in turn, not only caused the signals per cluster but even the total number of signals to decrease. This implies that the higher dose, in addition to disintegrate clusters within the plane of the membrane, also induced endocytic retrieval of integrins and thus induced both lateral and axial membrane transport. In 3D culture cells, the same combination of axial and lateral membrane transport was taking place, however at much higher doses. An irradiation 15 Gy lead to a decrease in the clustering, the cluster radius and cluster area, as well as to an decrease in the total number of molecules. Hence, while the mechanism of the response to high doses of were the same for both 2D and 3D cultured cells, the kinetics and the severity differ significantly (Fig. 4).

Thus, as stated above, the membrane organization of β1 integrins in 2D is less defined and therefore more vulnerable to disturbance than in 3D cultured cells. Notably, however, as our results on β3 and αv integrins show, this behaviour is protein specific and does not apply to the nanoscale organization of the membrane in general. The impact of IR on integrin clustering are also directly reflected by the effects on integrin signalling. As 3D cells did not respond with any change in the number of pFAK, the high levels found in untreated 2D cells collapsed to a very low amount after X-irradiation, indicating a severe impairment of signalling and IR load. Hence, the ability to maintain integrin clusters against IR is a direct consequence of intact integrin signalling.

Using a treatment of cells with H_2O_2 we were able to recreate the effect of IR to break down β1 integrin clusters in 2D (100 µm H_2O_2) and 3D (500 mM H_2O_2) cultured cells, demonstrating that ROS produced by IR are potentially the prime reason behind the observed effects of X-irradiation. While an identical treatment with H_2O_2 on 3D cultured cells would have been desired we were not able to produce an effect on the integrin clustering with low concentrations of H_2O_2. This may be explained by a very fast scavenging of ROS within 1–2 min in 3D cultured cells as it was reported for the generation of ROS in cells by gas plasma treatment[44]. As this method produces ROS in an abiotic way as does IR, we assume that 3D cultured cells have a high capacity to scavenge ROS.

But regardless, whether 3D cultured cells are able to scavenge ROS more efficiently or whether their membranes tolerate higher ROS levels, both accomplishments would simply be a direct result of the fact that the integrin signalling system of these cells is intact and tolerant to some degree of disturbance. This is reflected by our observations of (i) stable integrin clusters and (ii) stable levels of pFAK in presence or absence of IR and (iii) a different distribution of lamin A/C, which demonstrates the continuous signalling connection between the PM and the nucleus.

Our detailed view on the membrane located events involving integrin β1 and its downstream partner pFAK, allows us to conclude that CAM-RR starts at maintaining integrin clusters, as we show that only 3D cells possess and maintain integrins in a firm and defined organization of clusters and a signalling which, via FAK, eventually propagates all the way to the nucleus and impacts the distribution of the nuclear scaffold protein lamin A/C, which is known to influences the chromatin organization and even the stiffness of the nucleus itself[18,19]. This connection from integrins to chromatin nicely links our results to the work of Cordes and coworkers who showed that the ratio of hetero to euchromatin changes with the cell culture condition, (1:1 for 2D, 2:1 for 3D cultured cells)[21]. Moreover, they were able to directly link the increased chromatin condensation with the ability of cells to survive after irradiation and the total number of DNA double strand breaks.

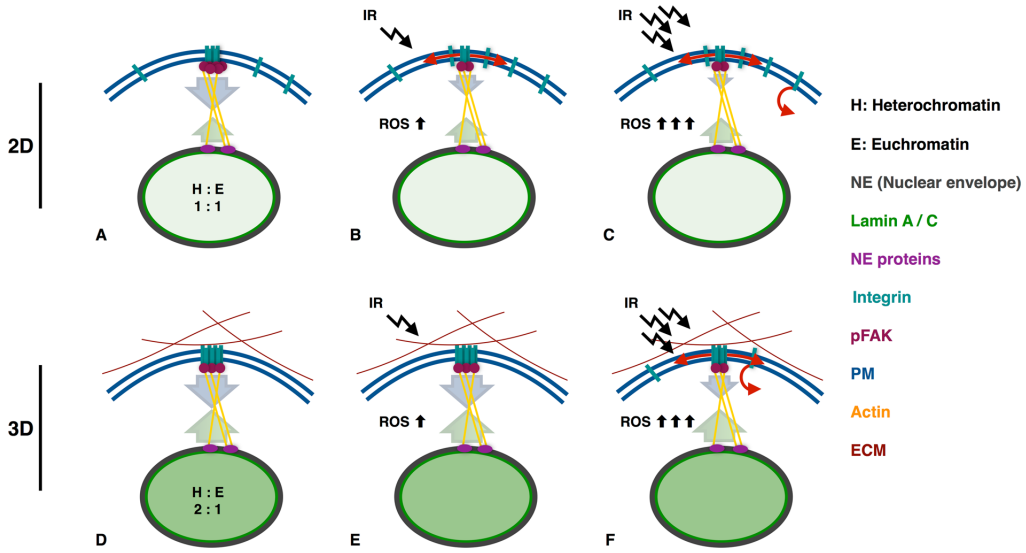

Figure 7. Mechano imbalance of 2D cells leads to their radio-sensitivity. (**A**) 2D cells show a different organisation of the nuclear matrix (Lamin A/C) and the chromatin condensation (ratio of hetero to euchromatin) if compared to 3D cells (**D**). The counterbalance of the nuclear force feedback between the integrin - cytoskeleton - nucleus link is imbalanced leading to a loose, dynamic integrin organisation in 2D cells (**A**). In 3D cells the mechanical link is well-balanced leading to firm and defined integrin clusters (**D**). An irradiation with a low dose (2 Gy) of 2D cells leads to integrin cluster disintegration by lateral diffusion and down regulation of downstream signals (pFAK) by up regulation of ROS. The imperfect force feedback combined with loose integrin clusters is responsible for the observed effects (**B**). As 3D cells exhibit a mechano-homeostasis, low doses can not effect integrin and pFAK signalling, although ROS is upregulated (**E**). (**C**) An irradiation with a high dose (15 Gy) exceeds the threshold for endocytosis leading not only to cluster disintegration by lateral diffusion but also by axial membrane transport. (**F**) 3D cells irradiated with a high dose (15 Gy) lead to a slight integrin cluster disintegration by a lateral and axial membrane transport. The equilibrium of the force feedback leads to effects that are shifted in their time dependence and in their intensity.

Taken together, we assume that the mechanical link connecting integrins with the nuclear lamina and therefore with the chromatin organization itself is differently balanced in cells cultured in 2D or 3D, leading to a different mechanosensitive homeostasis and to a different integrin cluster reaction upon irradiation. Our results involving the pFAK signalling support this assumption. pFAK signalling of unirradiated 2D cells is twice as intensive as detected for 3D cultured cells. This obvious imbalance of 2D cells leads to an incomplete nuclear force feedback and to a loose, dynamic integrin organization which is easily distributed. This leads to a integrin cluster disintegration and the loss of pFAK signalling at low dosages. The counterbalanced nuclear force feedback of 3D cells results in defined and firm integrin clusters. These clusters can only be disrupted at very high dosages resulting in a higher ROS level. This view is summarized in our model (Fig. 7).

Conclusion

In conclusion, CAM-RR is based on an intact integrin signalling system connecting the PM with chromatin, which has its origin in the proper nanoscale organization of integrins. Only with this balanced system in place, the long term observations of CAM-RR (chromatin organization → lower amount of DSB → higher tolarance to IR → cell survival) are able to unfold. Consequently, it is reasonable to assume that if radioresistance relies on intact integrin clusters, an active disintegration of integrin clusters may in turn induce radiosensitivity - and probably also chemosensitivity, making the nanoscale distribution of integrins a potential drug target for radiosensitization. While integrin receptors have been in the focus as a drug target for a long time, almost all antagonists (antibodies, peptides or small molecules) so far targeted either the ligand-binding site or the ligand itself[45]. Based on our study, we propose in turn to target antagonists against the ability to form clusters. Along with this suggestion, however, microscopy capable to monitor the nanoscale distribution in cells cultured in meaningful 3D environments would need to become an integral part of the preclinical screening process.

Materials and Methods

Cell culture. MEF cells (mouse embryonic fibroblasts) were cultured in DMEM/Ham's F-12 (1:1) (Biochrom, Berlin, Germany) supplemented with 10% FCS (Sigma-Aldrich, St. Louis, Missouri, USA) and 1% NEAA (Biochrom, Berlin, Germany) in a humidified chamber at 37 °C and 5% CO_2. All cell cultures were prepared on round coverslips (Karl Hecht GmbH, Sondheim, Germany, NO. 1.5, Ø = 25 mm).

3D cell culture. MEF cells were cultured in 1.5 mg/ml collagen I hydrogels for 4 to 5 days prior to use. Functionalization of the coverslip surface with APTS is crucial for the immobilization of the hydrogels on the coverslip.

Coverslip coating with APTS ((3-Aminopropyl)triethoxysilane, Sigma-Aldrich, St. Louis, Missouri, USA). Coverslip were washed for 10 min in technical acetone (AppliChem, Darmstadt, Germany) and were dried afterwards. APTS solution was prepared freshly containing 2% (v/v) of APTS in acetone. 40 µl of the APTS solution was spined onto a dried, pre-cleaned coverslip using a spin coater. Coverslips were dried afterwards followed by two washing steps in H_2O, each 10 min. Coverslips were dried and stored in the dark until use.

Hydrogel preparation. Collagen I hydrogels were prepared similar to Vira *et al.*[46]. A 1.5 mg/ml collagen solution was prepared with 50% (v/v) of a 3 mg/ml rat-tail collagen I stock solution (Thermo Fischer Scientific, Waltham, Ma, USA), 7.5% (v/v) of 10x PBS (Thermo Fischer Scientific, Waltham, Ma, USA), 2.8% (v/v) of a 7.5% NaHCO3 (AppliChem, Darmstadt, Germany) solution and with 14.7% (v/v) of a cell suspension containing 5×10^3 cells per µl. Cell suspension was obtained from one t25 flask of 80% confluent MEF cells. Cells were centrifuged after trypsin treatment and subsequently suspended in 1 ml media. 15 µl of the 1.5 mg/ml collagen solution was pipetted on a APTS coated coverslip. Hydrogels were incubated for 30 min at 37 °C and 5% CO_2, afterwards fresh media was added and cells were cultured as described above.

Radiation experiments. Irradiation was carried out using an Isovolt 160 Titan E (GE Sensing & Inspection Technologies, Alzenau, Germany) x-ray source. Cells were irradiated with a voltage of 90 kV and a current of 19 mA (for 0.5, 2 and 6 Gy) or 33.7 kV (for 15 Gy). Doses were delivered at a 30 cm source to probe distance with cell cultures placed on a 2 mm aluminum filtering plate with respect to the glass doubling factor[30].

Cells were fixed at 2 and 15 min as well as at 1, 6 and 24 h after radiation with a protocol optimized for the fixation of membranes, to avoid antibody-induced clustering of incompletely immobilized membrane proteins[36]. In using 4% PFA (Carl Roth, Karlsruhe, Germany) supplemented with 0.2% glutaraldehyde (Serva Electrophoresis, Heidelberg, Germany) in PBS (Sigma-Aldrich, St. Louis, Missouri, USA), (pH 6.9) for 1 h at 4 °C. This protocol is optimized for the fixation of membranes. Controls were treated exactly as the irradiated cells, controls were fixed coincidently with the 2 min probes. Cells were washed once with PBS prior to fixation and three times after fixation followed by antibody labeling as described below.

ROS Treatment. Cells were treated with H_2O_2 for 1 min (2D 100 µM, 3D 500 mM, Sigma-Aldrich, St. Louis, Missouri, USA)[47] in HBSS buffer, afterwards they were washed 3 times with PBS and were incubated until fixation in HBSS (Biochrom, Berlin, Germany) buffer at 37 °C. Fixation with 4% PFA supplemented with 0.2% glutaraldehyde in PBS occurred 2 min for 2D and 15 min for 3D cells after treatment followed by antibody staining of β1 integrins.

Stainings. *Collagen staining.* To stain collagen I the 3D cell cultures were incubated in a 20 µg/ml Erioglaucine disodium salt (E133, Sigma-Aldrich, St. Louis, Missouri, USA) solution for 10 min. Hydrogels were washed 3 times with PBS and imaged (Em: 633 nm, Ex: 750–750 nm).

Plasma membrane staining. For the detection of the plasma membrane CellMask Orange (Molecular Probes, Thermo Fisher Scientific, Waltham, Ma, USA) was used at a concentration of 0.5 µg/ml. Cells were incubated for 15 min in CellMask orange and imaged.

Antibody stainings. All integrin antibodies were purchased by Biozol Diagnostica (Eching, Germany). The following antibodies were used: anti CD29 Alexa 488 (integrin β1), anti CD61 Alexa 488 (integrin β3), anti CD51 (integrin αV) and anti-rat Alexa 647 (Biozol Diagnostica, Eching, Germany). All primary antibodies bind to extracellular integrin domains, therefore no permeabilization was needed. For all SMD measurements a 1:10 000 antibody dilution was used for 2D cells, for 3D cultured cells antibodies were diluted 1:5 000. For live cell measurements of β1 integrins cells were washed twice with PBS. Cells were incubated for 15 min in β1 integrin antibody solution in HBSS buffer. Afterwards cells were washed with PBS and were imaged directly. To analyse single molecules of fixed cells, cells were blocked after fixation for 1 h with a 1% BSA (AppliChem, Darmstadt, Germany) solution at 37 °C, washed with PBS 3 times and were incubated for 3 h at 4 °C in the desired antibody solution. For labeling αV with a secondary antibody or for colocalization experiments cells were blocked and stained once more as described before. Cells were washed 3 times afterwards and were imaged using STORM buffer. For SMD measurements of pFAK cells were stained and imaged as described for the αV antibody combination, in addition cells were permeabilized with 0.2% Triton-X100 (AppliChem, Darmstadt, Germany). pFAK antibody (Santa Cruz, Dallas, Texas, USA) was applied 1:5000, anti-rabbit Alexa 488 antibody (Thermo Fisher Scientific, Waltham, Ma, USA) was applied 1:10000. All primary antibodies were used for CLSM measurements as 1:100 dilutions, secondary antibodies were applied as dilutions of 1:200. Cells were fixed with 4% PFA for 1 h at 4 °C, washed 3 times with PBS. Prior to the staining cells were permeabilized with 0.2% Triton X-100 solution in PBS for 10 min and were blocked for 1 h with a 1% BSA solution at 37 °C and were washed with PBS 3 times. For the visualization of the cytoskeleton, the nucleus and Lamin A/C, cells were stained with primary antibodies for β-tubulin (Sigma-Aldrich, St. Louis, Missouri, USA), H2A (Sigma-Aldrich, St. Louis, Missouri, USA), LMNA (abcam, Cambridge, UK) and secondary antibodies labeled with Alexa 568 (anti-mouse, Thermo Fisher Scientific, Waltham, Ma, USA) or 488 (anti-rabbit, Thermo Fisher Scientific, Waltham, Ma, USA), each 3 h at 4 °C.

Microscopy. *Microscopy buffers.* Live cell imaging was performed in HBSS buffer (Biochrom, Berlin, Germany). For single molecule detection of fixed cells a standard STORM buffer was used according to Dempsey *et al.*[48] and van de Linde *et al.*[49]. 100 mM MEA (beta-mercaptoethylamine, pH 8.5, Sigma-Aldrich, St. Louis,

Missouri, USA), 140 U catalase (Sigma-Aldrich, St. Louis, Missouri, USA, C3515) and 10 U glucose oxidase (Sigma-Aldrich, St. Louis, Missouri, USA, G0543) were added immediately before use into Tris-buffer (50 mM Tris, 10 mM NaCl (both AppliChem, Darmstadt, Germany), pH 8) supplemented with 10% (w/v) glucose (AppliChem, Darmstadt, Germany). Imaging was performed under oxygen exclusion conditions.

CLSM measurements. CLSM-measurements were performed using the Leica TCS SP5 II (Leica Microsystems, Mannheim, Germany) equipped with a 63 × 1.2 Water corr objective or with a 63 × 1.3–0.6 oil objective.

SMD measurements. Single molecule imaging was performed using a custom-built instrument: The outputs of four continuous-wave optically pumped semiconductor laserdiodes (OPSL, Coherent Inc., Santa Clara, CA, USA) with wavelengths of 405 nm (OBIS, 100 mW), 488 nm (Sapphire, 75 mW), 561 nm (Sapphire, 75 mW), and 640 nm (OBIS, 100 mW) were controlled by an acousto-optic tunable filter (AOTFnC-400.650-TN and MDSnC, AA Opto-Electronic, Orsay, France), coupled into a single mode fiber (kineFLEX™, Qioptiq, Excelitas Technologies Corp., Waltham, MA, USA), and cleaned by a quadband excitation filter (FF01–390/482/563/640–25, Semrock, Rochester, NY, USA).

For widefield illumination the beam exiting the fiber collimator was expanded 15-times and focused into the back focal plane (BFP) of a Nikon CFI Apo TIRF 100x objective (NA 1.49, WD 0.12 mm) via a quadband dichroic mirror (Di01-R405/488/561/635–25 × 36, Semrock, Rochester, NY, USA) to exit the objective as a collimated beam with a FWHM of ~42 µm. Objective and filters were mounted in a Nikon Ti-E stand (Nikon, Konan, Minato-ku, Tokyo, Japan) equipped with a Perfect Focus System (PFS). For HILO and TIRF imaging the focus in the BFP was moved off-center by controlling the position of a mirror with a single-axis stage M-126. DG controlled by a C-863 Mercury Servo Controller (Physik Instrumente (PI), Karlsruhe, Germany).

For standard widefield fluorescence illumination, light from a Prior Lumen 220 Pro metal halide lamp (Prior Scientific, Cambridge, UK) was filtered by singleband excitation filters (FF01–390/40–15, FF02–482/18–25, FF01–563/9–25, FF01–640/14–25, Semrock, Rochester, NY, USA) and coupled into the microscope via a liquid light guide using the second of two of the Nikon Microscope's 'stratum structure' beam paths. Fluorescence emission was imaged onto an Andor iXon EM + DU-897 (back illuminated) EMCCD camera (Andor, Belfast, UK) using either Semrock quadband (FF01–446/523/600/677–25), dualband (FF01–523/610–25) or singleband emission filters (FF01–445/45–25, FF03–525/50–25, FF01–612/69–25, FF01–731/137–25, Semrock, Rochester, NY, USA). The AOTF and single-axis stage were controlled by a custom written virtual instrument (VI) for Labview (National Instruments, Austin, TX, USA) using a NI PCIe-6323 data acquisition (DAQ) board (National Instruments, Austin, TX, USA) and the fire signals from the camera as timing triggers. The open source software Micro-Manager 1.4[50] was used for image acquisition.

Image acquisition and data analysis. Editing of confocal images was performed using Fiji (version: 1.48t)[51]. Single molecule signals were detected and filtered using the ThunderStorm plugin[52] for Fiji. For single particle tracking and mean square displacement analysis TrackMate[53] was used. As a model for confined diffusion, the following formula was used to fit the mean square displacement plots (see ref. 54 for further details on single molecule tracking analysis).

$$MSD\left(t_{lag}\right) = \frac{L^2}{3}\left(1 - e^{-\frac{12D_0 t_{lag}}{L^2}}\right) \tag{1}$$

Due to the limited positional accuracy of the localization procedure, even immobile objects have an apparent diffusion-like mobility that determines the minimal detectable square displacement. In our case, the positional accuracy was ~28 nm which leads to a minimal detectable square displacement of $4\times (28\,\text{nm})^2 = 0{,}003136\,\mu\text{m}^2$. This minimal detectable square displacement is indicated in the plot (Fig. 2E) by a horizontal line near the x-axis. Data analysis and simulations were performed with custom written software in MATLAB R2014b. For 2D cultured cells two 4 × 4 µm ROIs, for 3D cultured cells one 4 × 4 ROI per cell were analysed. In Fig. 4, in Fig. 5 and in supplementary table 1 medians of distributions of samples from the analyses parameters are visualized. All presented box plots (Figs 5 and S3, S6–18) show as a central line the median, the top and bottom of each box are the first and third quartile, top and bottom line represent the maximum and minimum values. Outliers are colored in red. Statistical analysis was performed with GraphPad Prism 7.

Ripley's K function analysis. For the analysis of the obtained single molecule data we used Ripley's K function. This function identifies the average number of signals within concentric rings centered on each molecule[37,38].

$$K(r) = \frac{1}{n}\sum_{i=1}^{n} N_{Pi}(r)/\lambda \tag{2}$$

Where N is the number of points within the radius r of another point normalized by the number of points per area λ, where pi is the ith point summed over n points[39]. This function was linearized to obtain the so-called L-function and it was further normalized to generate the H-function.

$$L(r) = \sqrt{K(r)/\pi} \tag{3}$$

$$H(r) = L(r) - r \tag{4}$$

H(r) is 0 if the obtained signals are randomly, poisson distributed. A positive H(r) value indicates clustered data, a negative value indicates dispersed signals. To obtain the degree of clustering and the mean cluster radius the H-function was plotted against the length scale r. The first local maxima provides the information of the clustering (H(r)max) as well as the maximal cluster radius (rmax)[39]. For statistical analysis confidence intervals of 68.27% were generated by simulating 100 random distributions with the same number of signals as a control data set.

To visualize the clustering a 2-dimensional pseudo colored heat map was prepared similar to Williamson *et al.*[55]. Local L(r) values for each point were determined (with r = 130 nm) and interpolated as a surface plot by using the MATLAB interpolation function 'v4' with a grid set to 10 nm.

The total number of integrins were determined by counting all signals, molecules that convert to the same position were removed within the distance of the uncertainty of each dataset.

Cluster area, number of clusters per μm^2, number of signals per cluster, cluster density (signals per area) and the ratio of clustered/unclustered signals were determined after generating binary cluster maps based on the publication of Owen *et al.*[56]. To generate binary cluster maps the threshold was adjusted for the controls and was set constant.

Statistical analysis. Effects of ionizing radiation or ROS treatment on ECM-binding integrins and pFAK were analyzed for significance using an one-way ANOVA test with a Tukey post hoc test. Homogeneity of variances was tested with the Brown-Forsythe test, if this test resulted in a small P value the Kruskal-Wallis test with a Dunn's multiple comparison test was used to determine significances. For both cases, $p \leq 0.05$ was considered significant (*), $p \leq 0.01$ very significant (**) and $p \leq 0.001$ extremely significant (***). Also $p \leq 0.0001$ (****) was noted.

References

1. Ghosh, S. *et al.* Three-dimensional culture of melanoma cells profoundly affects gene expression profile: a high density oligonucleotide array study. *J. Cell. Physiol.* **204**, 522–531 (2005).
2. Zschenker, O., Streichert, T., Hehlgans, S. & Cordes, N. Genome-wide gene expression analysis in cancer cells reveals 3D growth to affect ECM and processes associated with cell adhesion but not DNA repair. *PLoS One* **7**, e34279 (2012).
3. Kenny, P. A. *et al.* The morphologies of breast cancer cell lines in three-dimensional assays correlate with their profiles of gene expression. *Mol. Oncol.* **1**, 84–96 (2007).
4. Harunaga, J. S. & Yamada, K. M. Cell-matrix adhesions in 3D. *Matrix Biol.* **30**, 363–368 (2011).
5. Geraldo, S. *et al.* Do cancer cells have distinct adhesions in 3D collagen matrices and *in vivo*? *Eur. J. Cell Biol.* **91**, 930–937 (2012).
6. Meshel, A. S., Wei, Q., Adelstein, R. S. & Sheetz, M. P. Basic mechanism of three-dimensional collagen fibre transport by fibroblasts. *Nat. Cell Biol.* **7**, 157–164 (2005).
7. Windus, L. C. E., Kiss, D. L., Glover, T. & Avery, V. M. *In vivo* biomarker expression patterns are preserved in 3D cultures of Prostate Cancer. *Exp. Cell Res.* **318**, 2507–2519 (2012).
8. Hutmacher, D. W. Biomaterials offer cancer research the third dimension. *Nat. Mater.* **9**, 90–93 (2010).
9. Hutmacher, D. W. *et al.* Can tissue engineering concepts advance tumor biology research? *Trends Biotechnol.* **28**, 125–133 (2010).
10. Huveneers, S. & Danen, E. H. J. Adhesion signaling – crosstalk between integrins, Src and Rho. *J. Cell Sci.* **2** (2009).
11. Streuli, C. H. Integrins and cell-fate determination. *J. Cell Sci.* **122**, 171–177 (2009).
12. Tate, M. C. *et al.* Specific β 1 integrins mediate adhesion, migration, and differentiation of neural progenitors derived from the embryonic striatum. *Mol. Cell. Neurosci.* **27**, 22–31 (2004).
13. Maniotis, A. J., Chen, C. S. & Ingber, D. E. Demonstration of mechanical connections between integrins, cytoskeletal filaments, and nucleoplasm that stabilize nuclear structure. *Proc. Natl. Acad. Sci. USA* **94**, 849–854 (1997).
14. Balcioglu, H. E., van Hoorn, H., Donato, D. M., Schmidt, T. & Danen, E. H. J. The integrin expression profile modulates orientation and dynamics of force transmission at cell-matrix adhesions. *J. Cell Sci.* **128**, 1316–1326 (2015).
15. Ning Wang, J. D. T. A. D. E. I. Mechanotransduction at a distance: mechanically coupling the extracellular matrix with the nucleus. *NATuRE REVIEwS | Molecular cell Biology* **10** (2009).
16. Luxton, G. W. G., Gomes, E. R., Folker, E. S., Vintinner, E. & Gundersen, G. G. Linear arrays of nuclear envelope proteins harness retrograde actin flow for nuclear movement. *Science* **329**, 956–959 (2010).
17. Navarro, A. P., Collins, M. A. & Folker, E. S. The nucleus is a conserved mechanosensation and mechanoresponse organelle. *Cytoskeleton* **73**, 59–67 (2016).
18. Swift, J. *et al.* Nuclear lamin-A scales with tissue stiffness and enhances matrix-directed differentiation. *Science* **341**, 1240104 (2013).
19. Swift, J. & Discher, D. E. The nuclear lamina is mechano-responsive to ECM elasticity in mature tissue. *J. Cell Sci.* **127**, 3005–3015 (2014).
20. Fuks, Z., Vlodavsky, I., Andreeff, M., McLoughlin, M. & Haimovitz-Friedman, A. Effects of extracellular matrix on the response of endothelial cells to radiation *in vitro*. *Eur. J. Cancer* **28A**, 725–731 (1992).
21. Storch, K. *et al.* Three-dimensional cell growth confers radioresistance by chromatin density modification. *Cancer Res.* **70**, 3925–3934 (2010).
22. Storch, K. & Cordes, N. Focal adhesion-chromatin linkage controls tumor cell resistance to radio- and chemotherapy. *Chemother. Res. Pract.* **2012**, 319287 (2012).
23. Eke, I. & Cordes, N. Radiobiology goes 3D: How ECM and cell morphology impact on cell survival after irradiation. *Radiother. Oncol.* **99**, 271–278 (2011).
24. Miller, K. M. *et al.* Human HDAC1 and HDAC2 function in the DNA-damage response to promote DNA nonhomologous end-joining. *Nat. Struct. Mol. Biol.* **17**, 1144–1151 (2010).
25. Eke, I. *et al.* β1 Integrin/FAK/cortactin signaling is essential for human head and neck cancer resistance to radiotherapy. *J. Clin. Invest.* **122**, 1529–1540 (2012).
26. Hehlgans, S., Haase, M. & Cordes, N. Signalling via integrins: Implications for cell survival and anticancer strategies. *Radiat. Res.* **1775**, 163–180 (2007).
27. Goel, H. L. *et al.* Beta1 integrins mediate resistance to ionizing radiation *in vivo* by inhibiting c-Jun amino terminal kinase 1. *J. Cell. Physiol.* **228**, 1601–1609 (2013).
28. Sandfort, V., Eke, I. & Cordes, N. The role of the focal adhesion protein PINCH1 for the radiosensitivity of adhesion and suspension cell cultures. *PLoS One* **5** (2010).
29. Lauer, F. M., Kaemmerer, E. & Meckel, T. Single molecule microscopy in 3D cell cultures and tissues. *Adv. Drug Deliv. Rev.* **79–80**, 79–94 (2014).
30. Kegel, P., Riballo, E., Kühne, M., Jeggo, Pa & Löbrich, M. X-irradiation of cells on glass slides has a dose doubling impact. *DNA Repair* **6**, 1692–1697 (2007).

31. Fraley, S. I., Feng, Y., Wirtz, D. & Longmore, G. D. Reply: reducing background fluorescence reveals adhesions in 3D matrices. *Nat. Cell Biol.* **13**, 5–7 (2010).
32. Axelrod, D., Burghardt, T. P. & Thompson, N. L. Total Internal Reflection Fluorescence. *Annu. Rev. Biophys. Bioeng* **13**, 247–268 (1984).
33. Tokunaga, M., Imamoto, N. & Sakata-sogawa, K. Highly inclined thin illumination enables clear single-molecule imaging in cells. *Nat. Methods* **5**, 159–161 (2008).
34. Rust, M. J., Bates, M. & Zhuang, X. Sub-diffraction-limit imaging by stochastic optical reconstruction microscopy (STORM). *Nat. Methods* **3**, 793–795 (2006).
35. Rossier, O. *et al.* Integrins beta1 and beta3 exhibit distinct dynamic nanoscale organizations inside focal adhesions. *Nat. Cell Biol.* **14**, 1057–1067 (2012).
36. Tanaka, Ka. K. *et al.* Membrane molecules mobile even after chemical fixation. *Nat. Methods* **7**, 865–866 (2010).
37. Dixon, P. M. Ripley's K function. *Encyclopedia of environmetrics* (2002).
38. Haase, P. Spatial pattern analysis in ecology based on Ripley's K -function: Introduction and methods of edge correction. *J. Veg. Sci.* **6**, 575–582 (1995).
39. Kiskowski, Ma, Hancock, J. F. & Kenworthy, A. K. On the use of Ripley's K-function and its derivatives to analyze domain size. *Biophys. J.* **97**, 1095–1103 (2009).
40. Riley, P. A. Free radicals in biology: oxidative stress and the effects of ionizing radiation. *Int. J. Radiat. Biol.* **65**, 27–33 (1994).
41. Goswami, S. Importance of integrin receptors in the field of pharmaceutical & medical science. *ABC Decor* **03**, 224–252 (2013).
42. Clyman, R. I., Mauray, F. & Kramer, R. H. β1 and β3 Intregrins Have Different Roles in the Adhesion and Migration of Vascular Smooth Muscle Cells on Extracellular Matrix. *Exp. Cell Res.* **200**, 212–284 (1992).
43. Goldstein, M. & Kastan, M. B. The DNA damage response: implications for tumor responses to radiation and chemotherapy. *Annu. Rev. Med.* **66**, 129–143 (2015).
44. Xu, D. *et al.* Intracellular ROS mediates gas plasma-facilitated cellular transfection in 2D and 3D cultures. *Sci. Rep.* **6**, 27872 (2016).
45. Ley, K., Rivera-Nieves, J., Sandborn, W. J. & Shattil, S. Integrin-based therapeutics: biological basis, clinical use and new drugs. *Nat. Rev. Drug Discov.* **15**, 173–183 (2016).
46. Artym Vira, M. K. V. Imaging Cells in Three-Dimensional Collagen Matrix. *Curr. Protoc. Cell Biol.* 1–23 (2011).
47. Gibhardt, C. S. *et al.* X-ray irradiation activates K+ channels via H2O2 signaling. *Sci. Rep.* **5**, 13861 (2015).
48. Bates, M., Huang, B., Dempsey, G. T. & Zhuang, X. Multicolor super-resolution imaging with photo-switchable fluorescent probes. *Science* **317**, 1749–1753 (2007).
49. van de Linde, S. *et al.* Direct stochastic optical reconstruction microscopy with standard fluorescent probes. *Nat. Protoc.* **6**, 991–1009 (2011).
50. Edelstein, A., Amodaj, N., Hoover, K., Vale, R. & Stuurman, N. Computer control of microscopes using μManager. *Curr. Protoc. Mol. Biol.* Chapter 14, Unit14.20 (2010).
51. Schindelin, J. *et al.* Fiji: an open-source platform for biological-image analysis. *Nat. Methods* **9**, 676–682 (2012).
52. Ovesny, M., Křížek, P., Borkovec, J., Svindrych, Z. & Hagen, G. M. ThunderSTORM: a comprehensive ImageJ plugin for PALM and STORM data analysis and super-resolution imaging. *Bioinformatics* 1–2 (2014).
53. Tinevez, J.-Y. *et al.* TrackMate: An open and extensible platform for single-particle tracking. *Methods* **115**, 80–90 (2017).
54. Xu, X. *et al.* Coupling mechanism of a GPCR and a heterotrimeric G protein during chemoattractant gradient sensing in Dictyostelium. *Sci. Signal.* **3**, ra71 (2010).
55. Williamson, D. J. *et al.* Pre-existing clusters of the adaptor Lat do not participate in early T cell signaling events. *Nat. Immunol.* **12**, 655–662 (2011).
56. Owen, D. M. *et al.* PALM imaging and cluster analysis of protein heterogeneity at the cell surface. *J. Biophotonics* **3**, 446–454 (2010).

Acknowledgements

We thank A. Eigen and N. Dogan for measuring the pFAK data during their practical course at TU Darmstadt. This work was supported by the Deutsche Forschungsgemeinschaft (DFG, German Research Foundation) with grants to T. Meckel (Me3712/1-2 and GRK 1657).

Author Contributions

Conception or design of the work: L. Babel, T. Meckel. Data collection: L. Babel. Data analysis and interpretation: L. Babel, M. Grunewald, R. Lehn, T. Meckel. Drafting the article: L. Babel, T. Meckel. Critical revision of the article: L. Babel, M. Langhans, T. Meckel. Final approval of the version to be published: L. Babel, M. Grunewald, R. Lehn, M. Langhans, T. Meckel.

Additional Information

Supplementary information accompanies this paper at doi:10.1038/s41598-017-03414-4

Competing Interests: The authors declare that they have no competing interests.

Publisher's note: Springer Nature remains neutral with regard to jurisdictional claims in published maps and institutional affiliations.

Supplementary of:

Direct evidence for cell adhesion-mediated radioresistance (CAM-RR) on the level of individual integrin β1 clusters

Laura Babel[1,2], Miriam Grunewald[1,2], Robert Lehn[1], Markus Langhans[1], Tobias Meckel[1,2]

1 Membrane Dynamics, Department of Biology, Technische Universität Darmstadt, Germany
2 GRK 1657, Molecular and cellular responses to ionizing radiation, Technische Universität Darmstadt, Germany

β3 and αv integrins are affected by IR in an entirely different manner as β1 integrins

Results

Integrin heterodimers of αvβ1 and αvβ3 are well characterized ECM-binding integrins. To investigate if IR has an effect on integrins containing αv and β3 subunits comparative experiments were performed and results are displayed in in **S12 - 18** and in **S-table 1**. Both subunits showed a different reaction towards IR if compared to β1 integrins.

The most outstanding difference is shown in the effect of IR on integrins containing a β3 subunit. While the clustering (H max) shows a similar trend if compared to the results obtained from the β1 experiments, the severity of the initial effect 2 min after an irradiation with 2 Gy and 15 Gy of 2D cells is not comparable. R max is not affected if irradiated with 2 Gy and shows only a slight decrease after an irradiation with 15 Gy. An irradiation with 2 Gy of 3D cultured cells led to an increase in H max and r max, an irradiation with 15 Gy led only to a slight decrease in H max and had no effect on r max. In almost all parameters analyzed in **S-table 1** no or only slight differences were detected after an irradiation with 2 and 15 Gy of cells cultured in 2D or 3D. Only the number of molecules and the number of clusters increased significantly 2 min after an irradiation with 15 Gy of 2D cells.

Integrins containing a αv subunit of 2D cells show in their clustering (H max) and their cluster radius (r max) a comparable trend towards IR if compared to the β1 results seen in **Figure 4**. An irradiation with 2 Gy of 3D cultured cells led to an increase in H max with no significant effect on r max. 3D cells irradiated with 15 Gy showed no significant effect in H max as well as in r max (**S7**). The reaction of the parameters seen in **S-table 1** towards IR is comparable if the cells were cultured in 2D and irradiated with 2 and 15 Gy, only the number of clusters increases with the higher dose. All other parameters decreased and regenerated with time. The effect of 2 Gy on 3D cultured cells is comparable, but not as distinct as observed by 2D cultured cells. Surprisingly, the effects of IR on αv integrins of 3D cultured cells differ greatly if the cells was irradiated with 2 or 15 Gy. While an irradiation with 2 Gy led to a slight decrease in all parameters, an irradiation with 15 Gy led to an increase, while the ratio of clustered / unclustered signals of 3D cultured cells does not change. These results show that not only the ECM binding β1 integrins are affected by IR in dependence of the cell culture system, also integrins containing the αv or β3 subunit may contribute to CAM-RR.

Discussion

β3 integrins of 2D cultured cells are only slightly affected by an irradiation with 2 Gy (we could only detect a slight, still significant decrease in H max), an irradiation with 15 Gy had only a slight effect on the cluster radius but we could detect a significant decrease of the clustering 2 min after irradiation (**see S 12**). The most significant changes were detected in the number of molecule and clusters, both parameters increased 2 min after irradiation. Since the ratio of clustered / unclustered signals was constant as well as the cluster density and the signals per cluster, our results indicate that β3 integrins are upregulated and new clusters were generated. The effects of IR on β3 integrin differ in dependence of the cell culture system. 3D cultured cells irradiated with 2 Gy showed an increase in their clustering and cluster radius, but we could not detect distinct effects on the parameters in **S-table 1**, therefore we assume that β3 integrin clusters are compressed. Surprisingly, an irradiation with 15 Gy of 3D cultured cells revealed no such effects. Only a minor decrease of the clustering was detected. β3 integrin clusters of 3D cultured cells are affected after an irradiation with a low dose (2 Gy) but not after an irradiation with a high dose (15 Gy), 2D cultured cells are only affected after an irradiation with a higher dose (15 Gy) but show a completely different membrane located radiation response mechanismen.

Integrins containing the αv subunit are affected by IR in dependence of the dose and cell culture system. αv integrins of 2D cultured cells irradiated with 2 Gy showed a decrease in their clustering and cluster radius, as well as in all other parameter (except the number of clusters) from **S-table 1**. After an irradiation with 2 Gy we could detect more unclustered signals. Since the number of molecules decreased, we assume that the αv integrins emerge from the cluster by a combined axial and lateral membrane transport as reported for the β1 response mechanismen for higher doses. This mechanism also applies for 2D cells irradiated with 15 Gy. But, here we could also detect an increase in the number of clusters. This indicates, that the αv integrins do not simply emerge from the the clusters, they also form new clusters - αv clusters fragment after irradiation with 15 Gy of 2D cultured cells. An irradiation with 2 Gy on 3D cultured cells had the same effect on αv and β3 integrins: the clustering and the cluster radius increase, leading to a compression of the clusters by a lateral diffusion. The effects of 15 Gy on αv and β3 integrins of 3D cultured cells is not comparable: only minor decreases in the clustering and the cluster radius of αv integrins were detected, the number of molecules and clusters as well as the signals per cluster increased after IR. αv integrins are upregulated and form new clusters after irradiation.

Supplementary figures

S-table1: Percental change of various parameter after IR of β_3 and α_V integrins of 2D and 3D cultured MEF cells.

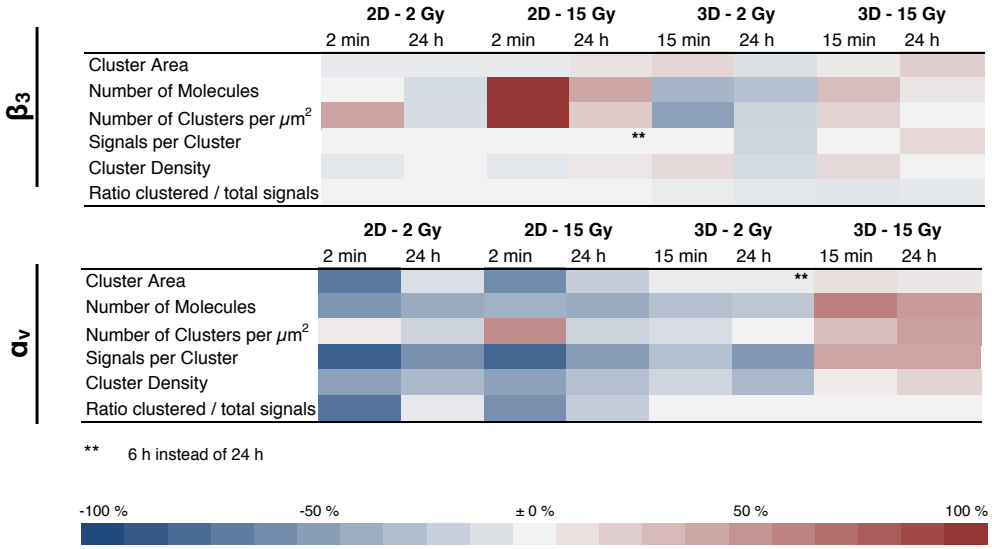

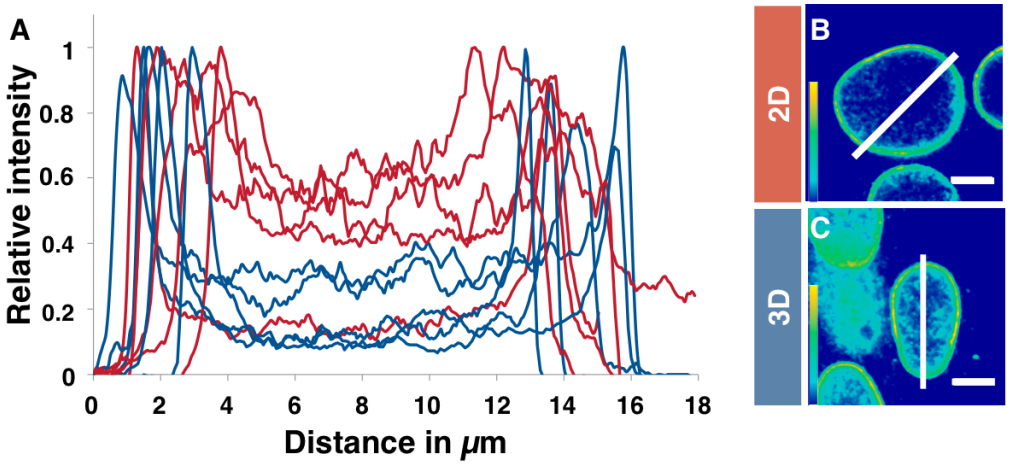

S 1: Line profiles of Lamin A/C of 2D (red) and 3D (blue) cultured cells. (A) Relative intensities of line profiles with a width of 3.5 µm of a Lamin A/C staining from cells cultured in 2D (red) and 3D (blue). N=1, n=5 for 2D and 3D cultured cells. (B, C) Heat map of a Lamin A/C immunostaining of 2D (B) and 3D (C) cultured cells including an exemplary line profile plotted in (A). Scale bar is 5 µm.

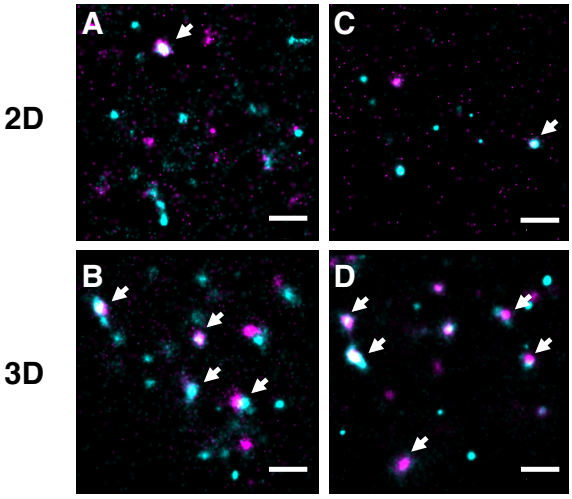

S 2: Colocalization of integrins of MEF cells cultured in 2D or 3D. (A) α_v (magenta) and β_1 (cyan) of 2D cultured cells. (B) Corresponding data for 3D cultured cells. (C) α_v (magenta) and β_3 (cyan) of 2D cultured cells. (D) Corresponding data for 3D cultured cells. Scale bar is 2 µm. Arrows indicate integrin-subunit colocalization (white).

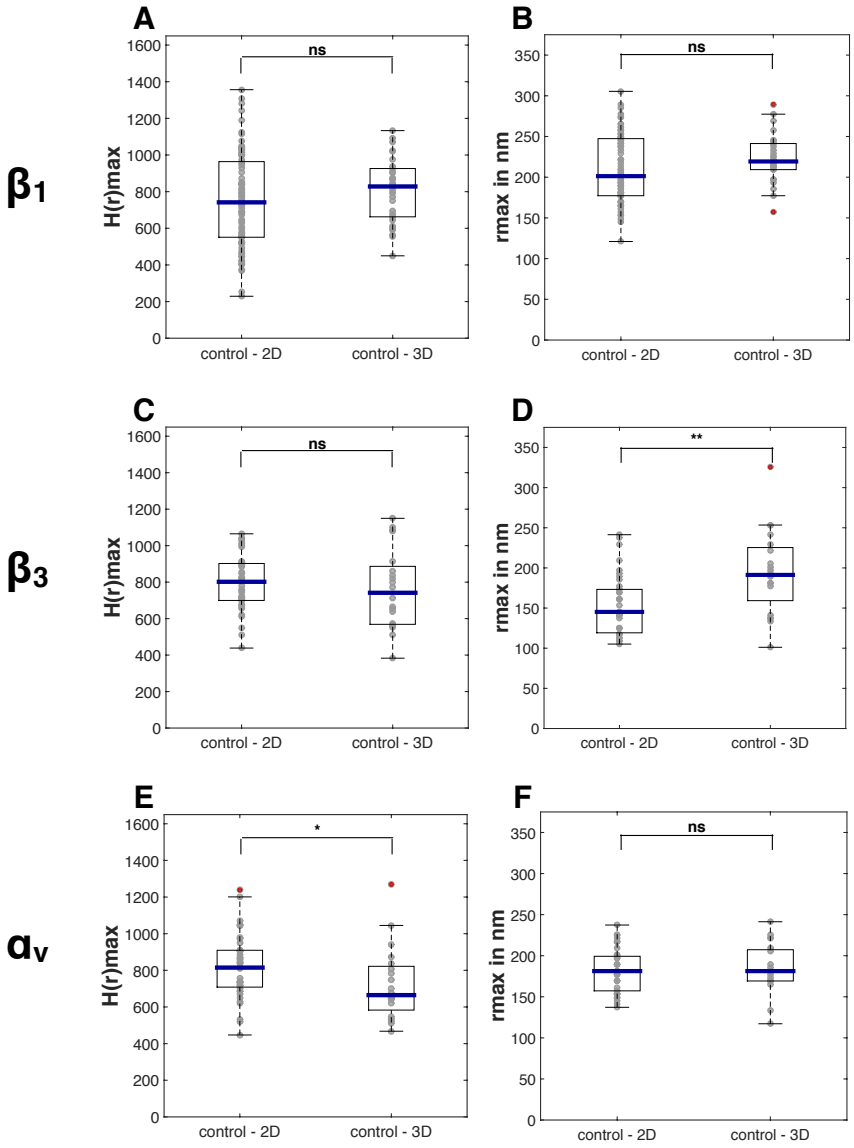

S 3: Clustering and cluster radius of all controls of β_1, β_3 and α_V integrins. (A) Box plot of the clustering (H(r)max) of β_1 integrins of 2D (N=8, n=80) and 3D (N=6, n=30) cultured control cells. (B) Box plot of the cluster radius r of β_1 integrins of 2D (N=8, n=80) and 3D (N=6, n=30) cultured control cells. (A, B) Statistical analysis was performed with an ordinary one-way ANOVA. (C) Box plot of the clustering (H(r)max) of β_3 integrins of 2D (N=4, n=40) and 3D (N=4, n=20) cultured control cells. (D) Box plot of the cluster radius r of β_3 integrins of 2D (N=4, n=40) and 3D (N=4, n=10) cultured control cells. (C, D) Statistical analysis was performed with an ordinary one-way ANOVA. (E) Box plot of the clustering (H(r)max) of α_v integrins of 2D (N=4, n=40) and 3D (N=4, n=20) cultured control cells. (F) Box plot of the cluster radius r of α_V integrins of 2D (N=4, n=40) and 3D (N=4, n=20) cultured control cells. (E, F) Statistical analysis was performed with a Kruskal - Wallis test. *p ≤ 0.05, **p ≤ 0.01. NS, not significantly different.

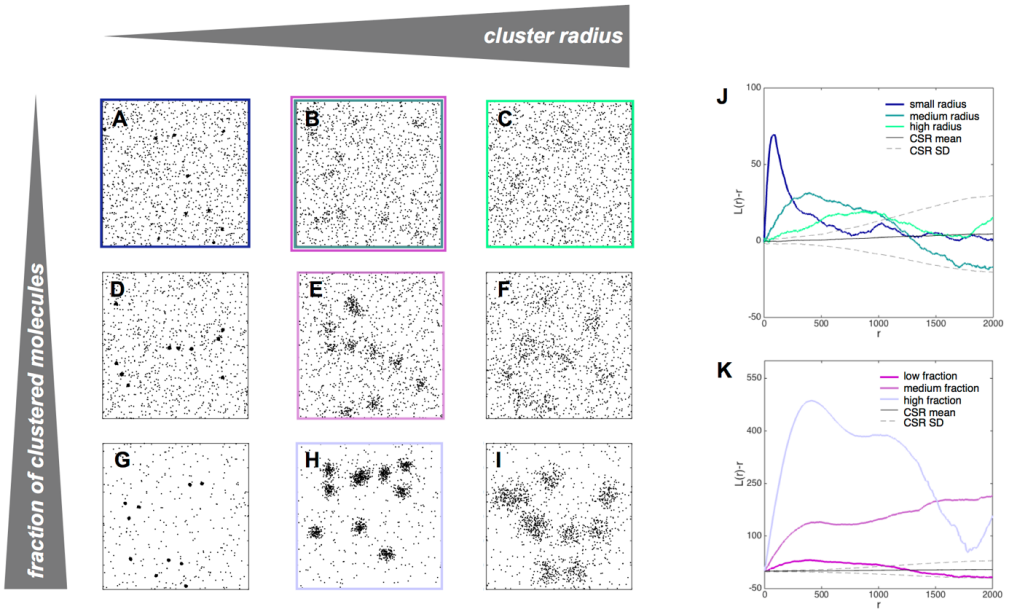

S 4: Simulated data demonstrating the influence of cluster radius and the fraction of clustered molecules on the H-function. While the cluster radius is depicted as the first maximum of the H-function, the clustering degree correlates with the value of L(r)-r. (A-I) Simulated distributions of 1500 molecules including 10 clusters with varying cluster radii and clustering degrees. In the upper row (A-C) the 10 cluster each consist of 20 molecules, in the middle row (D-E) clusters contain 50 molecules and in the lower row (G-I) clusters comprise 120 molecules. The cluster radius increases from left to right with a small radius in the left column (A, D and G), a medium radius for the middle column (B, E and H) and large radius in the right column (C, F and I). J and K show the corresponding H functions for the upper row (J) and the middle column (K) and the mean and standard deviation of 1500 completely random distributed molecules from 100 simulations. The cluster radius is depicted in the H-plot as the first maximum of the H-function at the scale of the highest clustering degree. Hence for expanding cluster radii r max increases (J). With higher cluster ratios the maximum of L(r)-r increases (K). The radius of clusters against a background of unclustered molecules likewise impacts the clustering degree, hence in J L(r)-r max decreases with higher cluster radii.

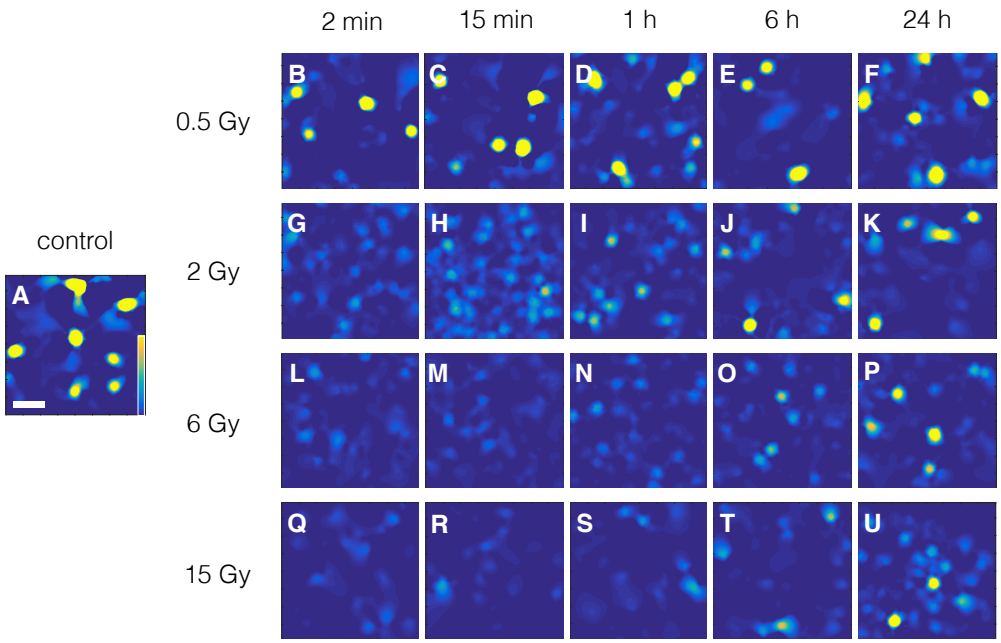

S 5: Effects of IR on the clustering of β_1 integrins of 2D cultured cells. Heat maps visualising unclustered (dark blue) and clustered (yellow) regions. Cells were irradiated with 0.5, 2, 6 and 15 Gy and were fixed 2 min, 15 min, 1 h, 6 h and 24 h after irradiation. (A) Control. (B-F) Cells irradiated with 0.5 Gy. (G-K) Cells irradiated with 2 Gy. (L-P) Cells irradiated with 6 Gy and (Q-U) cells irradiated with 15 Gy. Scale bar is 1 µm.

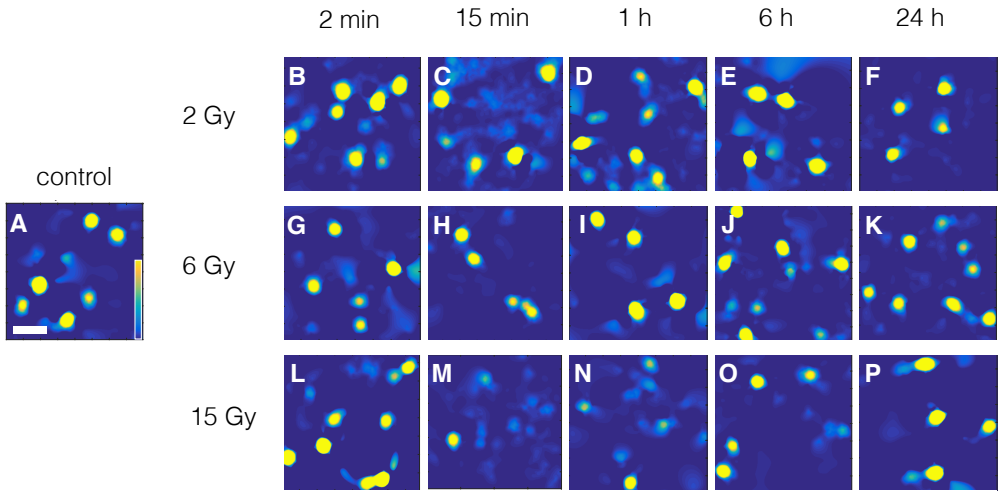

S 6: Effects of IR on the clustering of β_1 integrins of 3D cultured cells. Heat maps visualising unclustered (dark blue) and clustered (yellow) regions. Cells were irradiated with 2, 6 and 15 Gy and were fixed 2 min, 15 min, 1 h, 6 h and 24 h after irradiation. (A) Control. (B-D) Cells irradiated with 2 Gy. (G-K) Cells irradiated with 6Gy. (L-P) Cells irradiated with 15 Gy. Scale bar is 1 µm.

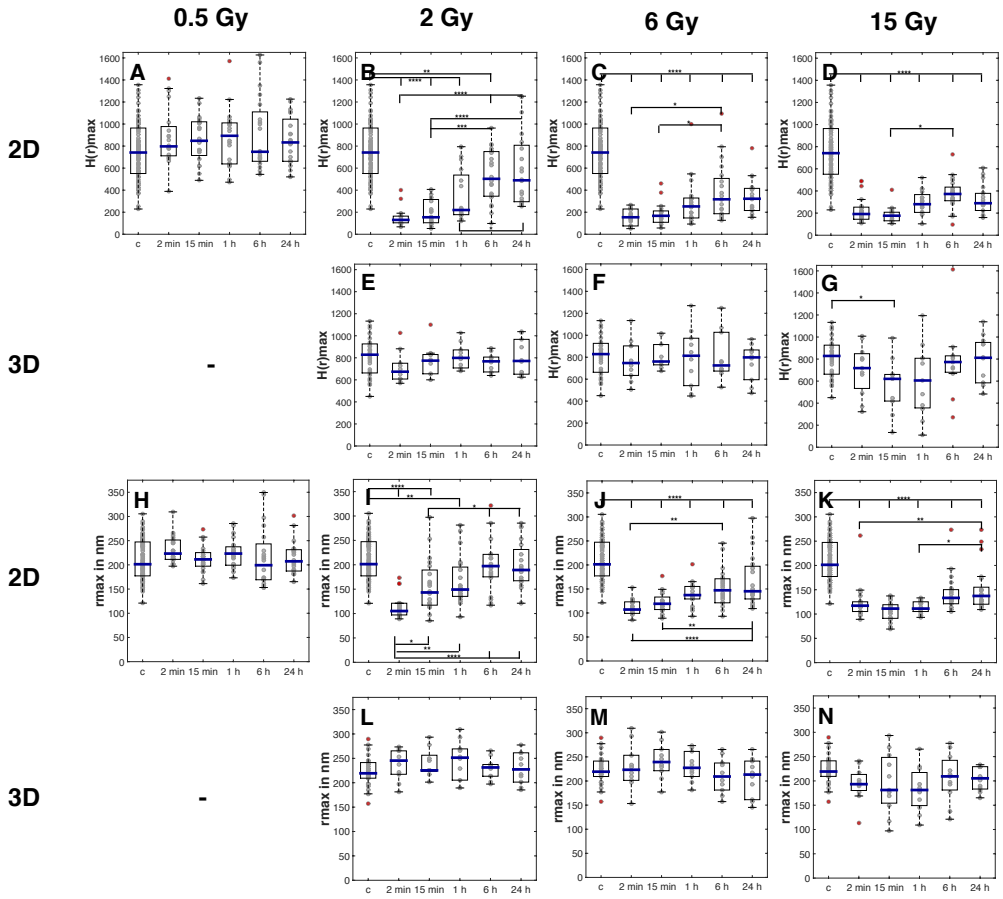

S 7: Effects of IR on the clustering (A-G) and the cluster radius (H-N) of β_1 integrins of 2D and 3D cultured cells. Box plots of the clustering H(r)max or the cluster radius r in nm plotted against the time (control (c), 2 min, 15 min, 1 h, 6 h and 24 h). 2D cultured cells were irradiated with 0.5, 2, 6 and 15 Gy (A-D, H-K), 3D cultured cells were irradiated with 2, 6 and 15 Gy (E-G, L-N). For 2D cells N=2, n=20. controls were pooled, N=8, n=80. For 3D cells N=2, n=10. Controls were pooled, N=6, n=30. Statistical analysis was performed with an ordinary one-way ANOVA (A, D, E, F, G, H, I, K, L, M) or with a Kruskal -Wallis test (B, C, F, N). *p ≤ 0.05, **p ≤ 0.01,***p ≤ 0.001 and ****p ≤ 0.0001. If not further noted no significance was detected.

2D

3D

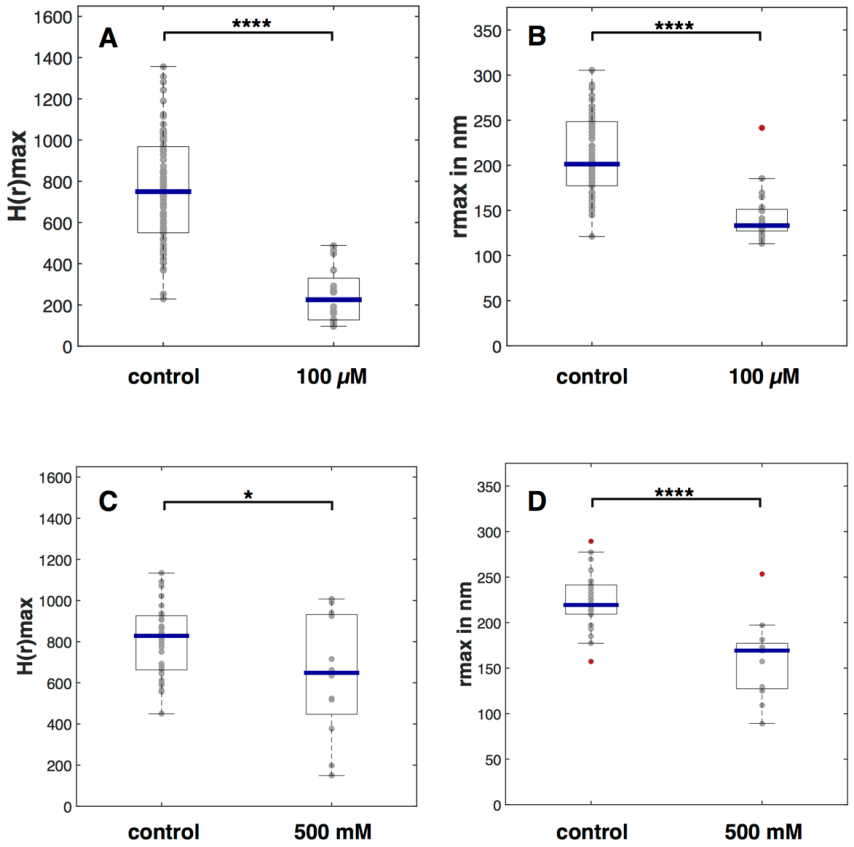

S 8: Cluster disintegration is induced by ROS. Box plots of the clustering H(r)max (A, C) and the cluster radius r in nm (B, D) of controls and cells treated with 100 µM H_2O_2 (2D, A and B) or of controls and cells treated with 500 mM H_2O_2 (3D, C and D). N=1, n=20. Statistical analysis was performed with a two-tailed Mann-Whitney test for (A) or with a two-tailed, unpaired t-test for (B, C, D). *p ≤ 0.05, ****p ≤ 0.0001.

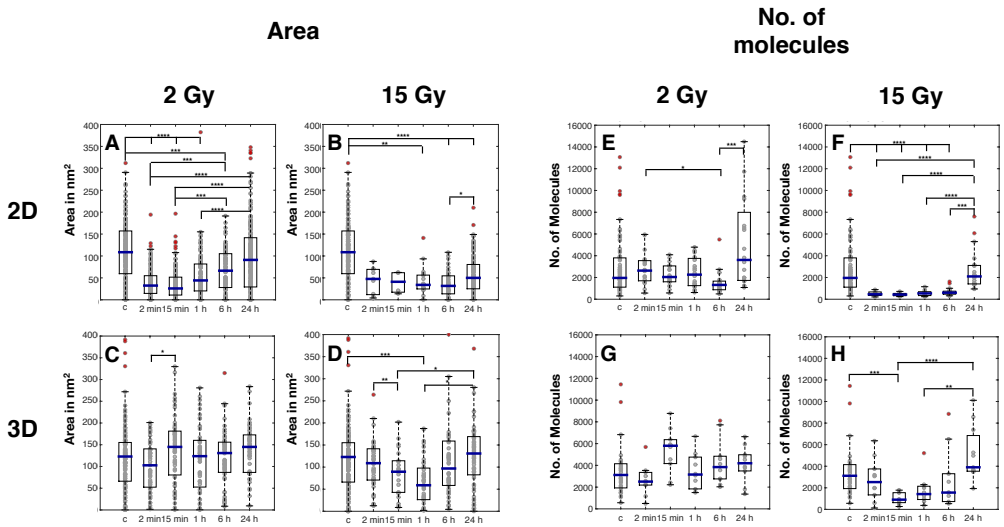

S 9: Effects of IR on the cluster area (A-D) and the number of molecules per ROI (E-H) of β_1 integrins of 2D (A/B, E/F) and 3D (C/D, G/H) cultured cells. Box plots of the cluster area and the number of molecules, plotted against the time (2 min, 15 min, 1 h, 6 h, 24 h and the control (c)). Cells were irradiated with 2 or 15 Gy. For 2D cells N=2, n=20. controls were pooled, N=8, n=80. For 3D cells N=2, n=10. Controls were pooled, N=6, n=30. Statistical analysis was performed with an ordinary one-way ANOVA (B, C, D, H) or with a Kruskal - Wallis test (A, E, F, G). *p ≤ 0.05, **p ≤ 0.01,***p ≤ 0.001 and ****p ≤ 0.0001. If not further noted no significance was detected.

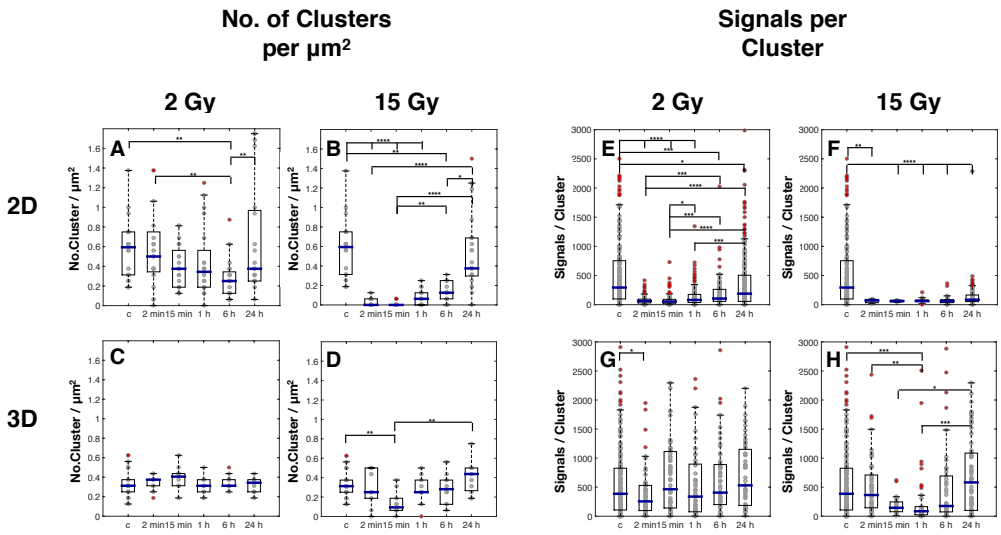

S 10: Effects of IR on the number of clusters per µm² (A-D) and the number of signals per cluster (E-H) of β_1 integrins of 2D (A/B, E/F) and 3D (C/D, G/H) cultured cells. Box plots of the number of clusters per µm² and the number of signals per cluster, plotted against the time (2 min, 15 min, 1 h, 6 h, 24 h and the control (c)). Cells were irradiated with 2 or 15 Gy. For 2D cells N=2, n=20. controls were pooled, N=8, n=80. For 3D cells N=2, n=10. Controls were pooled, N=6, n=30. Statistical analysis was performed with an ordinary one-way ANOVA (A, C, D, E, F, H) or with a Kruskal - Wallis test (B, G). *p ≤ 0.05, **p ≤ 0.01,***p ≤ 0.001 and ****p ≤ 0.0001. If not further noted no significance was detected.

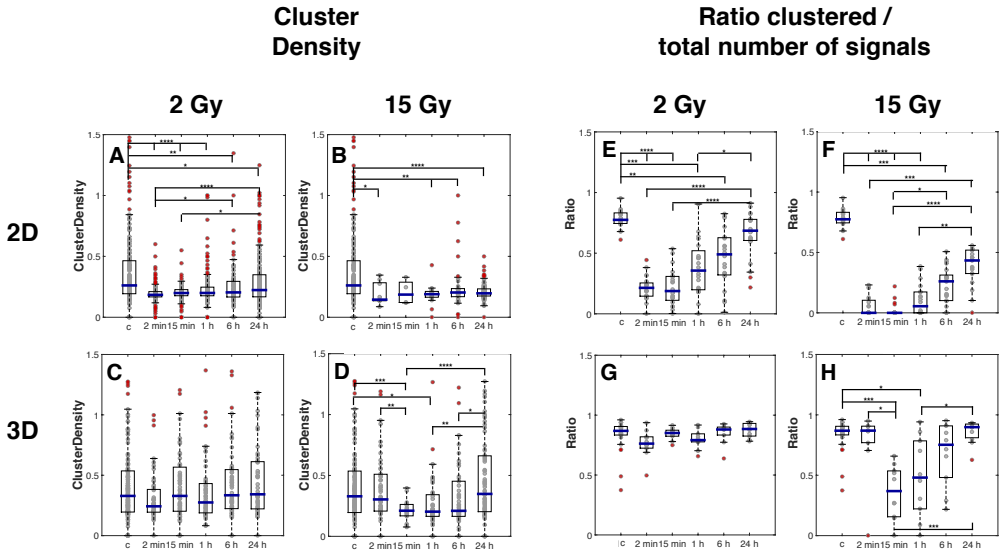

S 11: Effects of IR on the cluster density (A-D) and the ratio of clustered / total number of signals (E-H) of β_1 integrins of 2D (A/B, E/F) and 3D (C/D, G/H) cultured cells. Box plots of the cluster density and the ratio of clustered/unclustered signals, plotted against the time (2 min, 15 min, 1 h, 6 h, 24 h and the control (c)). Cells were irradiated with 2 or 15 Gy. For 2D cells N=2, n=20. controls were pooled, N=8, n=80. For 3D cells N=2, n=10. Controls were pooled, N=6, n=30. Statistical analysis was performed with an ordinary one-way ANOVA (C, G) or with a Kruskal - Wallis test (A, B, E, F, H). *p ≤ 0.05, **p ≤ 0.01,***p ≤ 0.001 and ****p ≤ 0.0001. If not further noted no significance was detected.

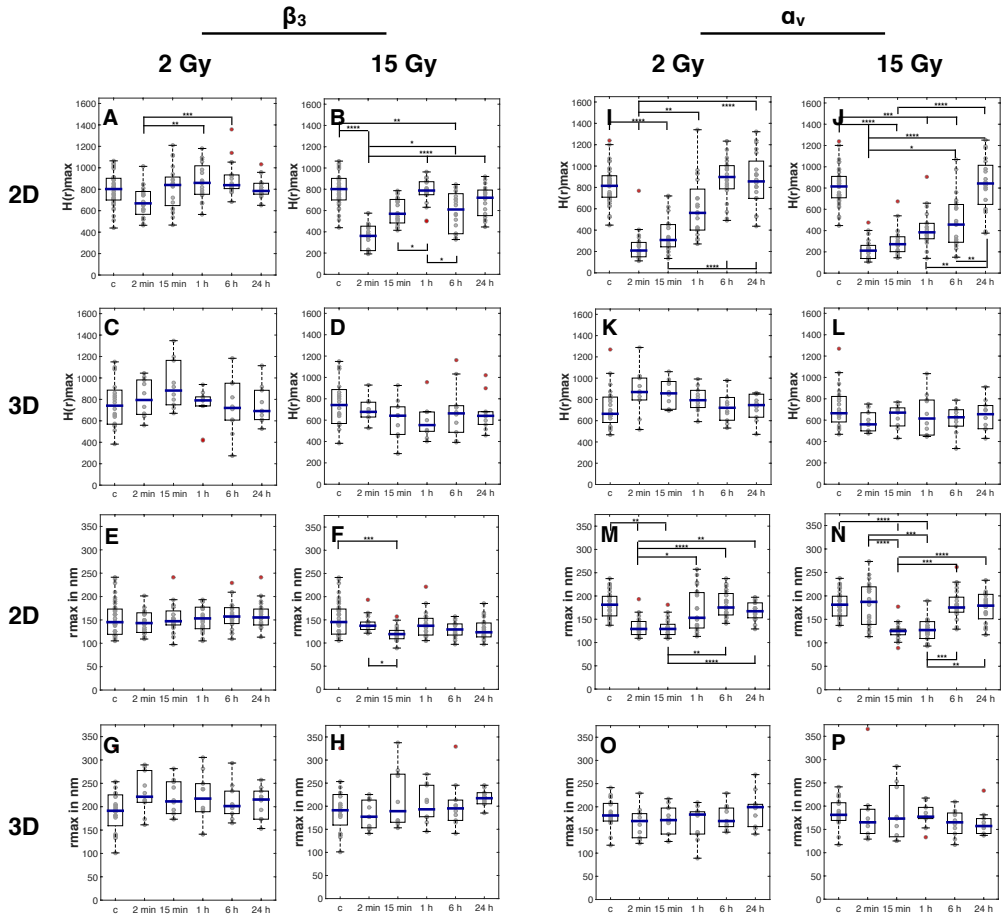

S 12: Effects of IR on the clustering and the cluster radius of β_3 (A-H) and α_V (I-P) integrins of 2D (A/B, e/F, I/J, O/P) and 3D (C/D, E/F, K/L, M/N) cultured cells. Box plot of the clustering H(r) max or the cluster radius r in nm plotted against the time (control (c), 2 min, 15 min, 1 h, 6 h and 24 h). Cells were irradiated with 2 or 15 Gy. For 2D cells N=2, n=20. controls were pooled, N=4, n=40. For 3D cells N=2, n=10. Controls were pooled, N=4, n=20. Statistical analysis was performed with an ordinary one-way ANOVA (A, C, D, E, G, H, K, L, O, P) or with a Kruskal - Wallis test (B, F, I, J, M, N). *p ≤ 0.05, **p ≤ 0.01,***p ≤ 0.001 and ****p ≤ 0.0001. If not further noted no significance was detected.

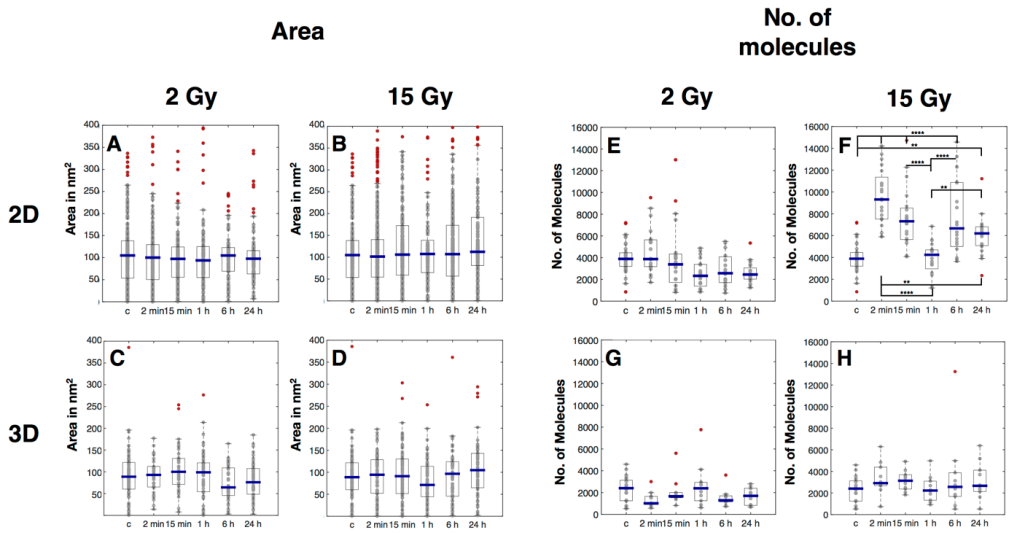

S 13: Effects of IR on the cluster area (A-D) and the number of molecules per ROI (E-H) of β_3 integrins of 2D (A/B, E/F) and 3D (C/D, G/H) cultured cells. Box plots of the cluster area and the number of molecules, plotted against the time (2 min, 15 min, 1 h, 6 h, 24 h and the control (c)). Cells were irradiated with 2 or 15 Gy. For 2D cells N=2, n=20. controls were pooled, N=4, n=40. For 3D cells N=2, n=10. Controls were pooled, N=4, n=20. Statistical analysis was performed with an ordinary one-way ANOVA (A - H). *p ≤ 0.05, **p ≤ 0.01,***p ≤ 0.001 and ****p ≤ 0.0001. If not further noted no significance was detected.

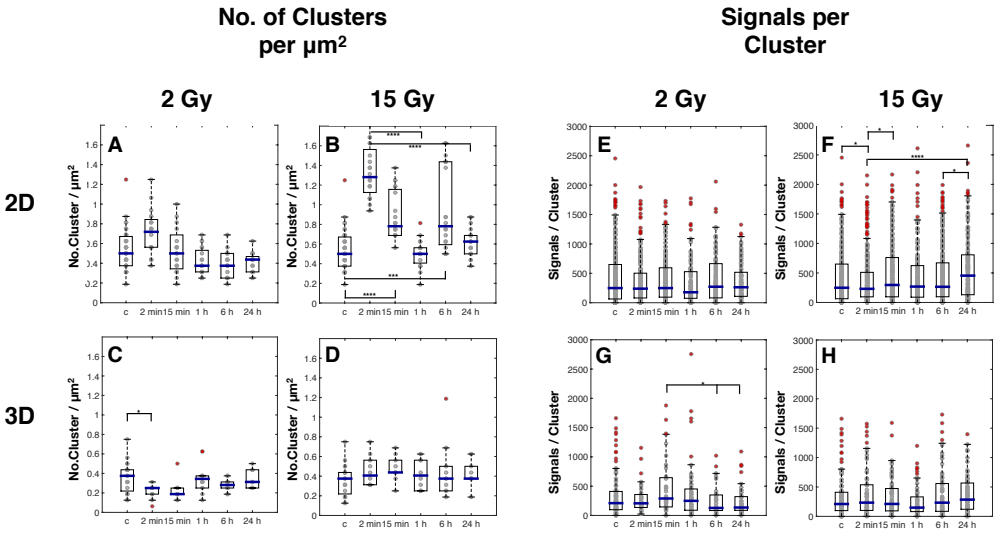

S 14: Effects of IR on the number of clusters per µm² (A-D) and the number of signals per cluster (E-H) of β_3 integrins of 2D (A/B, E/F) and 3D (C/D, G/H) cultured cells. Box plots of the number of clusters per µm² and the number of signals per cluster, plotted against the time (2 min, 15 min, 1 h, 6 h, 24 h and the control (c)). Cells were irradiated with 2 or 15 Gy. For 2D cells N=2, n=20. controls were pooled, N=4, n=40. For 3D cells N=2, n=10. Controls were pooled, N=4, n=20. Statistical analysis was performed with an ordinary one-way ANOVA (A, C - H) or with a Kruskal - Wallis test (B). *p ≤ 0.05, **p ≤ 0.01,***p ≤ 0.001 and ****p ≤ 0.0001. If not further noted no significance was detected.

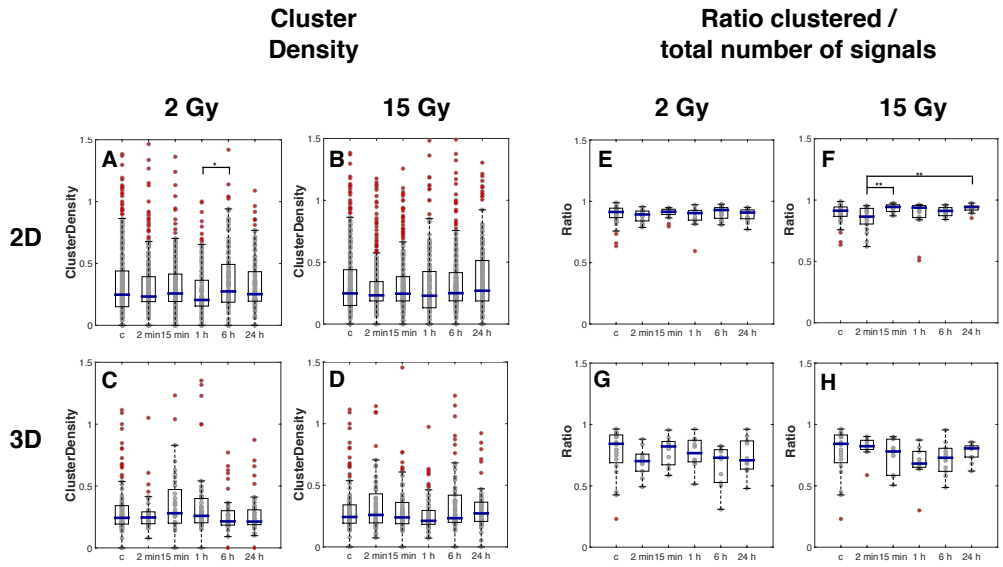

S 15: Effects of IR on the cluster density (A-D) and the ratio of clustered / total number of signals (E-H) of β_3 integrins of 2D (A/B, E/F) and 3D (C/D, G/H) cultured cells. Box plots of the cluster density and the ratio of clustered/unclustered signals, plotted against the time (2 min, 15 min, 1 h, 6 h, 24 h and the control (c)). Cells were irradiated with 2 or 15 Gy. For 2D cells N=2, n=20. controls were pooled, N=4, n=40. For 3D cells N=2, n=10. Controls were pooled, N=4, n=20. Statistical analysis was performed with an ordinary one-way ANOVA (A, C, D, E, G, H) or with a Kruskal - Wallis test (B, F). *p ≤ 0.05, **p ≤ 0.01,***p ≤ 0.001 and ****p ≤ 0.0001. If not further noted no significance was detected.

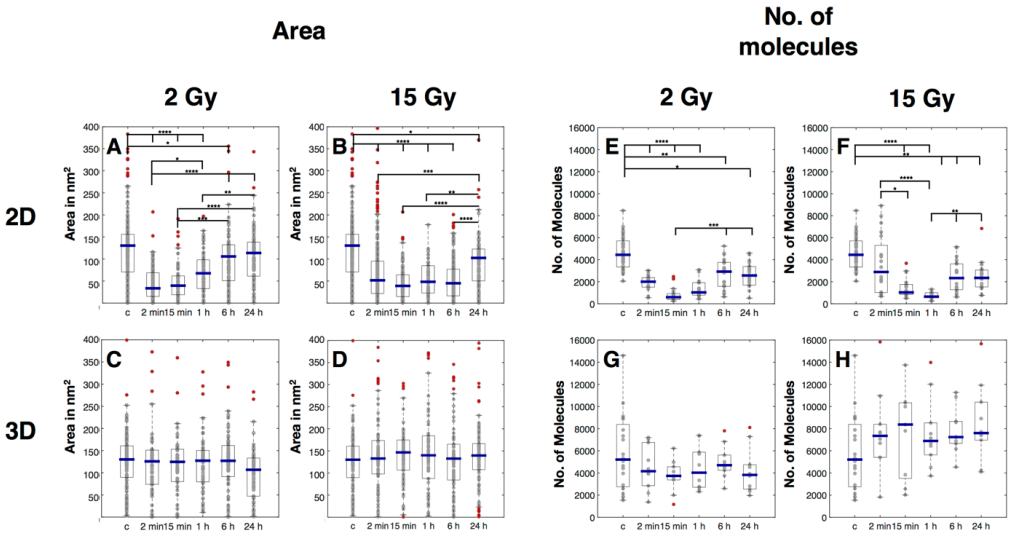

S 16: Effects of IR on the cluster area (A-D) and the number of molecules per ROI (E-H) of α_V integrins of 2D (A/B, E/F) and 3D (C/D, G/H) cultured cells. Box plots of the cluster area and the number of molecules, plotted against the time (2 min, 15 min, 1 h, 6 h, 24 h and the control (c)). Cells were irradiated with 2 or 15 Gy. For 2D cells N=2, n=20. controls were pooled, N=4, n=40. For 3D cells N=2, n=10. Controls were pooled, N=4, n=20. Statistical analysis was performed with an ordinary one-way ANOVA (C, G, H) or with a Kruskal - Wallis test (A, B, D, E, F). *p ≤ 0.05, **p ≤ 0.01,***p ≤ 0.001 and ****p ≤ 0.0001. If not further noted no significance was detected.

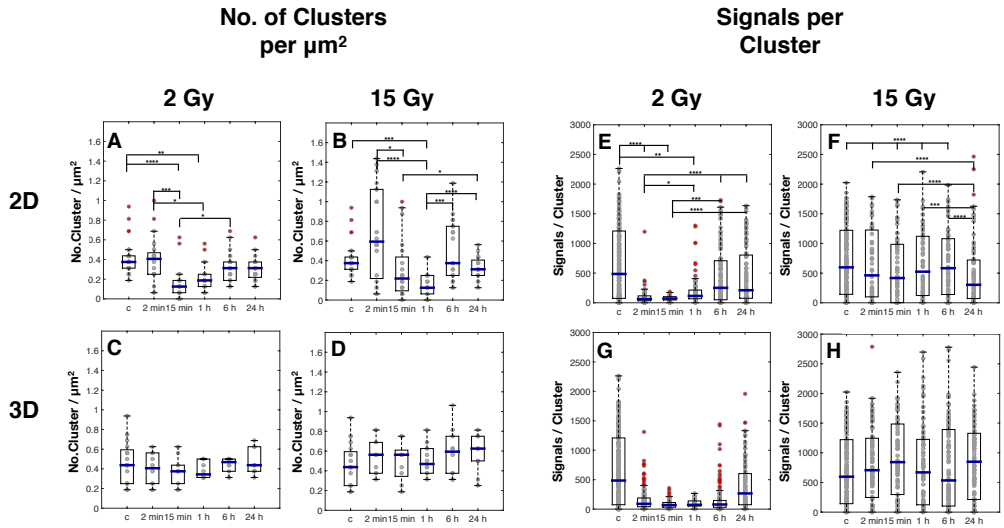

S 17: Effects of IR on the number of clusters per µm² (A-D) and the number of signals per cluster (E-H) of α_V integrins of 2D (A/B, E/F) and 3D (C/D, G/H) cultured cells. Box plots of the number of clusters per µm² and the number of signals per cluster, plotted against the time (2 min, 15 min, 1 h, 6 h, 24 h and the control (c)). Cells were irradiated with 2 or 15 Gy. For 2D cells N=2, n=20. controls were pooled, N=4, n=40. For 3D cells N=2, n=10. Controls were pooled, N=4, n=20. Statistical analysis was performed with an ordinary one-way ANOVA (A, C, D, G, H) or with a Kruskal - Wallis test (B, E, F). *p ≤ 0.05, **p ≤ 0.01,***p ≤ 0.001 and ****p ≤ 0.0001. If not further noted no significance was detected.

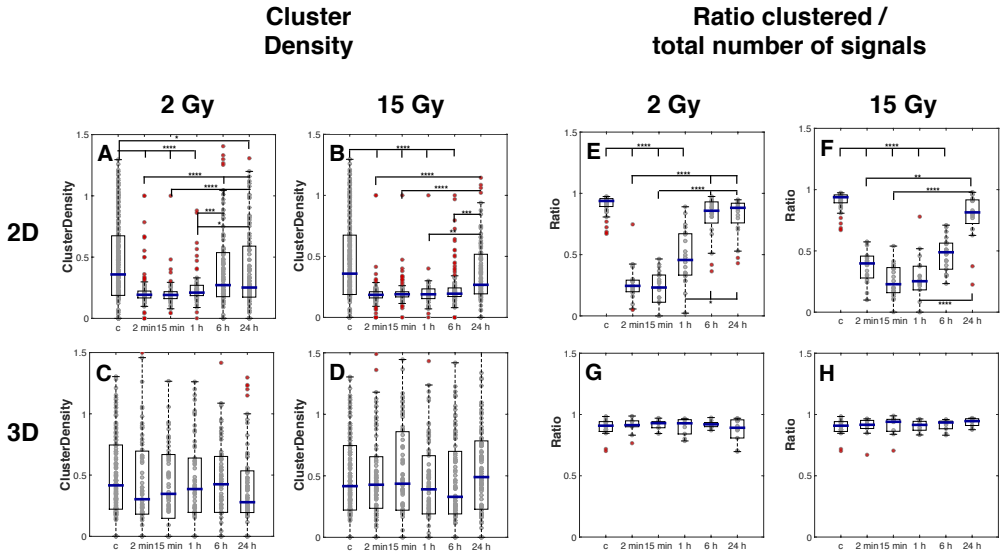

S 18: Effects of IR on the cluster density (A-D) and the ratio of clustered / total number of signals (E-H) of α_V integrins of 2D (A/B, E/F) and 3D (C/D, G/H) cultured cells. Box plots of the cluster density and the ratio of clustered/unclustered signals, plotted against the time (2 min, 15 min, 1 h, 6 h, 24 h and the control (c)). Cells were irradiated with 2 or 15 Gy. For 2D cells N=2, n=20. controls were pooled, N=4, n=40. For 3D cells N=2, n=10. Controls were pooled, N=4, n=20. Statistical analysis was performed with an ordinary one-way ANOVA (C, D, G, H) or with a Kruskal - Wallis test (A, B, E, F). *p ≤ 0.05, **p ≤ 0.01,***p ≤ 0.001 and ****p ≤ 0.0001. If not further noted no significance was detected.

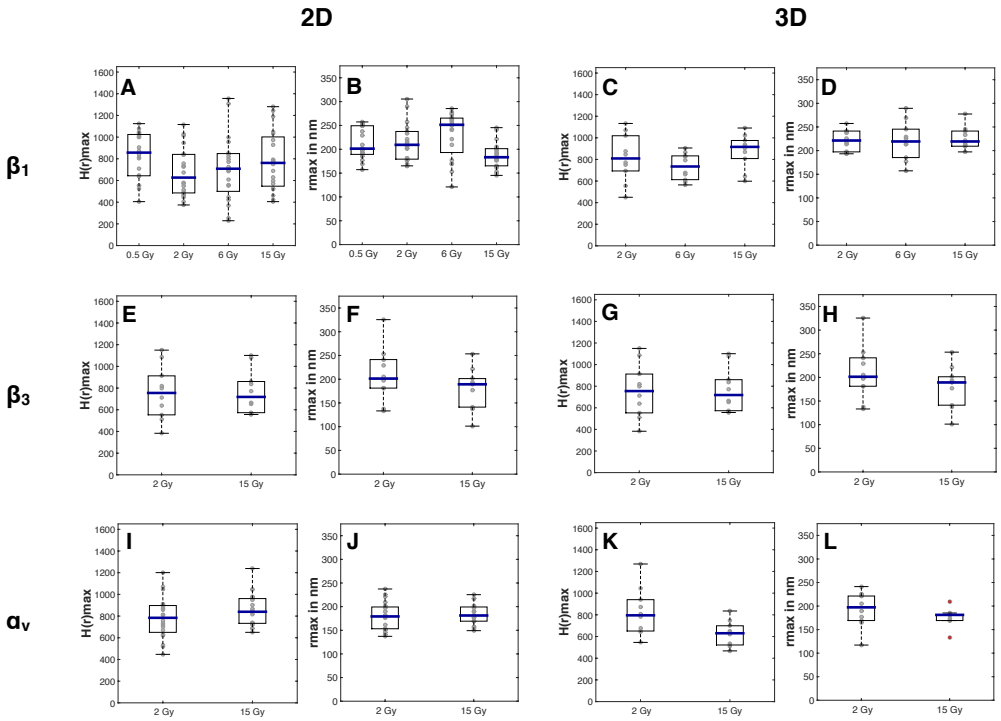

S 19: All pooled controls of β_1(A-D), β_3 (E-H) and α_V (I-L) integrins of 2D (A/B, E/F, I,J) and 3D cultured cells (C/D, G/H, K/L). Box plots of the clustering H(r)max and the cluster radius r in nm plotted against the dose. Cells stained for β_1 integrin were irradiated with 0.5, 2, 6 and 15 Gy if cultured in 2D, 3D cultured cells were irradiated with 2, 6 and 15 Gy. 2D and 3D cultured cells stained for β_3 and α_V were irradiated with 2 and 15 Gy. For 2D cells N=2, n=20. For 3D cells N=2, n=10.

Chapter II

Radiosensitization by anti-integrin β1 (AIIB2) is based on integrin cluster breakdown and subsequent loss of nuclear mechanosensing

5.1 Abstract

Resistance to ionizing radiation has been found to be higher in cells cultured in presence of a 3D matrix, a process, which has been termed cell-adhesion mediated radio-resistance (CAM-RR). As cell adhesion is - to a large amount - facilitated by integrin receptors and it was recently found that integrin clustering is a sensitive and robust indicator of radioresistance, it is reasonable to ask, whether disintegration of integrin clustering may in turn be a target to induce radioresistance in 3D cultured cells. With the use of the integrin $\beta 1$ inhibitory antibody AIIB2, a well-known radiosensitizer, it is possible to completely abolish integrin clustering in 2D cultured cells, while only a reduced clustering is observed in cells cultured under 3D conditions. There, an additional treatment with low dose (2 Gy) X-ray ionizing irradiation (IR) is required to remedy all clusters of integrin $\beta 1$. By following the actin-lamin interaction at the nuclear envelope with single molecule localization microscopy, it was found that the disintegration of integrin clusters has a direct impact on this nuclear mechanosensor. Collectively, the here presented results show that, in addition to biochemical, also mechanobiological cues and in particular nuclear mechanosensing have to be considered as relevant to uncover the molecular events behind adhesion related radiosensitivity.

5.2 Introduction

Integrins are front and center in the cellular processes that belong to the emerging field of mechanobiology. By linking the extracellular matrix (ECM) with the intracellular cytoskeleton they enable a cell to sense and produce mechanical forces that in turn are produced and sensed by neighboring cells [117]. This exchange of information between cells by mechanotransduction rather than diffusion of soluble molecules is gaining more and more attention in the quest to understand multicellular organization, development and diseases.

Cells use a multitude of different proteins acting in a concerted fashion to realize mechanosensation. Direct conversion of force into biochemical changes is realized by force-induced unfolding of proteins in the extracellular matrix, focal adhesions and at the nuclear envelope. Filamentous proteins like collagen, fibronectin, actin, microtubules, intermediate filaments and lamin provide the physical coupling between these force sensors, thereby enabling a continuous propagation of force throughout the network(s) and, finally, myosins maintain tension to add adaptive and responsive capabilities [92]. Importantly, this system allows the nucleus to not only receive biochemical but also mechanical cues about the cell's environment and, next to diffusion-based signaling through the cytoplasm, a direct and much faster route exists to modulate the expression of genes. In more detail, the integration of the nucleus is realized through the so-called LINC (linker of the nucleoskeleton and cytoskeleton) complex, composed of KASH (nesprin) and SUN domain proteins, which are located at the outer and inner nuclear membrane, respectively [117]. Much like integrins bridge the plasma membrane to couple the ECM with the cytoskeleton, the LINC complex bridges both nuclear membranes to physically link actin, microtubules, or intermediate filaments to lamins [118], turning the nuclear envelope into a force-sensitive interface between the cytoplasm and chromatin [95].

Inside the nucleus the 'nucleoskeleton' lamin forms a meshwork of intermediate filaments on the nucleoplasmic surface of the inner nuclear membrane and is mechanically interconnected with chromosomes, which are positioned in distinct locations [102, 103]. Lamin associated proteins (e.g. lamin B receptor, emerin) anchor the lamin network with chromatin structures and enable lamins to regulate DNA synthesis, chromatin organization and gene transcription [104, 105]. In particular lamins A and C provide structural support to the nucleus and define, together with the ECM, the final ends of the mechanotransduction system [96, 98, 97, 101]. Notably, the stiffness of the lamin nucleoskeleton mirrors the stiffness of the cell's environment, linking culture conditions with intranuclear architecture. Soft environments yield a reduced cytoskeletal tension and lead to higher levels of lamin A/C phosphorylation [100] which, in turn, yields a more soluble and mechanically weaker lamin network [92]. In other words, the softer the cellular environment, the more flexible and mobile the nuclear space.

As the integrin - actin - LINC - lamin connection is able to mirror the mechanical properties of the ECM in the nucleus [100, 99], any treatment of cells with the nucleus as the prime target needs to take this connection into account. In cancer treatment, ionizing radiation (IR) is used to cause DNA damage that leads to cell death. It was found that cells embedded in an ECM show a distinct radioresistance towards IR if compared to conventionally cultured 2D cells [27]. This effect, termed „cell-adhesion mediated radio-resistance“ (CAM-RR), shows that not only the effects of IR on DNA has to be considered, but rather a combination of damaging effects on DNA and on the ECM-nucleus connection needs to be understood [70, 17]. Of particular importance for the here presented work is the interaction of lamin A/C with proteins involved in DNA repair. Lamin has been shown to affect the stability and recruitment of 53BP1 resulting in an overall impairment of non-homologous end joining (NHEJ) [119]. Upon DNA damage, it is thought that chromatin-bound 53BP1 relocates to damage sites to form foci and, in addition, lamin A/C-associated 53BP1 proteins are released, to further increase the pool of free 53BP1 for a recruitment to damage sites [120] Likewise, also β1 integrin signaling has been shown to be involved in the regulation of DNA repair, in particular NHEJ [110].

Attention to the environment of cells in the context of cell survival and cancer treatment led to a number of publications addressing integrin signaling and its inhibition with inhibitory antibodies like the integrin β1 inhibitory antibody AIIB2. In these, the 3D environment was identified as a strong contributor to cell survival and numerous signaling pathways like Akt [109] or NF-κB [106] were found to be involved. Recently, the inhibition of β1 integrin was also shown to reduce the expression of proteins involved in DNA repair, mainly those involved in non-homologous end joining (NHEJ) [110], providing direct evidence for the reason behind CAM-RR. Mechanosensing as a contributor to β1 integrin mediated resistance of cells in a 3D environment was, however, not addressed in detail, thereby leaving mechanisms and targets unidentified that could aid in the radiosensitization of tumors. This chapter aims to show, how the nuclear mechanosensing system, with its origin at integrin containing focal adhesions, responds to ionizing radiation in dependence of the culture conditions and integrin inhibition.

Previously, it was identified that focal adhesions containing the integrin β1 subunits are a sensitive and fast compound to react on ionizing radiation (IR), as it was found that the radioresistance of 3D cultured cells is linked to their ability to maintain stable integrin β1 clusters upon irradiation. By using single molecule localization and tracking microscopy compatible with 3D cultured cells [42], it was found that the culture conditions cause marked differences in the organization of integrins. 2D cells were not able to organize integrins into firm and stable clusters, but instead display a rather loose and heterogeneous organization of the adhesion receptor. Moreover, a significant fraction of integrins in 2D cultured cells was found to be highly mobile in the plasma membrane, in contrast to integrins in 3D cultured cells. In addition, it was found that the integrin signaling is ineffective under the planar 2D culture conditions. Upon irradiation this unstable organization maintained by 2D cultured cells was severely disturbed by low doses of radiation, which did not have an effect on the clustered organization of integrins in 3D cultured cells [41].

Hence, as stable integrin clusters contribute to the radioresistance of 3D cultured cells, it is reasonable to ask whether an active destabilization of integrin clusters may induce mechanosensation that renders 3D cultured cells as sensitive as those under 2D culture conditions. Therefore, 2D and 3D cultured cells were treated prior to irradiation with the integrin β1 inhibitor AIIB2, an antibody well known to enhance the radiosensitivity towards IR of 3D cultured cells and mice xenografts [110, 109, 121]. Therein, subsequent analysis on the nanoscale distribution of the key components of (nuclear) mechanosensing system, namely integrin β1, actin, nesprin and lamin were done. In brief, it could be shown that an inhibition of β1 integrins with AIIB2 leads to a reduction of integrin clustering in cells embedded in an ECM followed by a complete cluster breakdown after IR and it was possible to show how the information of clustered/unclustered β1 integrins propagates through the mechanosensing system ultimately influencing intranuclear lamin distribution.

5.3 Results

5.3.1 AIIB2 and IR have a cooperative effect on integrin β1 cluster break-down in 3D cultured cells

To investigate the nanoscale effects of AIIB2 and IR co-treatment on integrin $\beta 1$ clustering, cells were incubated with the integrin $\beta 1$ inhibitory antibody 24 h prior to irradiation. Cells were irradiated with either (i) a low dose of X-rays were integrin clusters were not affected under non-inhibitor conditions (0.5 Gy for 2D and 2 Gy for 3D cells) and (ii) with a higher dose, were clusters disintegrated upon x-irradiation (6 Gy for 2D and 15 Gy for 3D cells). Cells were fixed 15 min after irradiation with a rapid and complete immobilization fixation protocol [86] so that the following results represent snapshots of the current integrin organization. The effects of AIIB2 treatment on the integrin clustering can be directly recognized by a visual inspection of the single molecule localization results. Each point in the scatterplots of Figure 5.1 represent an individual detection of an integrin $\beta 1$ molecule. While measurements of untreated, control cells reveal that $\beta 1$ integrins are organized as clusters, this picture changes after a treatment with AIIB2 or a combined treatment with AIIB2 and radiation. To put the visual inspection on quantitative grounds, a Ripley's K function cluster analysis was performed. This function counts the number of signals that fall within a defined radius of each detected signal. By plotting this number versus the respective radii a distribution (H-plot) is yielded, whose first local maximum represents the most prominent cluster formation of the data set. The height of this maximum gives (i) a measure of the clustering (H(r) max) and (ii) its position the cluster radius (r max). For a better visualization of the single molecule localizations, 2D plots of the H(r) max values are represented as heatmaps to visualize clustered regions with a higher density of signals as yellow areas. The degree of clustering (H(r) max) and the corresponding cluster radii for all AIIB2 and combined radiation treatments are summarized in Figure 5.1 (J, I and S, T).

The treatment of 2D cultured cells with the integrin inhibitor AIIB2 leads to a complete break-down of the loose and dynamic cluster organization. While in the control measurements clear integrin clusters were detected (Figure 5.1, A and B), this changes after the treatment with AIIB2 (Figure 5.1, C and D). Also an irradiation with a low dose (0.5 Gy) or with a high dose (6 Gy) could not increase this effect any further (Figure 5.1, E - H). AIIB2 treatment decreases the clustering (****$p \leq 0.0001$, Figure 5.1 I) and also the cluster radius (****$p \leq 0.0001$, Figure 5.1 J). AIIB2 treatment of 3D cultured cells also reduces the integrin clustering significantly (****$p \leq 0.0001$, Figure 5.1 S), but not as severe as detected for the 2D cells - some integrin clusters remain (Figure 5.1 M, N). Through an irradiation with a low dose (2 Gy) it is possible to break the integrin clustering to the same level as detected for 2D cultured cells treated with AIIB2 (*$p \leq 0.05$, Figure 5.1 O, P and S). An irradiation with a higher dose (15 Gy) revealed the same effect (****$p \leq 0.01$, Figure 5.1 Q and R).

Taken together, the integrin $\beta 1$ inhibitor AIIB2 has a strong impact on the cell's ability to maintain well organized integrins clusters, as in both cell culture systems the clustering is significantly reduced upon antibody treatment. While this inhibitor completely destroys the already impaired integrin organization of 2D cells, 3D cells show indeed a reduced clustering but are still able to maintain intact integrin clusters. Under non-inhibitory conditions a dose of 15 Gy was needed to trigger a slight (but significant) cluster disintegration of 3D cultured cells. Here, AIIB2 treatment of 3D cells leads to a complete cluster break-down after an irradiation with a low dose of only 2 Gy. These results prove, that it is possible to target integrin clustering itself. Still, the molecular connection that leads to AIIB2 induced radiosensitization is not known. The following results will show that the physical connection between integrins and nucleus, involving actin, nesprin and lamin, is highly affected by radiation and is further destabilized upon AIIB2 treatment.

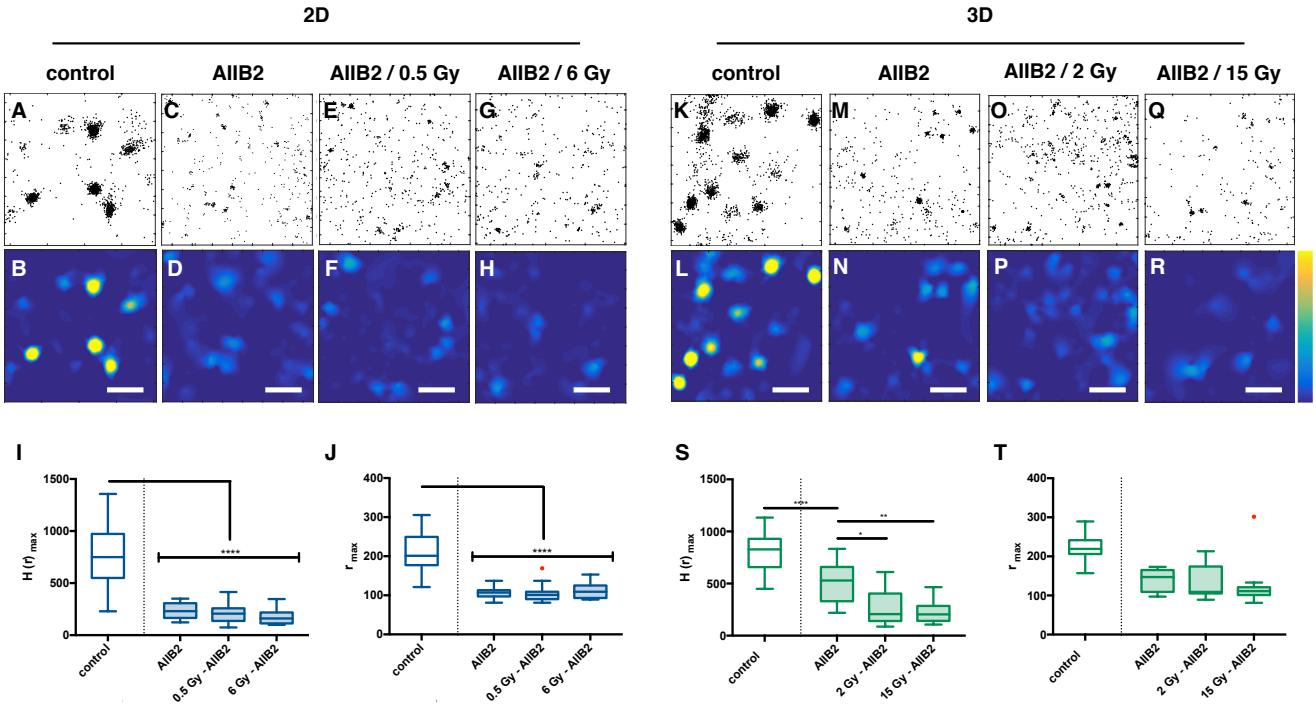

Figure 5.1: Combined radiation and AIIB2 treatment leads to a significant integrin β1 cluster disintegration. Single molecule localization data of β1 integrin immunostainings obtained from fixed cells 15 min after treatment and from untreated controls. Scatter plots show all detected β1 integrin localizations (A, C, E, G and K, M, O, Q), corresponding heat maps visualize clustered (yellow) and unclustered (dark blue) regions (B, D, F, H and L, N, P, R), scale bar is 1 μm. Statistical analysis with the Ripley's K function reveals the clustering (H(r) max) and the cluster size (r max). Shown are the distributions of β1 integrins found for untreated 2D cells (A and B), for 2D cells only treated with AIIB2 (C and D), for 2D cells treated with AIIB2 and irradiated with 0.5 Gy (E and F) and for 2D cells treated with AIIB2 and irradiated with 6 Gy (G and H). (I and J) Results of statistical analyzed 2D single molecule data for the clustering (I) and for the cluster radius (J), where N=2, n=20 (controls: N=4, n=80). (K - T) Corresponding data for 3D cultured cells, but irradiated with 2 and 15 Gy, N=2 and n=12 (controls: N=3, n=60). Statistical analysis was performed with a Kruskal - Wallis test. *p $\leq$ 0.05, **p $\leq$ 0.01 and ****p $\leq$ 0.0001

5.3.2 IN-Lamin: Intranuclear lamin organization changes in response to irradiation only in 3D cultured cells

With the integrin - actin - LINC - chromatin connection cells are able to mirror the mechanical properties of the ECM in the nucleus. The nuclear lamina forms a network of intermediate filaments on the nucleoplasmic surface of the inner nuclear membrane which can be easily recognized as a ring-like structure in confocal images (Figure 5.2, A and D). The distribution of Lamin A/C is highly ECM dependent, as the location beneath the inner nuclear membrane versus intranuclear signals differ if line profiles of 2D and 3D cells are analyzed (Figure 5.2, A - G). Intensity values of non NE-Lamin are 1.5x higher in 3D cells if compared to 2D cells (****p $\leq$ 0.0001, Figure 5.2, H).

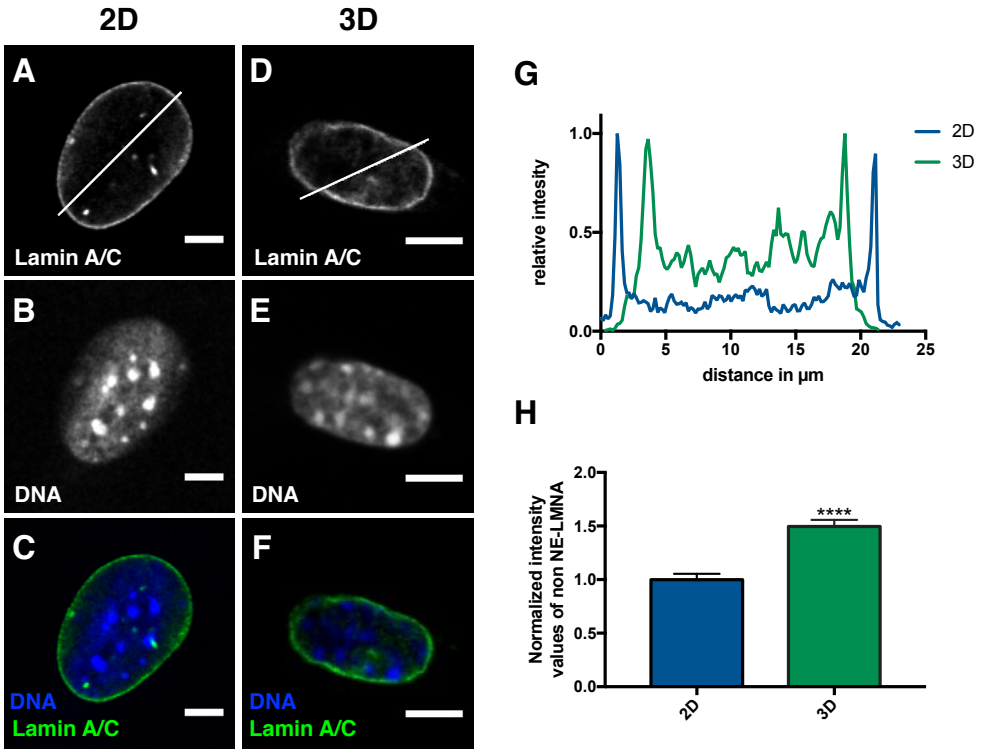

Figure 5.2: Intranuclear lamin organization is cell culture dependent. Lamin A/C immunostaining (A), DNA counterstaining (B) and overlay (C, green: Lamin, blue: DNA) of 2D cultured cells, scale bar is 5 μm. (D - F) Corresponding data for 3D cultured cells. (G) Relative intensity line profiles of 2D (blue) and 3D (green) cells as marked in (A) and (D). (H) Bar blots of normalized intensity values of intranuclear lamin (2D: blue, 3D: green), N=3, n=60. Statistical analysis was performed with an unpaired t-test, ****p $\leq$ 0.0001.

Hence, the lamin distribution already differs in dependence of the culture conditions alone. Upon IR, however, the response of cells gives valuable insights on the different statuses of the mechanosensing system in 2D and 3D cultured cells. Following the lamin distribution by quantifying the ratio of nuclear envelope vs. intranuclear located lamin (NE/IN-Lamin) it is possible to show that changes in response to IR are only observed in 3D cultured cells. Here, β1 integrin clusters disintegrate 15 min after irradiation with a high dose of 15 Gy. The ring-like structure of NE-lamin blurs 15 min after irradiation and regenerates overtime. As the intranuclear lamin signal increases significantly (*p $\leq$ 0.05), the signal transition towards the ring-like structure vanishes (Figure 5.3, G - L). Notably, the time point after IR at which lamin rearrangement occurs matches the time point of integrin cluster break-down after the same IR dose, indicating a close relation between both molecular rearrangements. In contrast, the distribution of lamin A/C in 2D cultured cells does not directly change in response to an IR dose that otherwise results

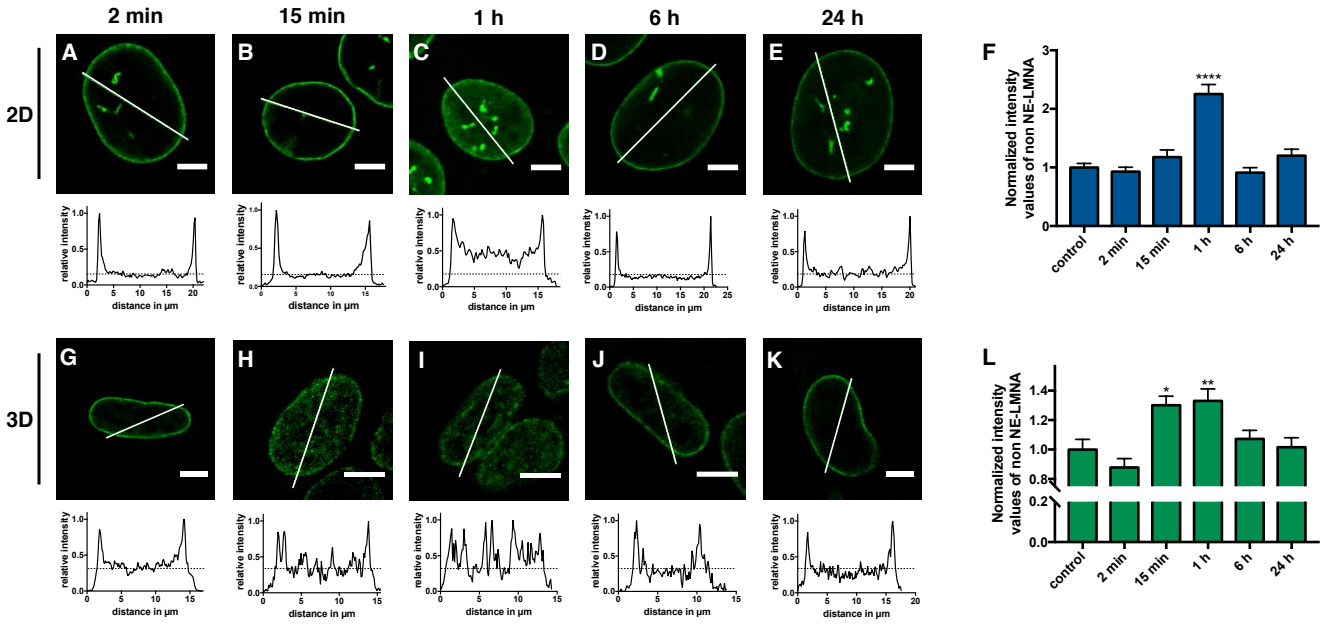

Figure 5.3: Only the nuclear lamina of 3D cells changes in response to IR. Immunostaining of Lamin A/C with relative intensity line profiles as marked in the confocal slices. Scale bar is 5 μm. Dotted line in the profiles represents the mean intensity value of intranuclear lamin of control cells. Shown are Lamin A/C stainings of 2D cells fixed 2 min (A), 15 min (B), 1h (C), 6 h (D) and 24 h (E) after an irradiation with 6 Gy. (F) Bar plot of normalized intensity values of intranuclear lamin A/C. (G - L) Corresponding data for 3D cultured cells, cells were irradiated with 15 Gy. Statistical analysis was performed with a Kruskal - Wallis test with N=2, n=20 (2D control: N=5, n=50, 3D control: N=3, n=30). *p $\leq$ 0.05, **p $\leq$ 0.01 and ****p $\leq$ 0.0001.

in the complete disintegration of integrin clustering (Figure 5.3, A - F). Only 1h after irradiation the concentration of IN-Lamin increased. The fact that this timing clearly does not correlate with the observed effects on integrin clustering in 2D irradiated cells indicates an impaired mechanosensing under these culture conditions. This point will be addressed in more detail in the discussion. Low dose irradiation - where integrin clustering is not affected - does not influence the intranuclear lamin organization in both cell culture systems (S 5.9).

5.3.3 NE-Lamin: Lamin organization at the NE follows IR induced apical f-actin destruction only in 2D cultured cells

To gain further insights in the nuclear envelope located events of lamin in response to IR and in dependence of the cell culture system, 2D and 3D cultured cells were x-irradiated with a high dose were integrin clusters disintegrated in previous experiments and with a low dose, were integrin clusters were not affected. To investigate the effects of IR on the mechanical link between integrins and chromatin, we also stained for actin. Actin and lamins are linked via nesprins and SUN proteins, transporting the information from integrins across the nuclear membrane. To analyze the effects of IR on this critical region single molecule microscopy is used to generate nanoscale colocalization snapshots of both proteins. The effects can directly be recognized by a visual inspection of the super-resolution images of Figure 5.4 and 5.5. 2D cells exhibit a strong colocalization of apical f-actin and lamin A/C. While the actin appears as distinct fibers, which always colocalize with lamin, lamin signals are also found in between actin fibers (Figure 5.4, A - C). An irradiation with a low dose of IR did not affect actin, lamin and consequently their colocalization (Figure 5.4, D - L). On the contrary, an irradiation with a dose of 6 Gy leads to a

fragmentation of actin fibers and to a scattering of lamin across the inner nuclear membrane and therefore to a complete loss of colocalization. 1 h after irradiation actin fibers start to regenerate while lamin signals are still unorganized. After 6 h, actin - lamin organization and colocalization have recovered (Figure 5.4, M - U).

At this point it is not clear if the actin - nesprin, or the nesprin - lamin connection of 2D cells is disrupted upon IR. Therefore, the same experiments were also performed with an costaining of actin and nesprin-2 (S 5.11 and 5.13), showing the same results. This leads to the suggestion that due to the actin fragmentation the connection to the nucleus is lost. The colocalization of actin and lamin A/C or nesprin-2 strongly depends on the organization of actin as strong, apical fibers. Confocal images of actin reveal that prominent f-actin bundles are more or less absent in 3D cultured cells (S 5.10, A - B). Therefore, the obvious colocalization of actin and lamin A/C is not present in these cells. The actin surrounding the nucleus of 3D cells is network-like organized and with a detailed inspection, some parts colocalize with lamin A/C, which is also organized as a meshwork (Figure 5.4, a - c). An irradiation with a low or with a high dose not lead to apparent effects, either the meshworks itself nor their colocalizing parts are influenced by IR (Figure 5.4, m - u). The same results were detected with an actin - nesprin-2 costaining (S 5.12).

To put the visual inspection on quantitative grounds we analyzed the number of lamin A/C molecules in dependence of the cell culture system combined with low and high dose irradiations (Figure 5.5, A). ROIs of 2.5 x 2.5 μm were placed in regions where no fibrous structures were present (Figure 5.5, B - E). Lamin A/C of 2D cells is mainly located on apical f-actin so that only very few signals were detected between these fibers. On the contrary, as no prominent f-actin is present in 3D cells, a significantly higher level of lamin A/C could be detected (****$p \leq 0.0001$). As IR does not affect the lamin organization at the NE of 3D cells, it was not possible to detect a significant effect on the number of lamin molecules. This also applies for 2D cells irradiated with 0.5 Gy, as most of the lamin molecules are still localized at f-actin fibers. An irradiation of 2D cells with a high dose leads to a significantly higher signal of lamin A/C 15 min and 1 h after irradiation (****$p \leq 0.0001$). As the connection between actin and lamin A/C is lost, lamin scatters across the inner nuclear membrane leading to a higher signal.

To receive a better understanding of the time dependence of actin destruction and reorganization and its influence on the lamin organization, an actin polymerization inhibition followed by actin and lamin A/C staining was performed. Therefore, a mild CytD treatment was chosen so that the cell morphology is still intact and 2D cells are able to adhere on the coverslip. With this CytD treatment the apical f-actin surrounding the nucleus of 2D cells was destroyed, as no actin stress fibers are present in 3D cells, an actin staining revealed no obvious difference (S 5.10, C - D). Superresolution images of CytD treated 2D cells fixed directly after the treatment reveal that actin fibers are not completely fragmented at this time point (Figure 5.6, D - F). Shreds of f-actin remain intact and colocalize with lamin A/C. After a regeneration time of 1 h most of the actin is completely fragmented, still some parts started to regenerate and at these regions we could not detect a lamin A/C colocalization (Figure 5.6, G - I). After a regeneration time of 6 h the actin - lamin A/C colocalization regenerated completely (Figure 5.6, J - L). With these results it can be concluded that (i) f-actin is able to move inner nuclear membrane located lamin (ii) and that after a f-actin destruction first actin and then lamin A/C is regenerated. A quantitative analysis of the number of lamin A/C molecules support these results. With the loss of apical f-actin lamin A/C molecules scatter across the nuclear envelope (Figure S 5.14 A; ***$p \leq 0.001$) as detected after an irradiation with a high dose of IR. Surprisingly, as shreds of f-actin are still present directly after the CytD treatment, line profiles of confocal lamin A/C stainings reveal a significant increase (****$p \leq 0.0001$) of the ratio of inner nuclear membrane located vs intranuclear lamin A/C (Figure S 5.14 B). Due to a lack of pronounced f-actin in 3D cells, f-actin inhibition does not change anything in the interaction of actin and lamin A/C (Figure 5.6, M - X) and in the number of lamin A/C molecules (Figure S 5.14 A). Also line profiles of confocal lamin A/C stainings reveal no significant effect of CytD treatment on the ratio of inner nuclear membrane located vs intranuclear lamin A/C (Figure S 5.14 C). This was not unexpected as the CytD did not affect 3D cells at all.

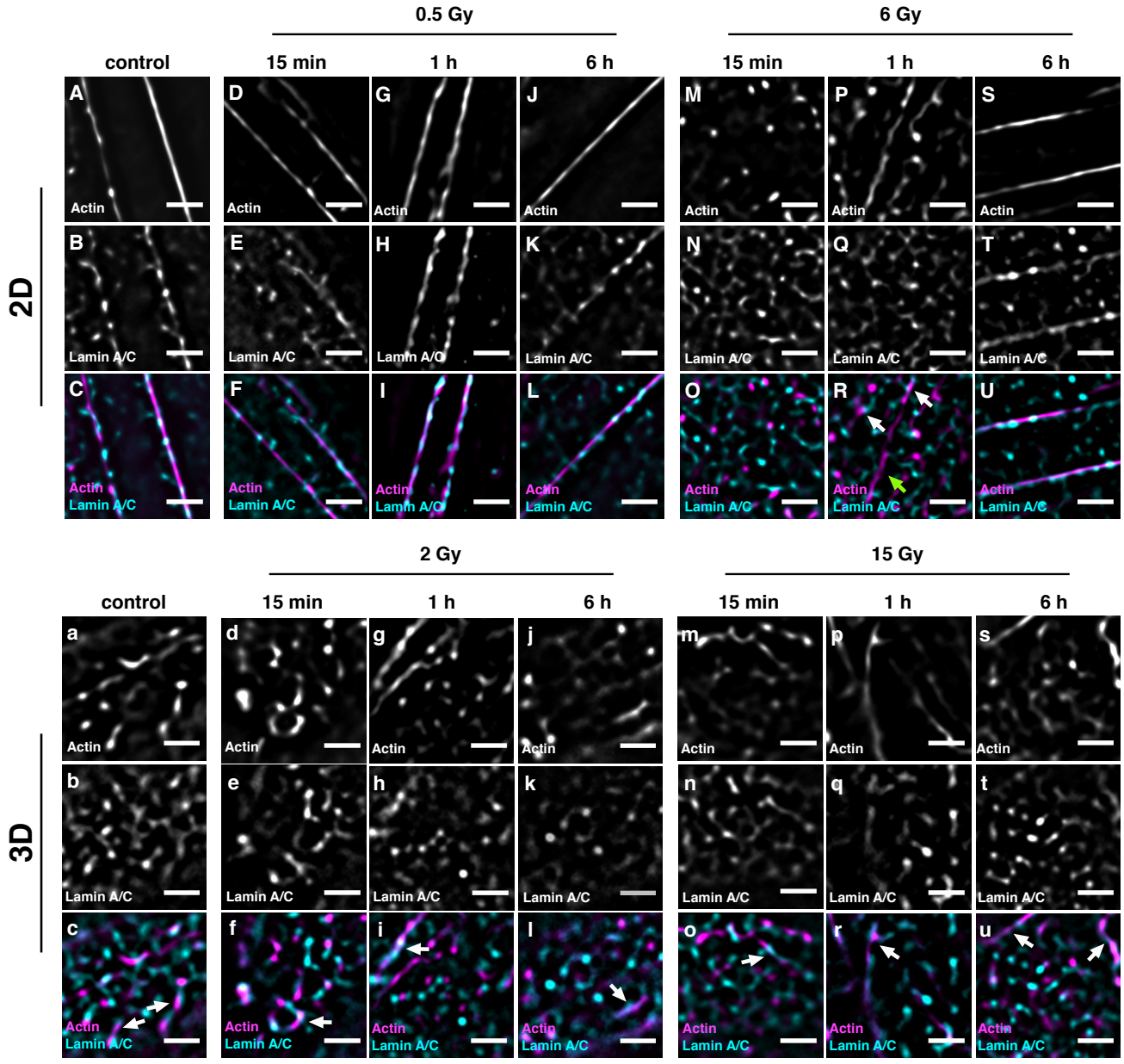

Figure 5.4: High doses of IR destroys lamin - f-actin connection only in 2D cells. Superresolution images of actin (A, D, G, J, M, P; S), lamin A/C (B, E, H, K, N, Q, T) and the corresponding overlay (C, F, I, L, O, R, U - actin: magenta, lamin A/C: cyan) of 2D control cells (A-C), 2D cells irradiated with 0.5 Gy (D-L) and 2D cells irradiated with 6 Gy (M-U). Cells were fixed 15 min after irradiation. (a-u) Corresponding data for 3D cultured cells. 3D cells were irradiated with 2 Gy (a-l) and 15 Gy (m-u). White arrows indicate regions with actin - lamin A/C colocalization (white), green arrow indicate regions where f-actin does not colocalize with lamin. Scale bar is 1 μm.

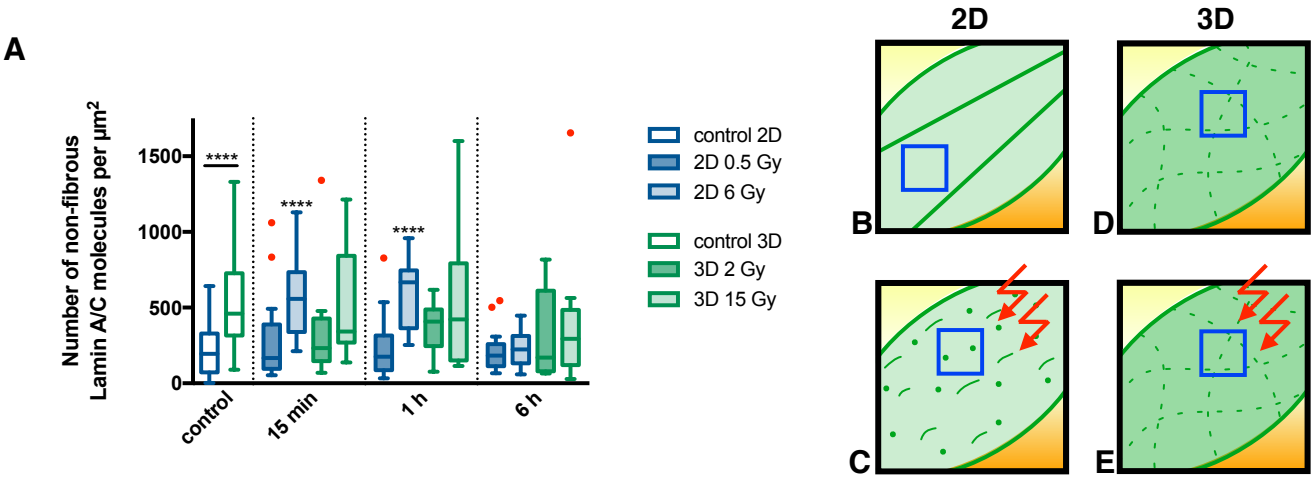

Figure 5.5: F-actin located lamin A/C molecules of 2D cells scatter after high dose irradiation. Single molecule localization data of inner nuclear membrane located lamin A/C molecules. (A) Box plots of the number of non f-actin located lamin A/C molecules of 2D and 3D cultured cells, fixed 15 min, 1h and 6 h after IR, as well as unirradiated controls. 2D cells were irradiated with 0.5 and 6 Gy, 3D cells were irradiated with 2 and 15 Gy. Statistical analysis was performed with an unpaired t-test and with a Kruskal-Wallis test (****$p \leq 0.0001$). For 2D cells N=2, n=20, for 3D cells N=2, n=10. (B - E) Sketch of the ROI (2.5 x 2.5 μm) placement for the data analyzed in (A). (B) Unirradiated 2D cells, ROI is placed between fibrous lamin A/C. For (C) irradiated 2D, (D) unirradiated 3D (E) and irradiated 3D cells the ROI is placed randomly as f-actin located lamin A/C is not present. Scale bar is 1 μm.

5.3.4 Only combined treatment of IR and AIIB2 significantly affects the nuclear lamina organization of 3D cells

To finally uncover the molecular link eventually leading to the radiosensitizing effect of AIIB2, irradiation experiments were combined with an AIIB2 treatment of cells cultured under both cell culture systems followed by actin and lamin A/C staining. Superresolution and confocal images of the actin - lamin A/C colocalization reveal that the actin organization 3D cells is not affected by the integrin inhibitor treatment, however 2D cells reveal a lesser amount of f-actin fibers spanning through the cell (see also S 5.10, E - F). Surprisingly, the molecular interference of the inhibitory antibody AIIB2 leads to a reorganization of inner nuclear membrane located lamin A/C in both cell culture systems.

As 2D cells still process apical f-actin the interaction with lamin is not influenced by the treatment - lamin colocalizes strongly with f-actin in presence of the inhibitor. Stunningly, the not-colocalizing signals of lamin A/C are dispersed (Figure 5.6, d - f). Under non-inhibitor conditions an irradiation with only 0.5 Gy did not affect the actin - lamin connection, only a high dose irradiation leads to f-actin destruction and lamin reorganization. The measurements of 2D cells treated with AIIB2 and 0.5 Gy show that the actin cytoskeleton is still not affected. However, lamin A/C is scattered across the inner nuclear membrane so that the actin - nucleus connection is disrupted (Figure 5.6, g - i). An irradiation with a high dose of 6 Gy leads to a combined f-actin break-down and lamin A/C scattering (Figure 5.6, j - l).

A quantitative analysis of the number of lamin A/C molecules support these results. With the AIIB2 treatment the signals of non-actin localized lamin molecules wanes (Figure 5.7 A; **$p \leq 0.01$), whereas an additional treatment with ionizing radiation leads to a scattering of the actin localized molecules across the nuclear envelope and therefore to a significant increase of lamin signals (***$p \leq 0.001$). The actin cytoskeleton of 3D cells is also not affected by the AIIB2 treatment. On the contrary, the overall signals of lamin A/C molecules are reduced while actin - lamin colocalizing regions still remain (Figure

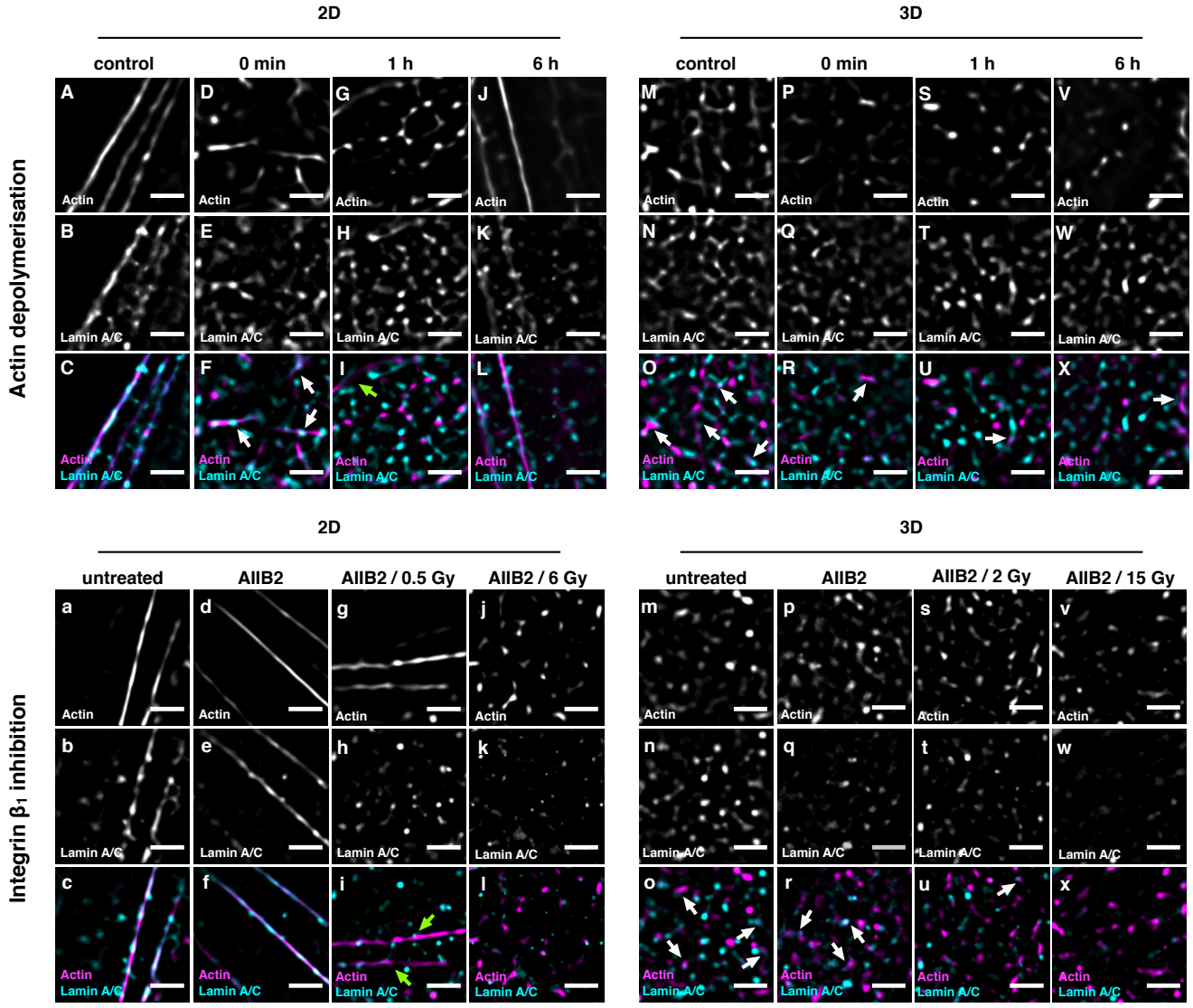

Figure 5.6: 3D cells are less disturbed by any treatment and only a combination of AIIB2 and IR leads to a significant effect on the nuclear lamina organization of 3D cells. Superresolution images of actin (A, D, G, J, M, P, S, V as well as a, d, g, j, m, p, s, v), lamin A/C (B, E, H, K, N, Q, T, W as well as b, e, h, k, n, q, t, w) and the corresponding overlay (C, F, I, L, O, R, U, X as well as c, f, i, l, o, r, u, x - actin: magenta, lamin A/C: cyan). Shown are superresolution images of 2D (A-L) cells fixed directly after CytD treatment (0 min, D-F), after a recovery time of 1 h (G-I) and 6 h (J-L), as well as untreated control cells (A-C). (M-X) Corresponding data for CytD treated 3D cultured cells. For the combined treatment of AIIB2 and IR untreated 2D cells (A-C), 2D cells only treated with AIIB2 (d - f), 2D cells treated with AIIB2 and irradiated with 0.5 Gy (g - i) and 2D cells treated with AIIB2 and irradiated with 6 Gy (j - l) are shown. (m - x) Corresponding data for 3D cultured cells, but irradiated with 2 Gy and 15 Gy. White arrows indicate regions with actin - lamin A/C colocalization (white), green arrows indicate regions where f-actin does not colocalize with lamin. Scale bar is 1 μm.

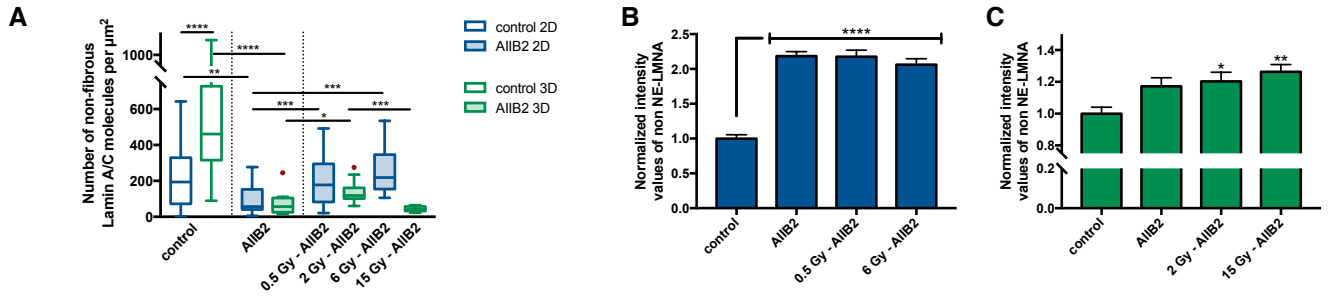

Figure 5.7: Combined treatment with AIIB2 and radiation leads to a loss of inner nuclear located lamin but to an increase of intranuclear lamin of 3D cells Single molecule data analysis and line profile analysis of confocal images of lamin A/C immunostainings. (A) Box plots of the number of non f-actin located lamin A/C molecules of 2D and 3D cultured cells of controls, AIIB2 treated cells and cells treated with AIIB2 and irradiation. 2D cells were irradiated with 0.5 and 6 Gy, 3D cells with 2 and 15 Gy. Statistical analysis was performed with an unpaired t-test and with a Kruskal-Wallis test. For 2D cells N=2, n=20 for 3D cells N=2, n=10 (2D control: N=5, n=50, 3D control: N=3, n=30). (B - C) Line profile analysis of confocal images of 2D (B) and 3D (C) cells, plotted are normalized intensity values of intranuclear lamin A/C. Same treatment as described above. Statistical analysis was performed with an one-way ANOVA. *p $\leq$ 0.05, **p $\leq$ 0.01,***p $\leq$ 0.001 and ****p $\leq$ 0.0001, N=2, n=20.

5.6, p - r and Figure 5.7 A, **p $\leq$ 0.01). A combined treatment with the integrin inhibitor and a low dose of IR did not further reduce the number of lamin signals beneath the NE (Figure 5.6, s - u and Figure 5.7 A). In contrast, a combined treatment of high dose irradiation and AIIB2 leads to a more or less complete loss of lamin molecules at the inner nuclear membrane (Figure 5.6, v - x and Figure 5.7 A).

To further investigate the combined effects of IR and integrin inhibition on the nuclear lamina, line profiles of confocal images were evaluated and the ratio of detected nuclear envelope located vs intranuclear lamin A/C signal were determined. While only an irradiation with a low or high dose did not influence this ratio, the treatment with AIIB2 alone leads to a significantly higher (****p $\leq$ 0.0001) intranuclear level of 2D cells. A combined treatment with low or high dose irradiation and AIIB2 treatment did not increase this ratio any further (Figure 5.7 B). The treatment with AIIB2 of 3D cells also leads to a higher, but not significant (p = 0.08), increase in intranuclear lamin A/C. Under non-inhibitor conditions only with a high dose irradiation a significant increase of non-NE lamin could be detected. Here, a combined treatment with AIIB2 and a low dose of IR lead to a significant increase of intranuclear signal (*p $\leq$ 0.05), the significance could be further increased with a high dose irradiation of 15 Gy (**p $\leq$ 0.01, Figure 5.7 C). Taken together, AIIB2 significantly enhances IR effects in 3D cultured cells, both at the level of integrin organization and - in consequence - organization and amount of NE-lamin.

5.4 Discussion

While studies on the cellular effects of IR are generally focused on DNA damage and its subsequent repair, it was identified that the adhesion of cells to a 3D environment leads to a higher resistance against ionizing radiation in comparison to cells grown under standard 2D conditions [41, 122]. To identify the link between adhesion and radioresistance, in principle all adhesion related proteins, such as integrins, immunoglobulins, cadherins, selectins, and syndecans come into focus as they all contribute to the complex process of the adhesion of cells to the extracellular matrix and adjacent cells. Among them, integrins are of particular interest as the key proteins that link the extracellular matrix with the intracellular cytoskeleton, enabling cells to sense and produce mechanical forces [123]. So far, mainly the connections between integrins and soluble multi-protein cascades have been thoroughly investigated in the context of adhesion related radioresistance (ILK, FAK, JNK1, AKT1, PINCH1, HDAC) [18, 19, 20, 21], while the mechanotransductive connection between the extracellular and intranuclear matrix, realized by integrins, actin, nuclear envelope proteins (nesprins, SUN proteins) and the nuclear lamina (lamin A/C), has not yet been studied in detail. To address this gap, the response of 2D and 3D cultured cells to ionizing radiation on the level of individual integrin $\beta 1$ clusters was previously investigated and it was found that culture dependent radioresistance (i.e. CAM-RR) is reflected in the ability of cells to maintain a stable organization of integrins into clusters leading to an intact and effective integrin signaling. Therefore, it can be concluded that an active disintegration of integrin clusters may in turn induce radiosensitivity, making the nanoscale distribution of integrins a potential drug target for radiosensitization [41]).

The aim of this study was to interfere with the clustering of integrins by using the inhibitory antibody AIIB2, a molecule already known to induce radiosensitization. However, a cell's ability to survive radiation treatments and, in particular, even maintain the ability to proliferate, is ultimately linked to nuclear activities. Hence, the view on the membrane located events of a cell's interaction with the ECM (i.e. integrin clustering) was extended by also following the nanoscale distribution of proteins that physically link integrins with the nuclear lamina. Thus, by combining treatments of ionizing radiation with integrin inhibition the consequences of AIIB2 induced radiosensitization was investigated by taking a detailed view on the molecular connection between the extracellular and the nuclear matrix, bringing mechanotransduction into focus to uncover the molecular events behind CAM-RR.

5.4.1 Culture conditions have a profound impact on the organization of proteins involved in nuclear mechanosensing

In this study, culture conditions in absence of any treatment were not only found to cause a marked difference in the ability to maintain well defined integrin clusters, but also in the organization of proteins involved the physical connection between the extracellular and the nuclear matrix. Hence, in order to elucidate the relevance of nuclear mechanosensing in the context of radiation treatment and culture conditions, the distribution and nanoscale organization of integrins, actin, nesprin, and lamin was followed.

As the pathways that propagate mechanical information from the extracellular environment to the nucleus converge on the main structural proteins of the nucleus, i.e. the lamins [95], this protein is central to investigate nuclear mechanosensing. In particular, as others have shown [100, 99], the differential distribution of lamin to form a thin layer beneath the NE (NE-Lamin) versus a rather dispersed intranuclear localization (IN-Lamin) is a useful indicator of the tensile forces that are transferred from the stiffness of the culture environment to the NE via actin and nesprin.

As it was shown earlier[41], mechanosensing in the here presented 3D culture system optimized for single molecule microscopy leads to a significantly higher ratio of NE- vs IN-Lamin and far less prominent f-actin fibers within the cytosol in comparison to the situation in 2D cultured cells. Intensity values of NE vs. IN-lamin were found to be 1.5x higher in 3D cells in comparison to 2D cells (****$p \leq 0.0001$, Figure 5.2 H and S5.10. More information about the influence of the culture conditions on nuclear

mechanosensing is obtained by a close look at the last step in the force propagation pathway from the extracellular to the nuclear matrix. Nanoscale colocalizations of actin and lamin at the NE reveal strong, fibrous colocalizations between both filamentous proteins in 2D cultured cells (Figure 5.4 C), whereas a far less intense colocalization and organization into fibers forms under 3D culture conditions (Figure 5.5 c).

Therefore, it can be concluded that the nucleus successfully senses the stiffness environment presented by these culture systems and that the different organization of the nuclear matrix protein lamin under both culture conditions is based on this sensing. Under stiff 2D culture conditions actin with its stress-strengthening properties [95] is under high tension, organized into distinct bundles and passes this status to the lamin network, which itself adopts a distinctly structured organization at the NE (Figure 5.8 B). Likewise, the flexible and pliable 3D culture conditions are reflected by the actin-lamin organization into a scattered and only partly colocalizing system (Figure 5.8 H).

5.4.2 Radiosensitivity is accompanied by peripheral lamin localization

As shown and mentioned above, already the culture conditions alone affect all components of the mechanosensing system (i.e. integrins, actin, nesprin, and lamin). Hence, 2D culture conditions can be viewed as a stress factor. With this in mind, it comes as no surprise that cells cultured under the two conditions show a different response to any additional stress treatment.

In response to high doses of IR, 3D cultured cells, with their intact and responsive nuclear mechanosensing, reorganize lamin A/C. Integrin clusters disintegrate to a small amount but actin or NE located lamin A/C do not fragment and more or less stay unchanged. Therefore, the actin-lamin connection can still sense the reduced tension resulting from integrin cluster breakdown, leading to a reorganization of the inner nuclear lamina (Figure 5.8 I). It is this less rigidly connected status between actin and lamin that seems to leave enough freedom for lamin to reorganize and redistribute to intranuclear regions in 3D cultured cells in situations of elevated stress and requirements for DNA repair.

In contrast, for cells cultured in 2D, the entire mechanosensing chain is affected by treatment with IR. Integrin clusters completely disintegrate and f-actin and NE located lamin fragment and separate from their previously strong colocalization (Figure 5.8 C). Accordingly, lamin does not redistribute towards the nucleus center, presumably as it does not receive the proper signal. Only at 1 h after x-irradiation - where f-actin and lamin A/C colocalization regions start to regenerate (Figure 5.6) - the nuclear lamina shows a higher amount of intranuclear signal (Figure 5.3). Intriguingly, it was possible to reproduce this effect by a mild CytD treatment, that yielded an actin-lamin distribution and level of colocalization that resembled the pattern found in 3D and 1 h after IR in 2D cultured cells (Figure 5.8 D). With this it can be concluded that also 2D cultured cells are able to reorganize their intranuclear lamina, if the strong actin-tension is alleviated which then allows for a more balanced mechano force propagation signaling. Otherwise, neither prominent f-actin bundles - as observed in all 2D cultured cells - nor depolymerized actin can act as a mechano component. In conclusion, the ability to redistribute lamin in response to IR is key to withstand IR treatment. As lamin is well known to have a strong impact on proteins involved in DNA repair, it is the lamin distribution that links the culture conditions with the intranuclear stress response to IR. From studies on laminophathys or $Lmna^{-/-}$ mice, which are characterized by low or zero levels of lamin A/C, it is known that, for example, the fast phase of DNA double strand break (DSB) repair, namely non-homologous end joining (NHEJ), is delayed [95] and 53BP1 recruitment is impaired [119, 120]. Hence, if these findings based on overall low levels of lamin are indicative for the situation found in 2D cultured cells with the low intranuclear lamin levels, then DNA repair is directly challenged by the 2D culture conditions.

Taken together, these results suggest that the integrin - actin - LINC - chromatin connection of 2D cells is too rigid to allow for lamin reorganization, while 3D cultured cells maintain a more balanced system that is able to respond to IR treatment with steps in favor of a fast DNA repair.

5.4.3 AIIB2 renders 3D cells radiosensitive due to breakdown of nuclear mechanosensing

Last but not least, to understand how the molecular components of the nuclear mechanosensing respond to the known radiosensitizer AIIB2, cells cultured under both culture conditions were treated with AIIB2 and IR.

A 24 h treatment of 2D cultured cells with AIIB2 led to a complete abolishment of integrin clusters with and without subsequent irradiation. Under these culture conditions, intranuclear lamin signals increased in both cases, even though f-actin bundles and the strong colocalization of apical f-actin and NE located lamin A/C remained intact in absence of an additional IR treatment. Thus, a release of actin from focal adhesions following AIIB2 treatment renders f-actin, that remains visible in 2D cultured cells, ineffective as a mechano component. The accompanied tension drop allows lamin to redistribute much like in cells grown in a soft 3D environment.

Even more, redistribution of lamin towards intranuclear regions in response to AIIB2 is so complete, that the nuclear envelope is virtually free of non-actin associated lamin. Likely, as AIIB2 not only impacts mechanotransduction but inhibits integrin $\beta 1$ signaling in general, diffusion based integrin signalling (e.g. via Akt [109] or NF-κB [106] pathways) may contribute to this behavior. Upon irradiation of AIIB2 treated cells, also the actin-lamin connection (i.e. colocalization) is lost, leading to the separation of both proteins and, as a result, the release of even more lamin from the NE. Hence, in order for lamin to colocalize with actin at the NE, actin tension is key.

On the contrary, the mechanical homeostasis of 3D cells is hard to break, which contributes to the observed radioresistance of 3D cultured cells. Targeting integrins with AIIB2 only leads to a reduction of clustering and consequently leaves some integrin-actin interactions still intact. Similar to 2D cells, were non-actin colocalizing lamin signals vanished upon AIIB2 treatment, the meshwork like structure of lamin A/C is reduced with AIIB2 (Figure 5.8 K). Importantly, however, it was found that AIIB2 significantly reduces the IR dose that leads to a complete integrin cluster breakdown in 3D cultured cells. While 15 Gy were required in the absence of AIIB2, the integrin inhibitor reduced this dose to only 2 Gy.

Only under the condition of a double treatment with AIIB2 and high (15 Gy) dose irradiation, a complete breakdown of the mechanosensitive system is observed in 3D cultured cells as apparent from the disappearance of NE located lamin A/C signals (Figure 5.8 L). In the 2D case these signals vanished under much milder treatment conditions.

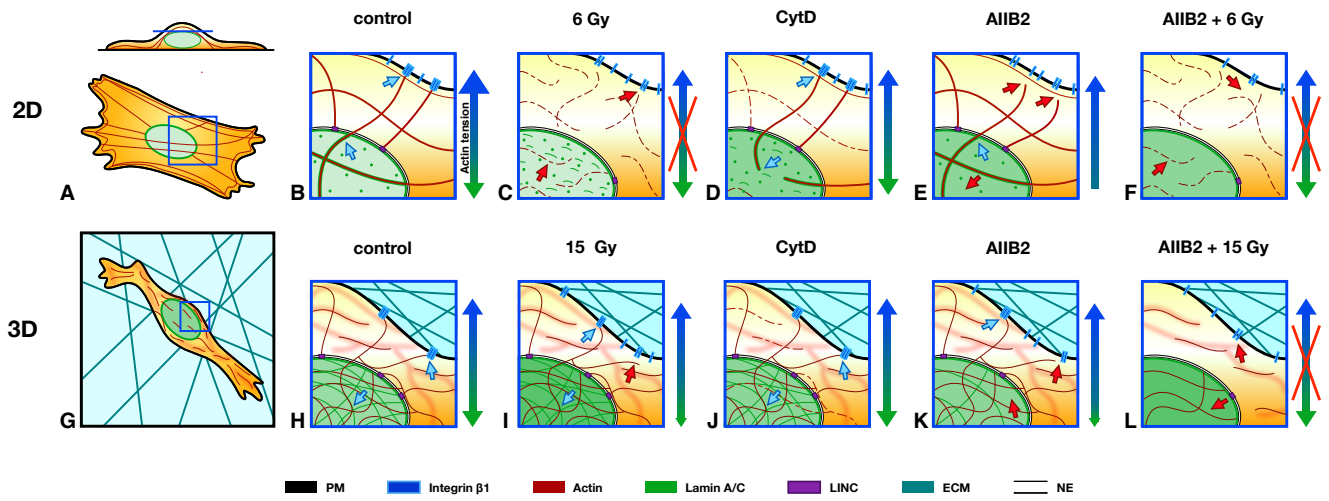

Figure 5.8: AIIB2 shifts the actin-tension equilibrium and induces IR sensitivity in 3D cells. (A) 2D cells possess a different organization of integrins, the nuclear lamina and actin if compared to 3D cells (G). (B) Apical f-actin of 2D cells leads to a strong, fibrous colocalization with Lamin A/C. This colocalization induces an imbalanced nuclear-force feedback leading to a loose and highly dynamic integrin organization and it prevents the reorganization of intranuclear lamin A/C. (C) This imperfect actin-force feedback combined with loose integrin clusters results in a complete break-down of force transmission upon irradiation with 6 Gy. Integrin clusters disintegrate, actin and lamin fragmentate leading to a scattering of lamin signals beneath the NE. Due to a complete loss of actin tension intranuclear lamin can not be reorganized. (D) Mild CytD treatment leads to a reorganization of intranuclear lamin as it only reduces the actin-lamin colocalization by not affecting the actin-integrin interactions. An actin-tension equilibrium is build up leading to the reorganization of intranuclear lamin. (E) AIIB2 treatment leads to integrin cluster disintegration and the loss of actin-integrin interactions. As the actin cytoskeleton remains intact the actin-lamin colocalization is not affected but non-colocalized lamin signals are loss. Whereas actin is not bound by integrins the actin-tension is shifted so that intranuclear lamin A/C can be reorganized. (F) An irradiation of cells under the condition of (E) leads to additional actin fragmentation and to a complete loss of actin-lamin colocalization as NE-located lamin signals are scattered leading to a actin-tension break-down. Intranuclear lamin is not further reorganized. (H) 3D cells exhibit a mechano-homeostasis. Firm and stable integrin clusters as well as only few actin-lamin colocalizations lead to an actin-tension equilibrium and to a higher amount of intranuclear lamin A/C if compared to 2D cells. (I) An irradiation with 15 Gy leads to a slight integrin cluster disintegration but not all integrin clusters and therefore not all integrin-actin interactions are disrupted. Actin-lamin interactions are not affected leading to a minor shift of the nuclear-force feedback and to a higher concentration of intranuclear lamin A/C. (J) Mild CytD treatment does not affect 3D cells. (K) AIIB2 treatment leads to a slight integrin cluster break down but not all integrin clusters and therefore not all integrin-actin interactions are affected leading to a minor change of the nuclear force-feedback. Integrin inhibition reduces the amount of NE-lamin A/C, intranuclear lamin is not significantly altered. (L) An irradiation of cells under the condition of (K) leads to a complete integrin cluster as well as actin-tension break-down. Integrin-actin interaction as well as actin-lamin colocalization are disrupted. NE-lamin A/C signals vanish, non-NE lamin A/C signals increase. The ability of AIIB2 to break integrin clustering leads to a destabilization of the actin-tension equilibrium and in turn induces sensitivity towards IR of 3D cells. Blue arrows indicate intact interactions between actin-lamin A/C or integrin-actin. Red arrows indicate disrupted interaction sides. Double arrows beside the zoom-ins indicate the change in action-tension.

5.5 Conclusion

In this chapter a connection between radiosensitivity and mechanobiological cues is drawn. With the use of single molecule localization microscopy, it was possible to follow the nanoscale distribution of integrin $\beta 1$, actin, nesprin and lamin, and it could be shown that intranuclear lamin redistribution is impaired under 2D culture conditions due to a non-functional mechanosensing system.

The involvement of mechanobiological cues in the radiosensitive response of 2D cultured cells is visible on many scales: (i) integrin clusters fall apart upon low dose irradiation (possible due to non-functional mechano-feedback that would favor their formation), (ii) the actin-lamin interface at the NE is patterned in an artificially ordered manner (not seen in 3D), (iii) IN-lamin is distributed differently if compared to 3D cells and (iv) after deliberate disruption of the mechano-system at numerous levels (inhibition of integrins with AIIB2, recovery of actin and lamin at the NE after IR, incomplete depolymerization of actin after mild CytD treatment), lamin redistribution returns. From that it can be concluded that the pre-tension of the mechanosensing machinery of 2D cultured cells is on a high level that does not allow for an adaptive response. If disturbed, this tension is released and permits lamin to redistribute within the nucleus. Hence, impaired lamin distribution may - in the same way laminopathies and Lmna $^{-/-}$ mice show DNA repair problems - be one of the prime reasons for 2D cells to be radiosensitive. Notably, and especially in the context of mechanobiology, 2D cultured cells should not be viewed as a „control“, as this culture condition represents a highly artificial mechano environment. In this sense, 3D cultured cells should not be termed „radioresistant“. Rather, 2D cells are „radiosensitive“.

3D cultured cells, in turn, have a level of pre-tension enabling them to properly respond to stressors, as it becomes evident from numerous observations: (i) Integrins are clustered, (ii) the actin/lamin interface at the NE is less rigidly structured, allowing it to respond to changing tension scenarios, and (iii) the presence of IN-lamin. The stability of this force feedback system can not be disrupted upon low dose irradiation, CytD or AIIB2 treatment alone. Only a combined treatment of IR and AIIB2 leads to an interruption of the mechanobiological balance with clear effects at both ends of the mechanobiological system: On one end, integrins decluster as the tension feedback is lacking, and on the other end, lamin redistribution, as a tension signal, is lost.

In closing, it once more becomes evident that 2D cell cultures present a highly artificial environment that does not provide the means to investigate mechanobiological aspects. The latter, however, should move into the focus of IR research, as potential new drug targets in the form of proteins or mechanisms may emerge, if the concepts of this important field are considered.

5.6 Material and Methods

5.6.1 Cell culture

Mouse embryonic fibroblasts (MEF cells) were cultured in DMEM / Ham's F-12 (1:1) (Biochrom, Berlin, Germany) supplemented with 10% FCS (Sigma-Aldrich, St. Louis, Missouri, USA) and 1% NEAA (Biochrom, Berlin, Germany) in a humidified chamber at 37 °C and 5% CO_2. Cell cultures were prepared on round coverslips (Karl Hecht GmbH, Sondheim, Germany, NO 1.5, $\varnothing$ = 25 mm). The preparation of 3D cells was described in Babel et al. [41]). In brief, MEF cells were cultured in 15 μl sized 1.5 mg/ml collagen I hydrogels (3 mg/ml rat-tail collagen I stock solution, Thermo Fischer Scientific, Waltham, Ma, USA) on APTS (3-Aminopropyl)triethoxysilane, Sigma-Aldrich, St. Louis, Missouri, USA) coated coverslips. Cells were incubated 4 to 5 days prior to use.

5.6.2 Radiation

Cells were irradiated with an Isovolt 160 Titan E (GE Sensing & Inspection Technologies, Alzenau, Germany) x-ray source. Cells were irradiated with a voltage of 90 kV and a current of 19 mA (0.5 and 2 Gy) or 33.7 mA (6 and 15 Gy). Doses were delivered at a 30 cm source to probe distance with cell cultures placed on a 2 mm aluminum filtering plate with respect to the glass doubling factor [124]. Cells were fixed at specific time points after irradiation.

5.6.3 Integrin β1 inhibition

Cells were incubated 24 h (humidified chamber at 37 °C and 5% CO_2) in medium supplemented with 10 μg/ml of the integrin β1 inhibitor AIIB2 (Merck KGaA, Darmstadt, Germany) prior to experiments.

5.6.4 Inhibition of actin polymerization

Cells were incubated for 30 min (humidified chamber at 37 °C and 5% CO_2) in serum-free medium supplemented with 0.8 μM CytochalasinD (Enzo Life Science GmbH, Lörrach, Germany). Cells were fixed directly after treatment.

5.6.5 Immunofluorescence

The following antibodies and dyes were used: anti Nesprin-2 (sc-99181, Santa Cruz, Dellas, Texas, USA), anti Lamin A/C (ab8984, abcam, Cambridge, UK), anti rabbit Alexa Fluor 488 (Thermo Fisher Scientific, Waltham, Ma, USA) and anti CD29 Alexa Fluor 488 (integrin β1, Biozol Diagnostica, Eching, Germany). Actin was stained with Phalloidin CruzFluor 555 (Santa Cruz, Dellas, Texas, USA), DNA was stained with Hoechst 33342 (Sigma-Aldrich, St. Louis, Missouri, USA). For SMD measurements all antibodies were diluted 1:10.000 for 2D and 1:5000 for 3D cells, for CLSM measurements primary antibodies were diluted 1:100 and secondary antibodies 1:200. 1000x stock solution of Phalloidin CruzFluor 555 was diluted 1:25.000 in 1% BSA (AppliChem, Darmstadt, Germany) for SMD measurements and was used as an dilution of 1:1000 in 1% BSA for CLSM measurements. For DNA staining Hoechst 33342 stock solution (2 mg/ml) was diluted 1:1000. Cells were fixed with 4% PFA (Carl Roth GmbH Karlsruhe, Germany) supplemented with 0.2% glutaraldehyde (Serva Electrophoresis, Heidelberg, Germany) in PBS (Sigma-Aldrich, St. Louis, Missouri, USA, pH 6.9) for 1 h at 4 °C. For stainings with nesprin-2, Lamin A/C or Phalloidin, cells were permeabilized with 0.2% Triton-X100 in PBS (AppliChem, Darmstadt, Germany)

for 10 min at RT prior to blocking with 1% BSA (3% for Lamin A/C staining) for 1 h at 37 °C. Cells were incubated with a primary antibody (or directly labeled anti integrin β1 antibody) for 3 h at 4 °C followed by an additional blocking step with 1% BSA at 37 °C for 1 h. Afterwards, cells were incubated with the secondary antibody for 3 h at 4 °C. For an additional actin staining cells were blocked with 1% BSA for 30 min followed by Phalloidin staining for 1 h at 4 °C. For DNA counterstaining cells were incubated in Hoechst dye for 5 min at RT. After every fixation, permeabilization and staining step, cells were washed 3 times with PBS-T.

5.6.6 Microscopy

Microscopy buffer
For SMD measurements a standard STORM buffer [125] containing 100 mM MEA (beta-mercaptoethylamine, pH 8.5, Sigma-Aldrich, St. Louis, Missouri, USA), 140 U catalase (Sigma-Aldrich, St. Louis, Missouri, USA, C3515) and 10 U glucose oxidase (Sigma-Aldrich, St. Louis, Missouri, USA, G0543) in Tris-buffer (50 mM Tris, 10 mM NaCl (both AppliChem, Darmstadt, Germany), pH 8) supplemented with 10% (w/v) glucose (AppliChem, Darmstadt, Germany) was used.

CLSM measurements
CLSM-measurements were performed using the Leica TCS SP5 II or the Leica SP8 (Leica Microsystems, Mannheim, Germany) equipped with a 63x 1.2 Water corr objective or with a 63x 1.3-0.6 oil objective.

SMD measurements
All SMD measurements were performed with a custom-built instrument. A detailed description of the setup was published previously [41].

5.6.7 Image acquisition and data analysis

Editing of images was performed using Fiji (version: 1.51h) [126]. To analyze the effects of ionizing radiation on β1 integrins of AIIB2 treated cells or to quantify the number of non-fibrous Lamin molecules, single molecule signals were detected and filtered using the ThunderStorm plugin for Fiji [127]. For the add-on cluster analysis custom written software in MATLAB R2014b was used. For non-quantitative analysis of single molecule data the NanoJ plug-in for Fiji was used [128]. For all SMD analysis 4x4 μm ROIs were quantified.

Cluster Analysis - Ripley's K function
The Ripley's K function is a standard method to analyze single molecule data. In brief, this function identifies the average number of signals within rings centered on each molecule [129, 88]. By plotting this number against the respective radii a distribution (the so called H plot) is yielded, where the maximum represents the most prominent cluster distribution. The height of the first local maximum (H(r)max) gives a measure of the degree of clustering and its position the radius of the most frequent clusters [129, 88, 89]. Based on the publication of Williamson et al [78], heat maps were created. A detailed description of our cluster analysis can be found in Babel et al. [41]. To remove duplicates, molecules that convert to the same position were removed within the distance of the uncertainty of each dataset.

5.6.8 Statistical analysis

Statistical analysis was performed with GraphPad Prism 7. For multiple comparisons, significances were analyzed with an one-way ANOVA test with a Tukey post hoc test. Homogeneity of variances was tested with the Brown-Forsythe test, if this test resulted in a small P value the Kruskal-Wallis test with a Dunn's

multiple comparison test was used. For simple comparisons, significances were analyzed with an unpaired, two-tailed t-test. For all cases, $p \leq 0.05$ was considered significant (*), $p \leq 0.01$ very significant (**) and $p \leq 0.001$ extremely significant (***). Also $p \leq 0.0001$ (****) was noted. All presented box plots show as a central line the median, the top and bottom of each box are the first and third quartile, top and bottom line represent the maximum and minimum values. Outliers are colored in red.

5.7 Supplementary figures

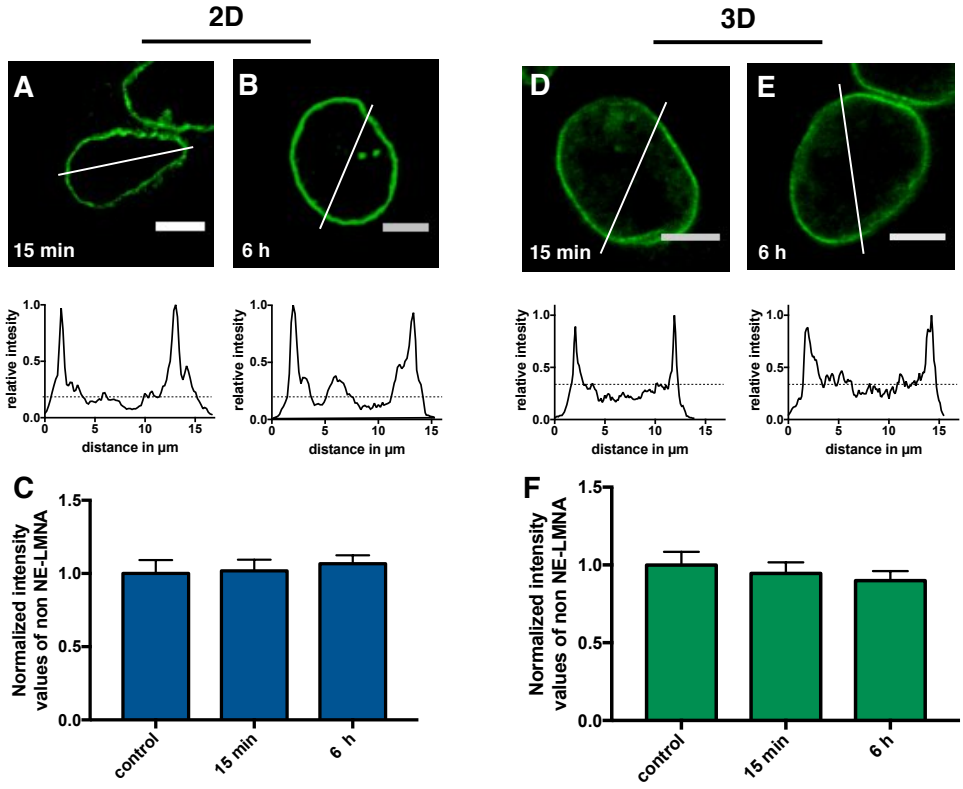

Figure 5.9: Low dose irradiation has no effect on the intranuclear lamin organization. Immunostainings of Lamin A/C with relative intensity line profiles as marked in the confocal slices. Dotted lines in the profiles represents the mean intensity value of intranuclear lamin of control cells. Shown are Lamin A/C stainings of 2D cells fixed 15 min (A) and 6 h (B) after an irradiation with 0.5 Gy. (C) Bar plot of normalized intensity values of intranuclear lamin A/C. (D - E) Corresponding data for 3D cultured cells, cells were irradiated with 2 Gy. Statistical analysis was performed with a Kruskal - Wallis test, N=2, n=20. No significance was detected. Scale bar is 5 μm.

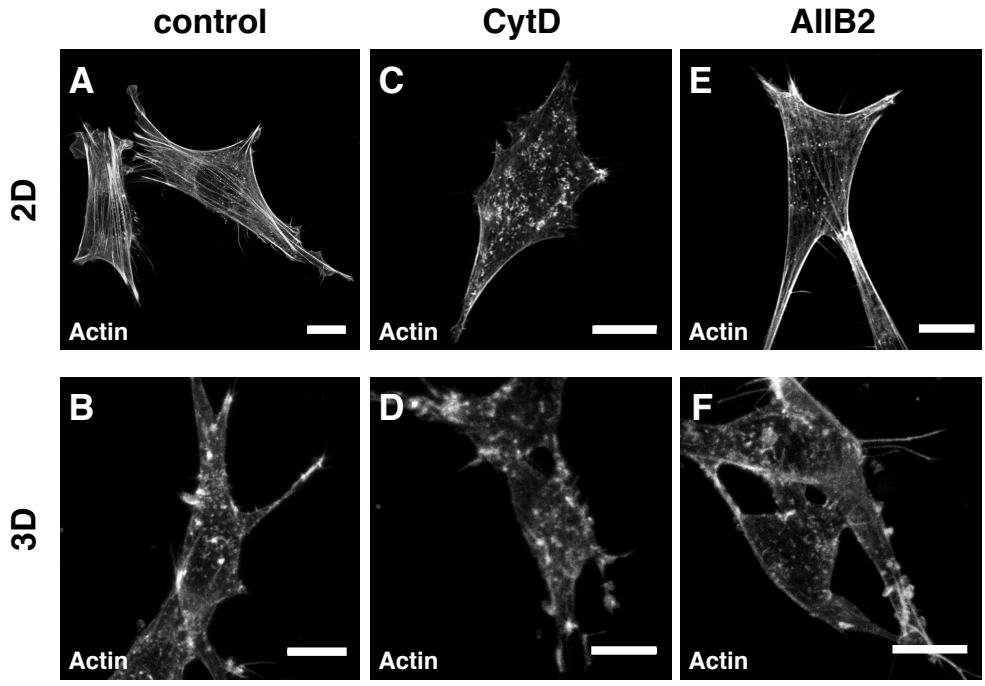

Figure 5.10: Actin organization is cell culture dependent. Phalloidin staining of actin from 2D (A, C, E) and 3D (B, D, F) cultured cells, fixed after CytD (C - D) or AIIB2 (E - F) treatment, as well as untreated controls (A - B). For 2D cells the scale bar is 15 μm, for 3D cells the scale bar is 10 μm.

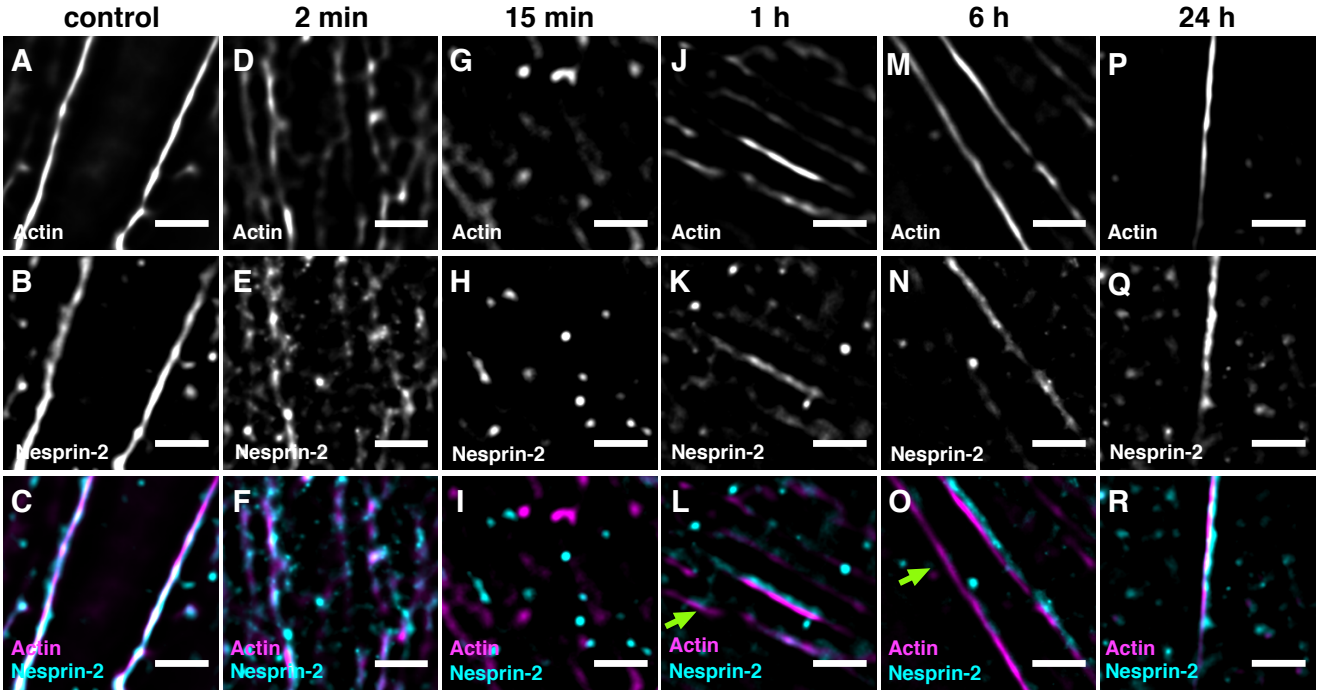

Figure 5.11: High doses of IR destroy nesprin-2 - f-actin connection in 2D cells. Superresolution images of actin (A, D, G, J, M, P), nesprin-2 (B, E, H, K, N, Q, T) and the corresponding overlay (C, F, I, L, O, R, U - actin: magenta, nesprin-2: cyan) of control cells (A-C) and cells irradiated with 6 Gy, fixed after 2 min (D - F), 15 min (G - I), 1 h (J - L), 6 h (M - O) and after 24 h (P - R). Arrow (green) in (R) indicate region where f-actin does not colocalize with lamin. Scale bar is 1 μm.

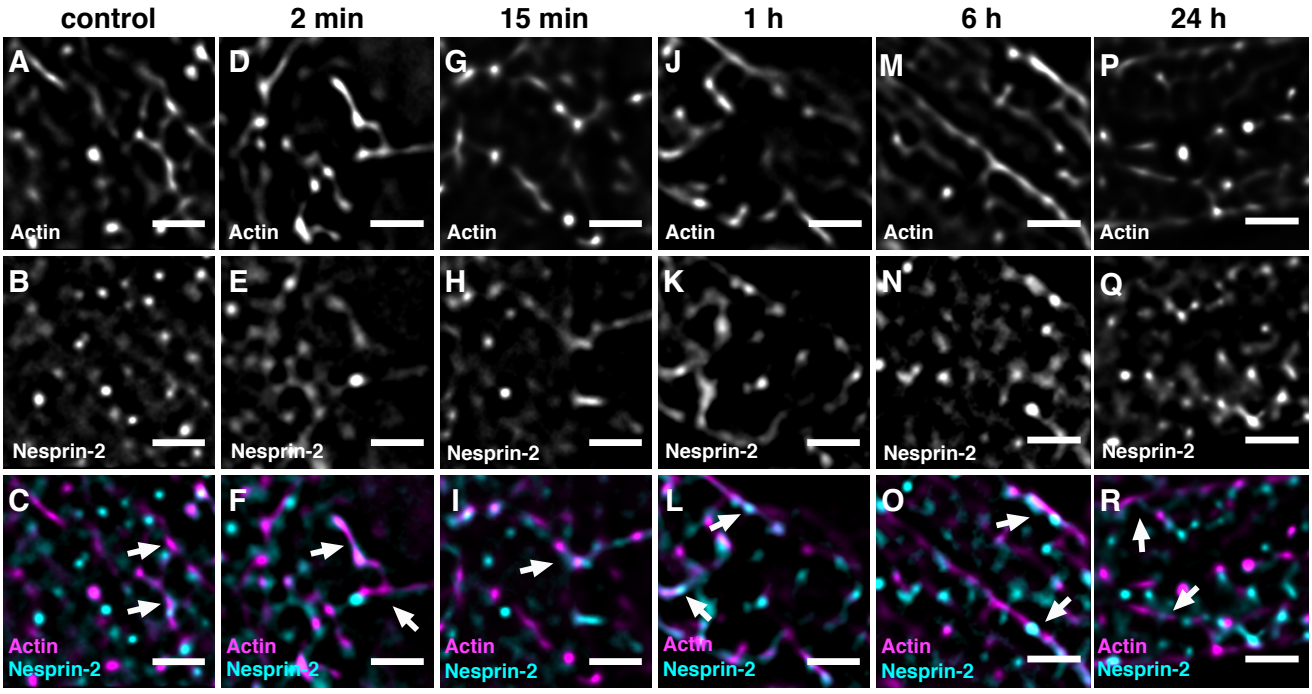

Figure 5.12: High doses of IR do not affect the nesprin-2 - f-actin connection of 3D cells. Superresolution images of actin (A, D, G, J, M, P), nesprin-2 (B, E, H, K, N, Q, T) and the corresponding overlay (C, F, I, L, O, R, U - actin: magenta, nesprin-2: cyan) of control cells (A-C) and cells irradiated with 15 Gy, fixed after 2 min (D - F), 15 min (G - I), 1 h (J - L), 6 h (M - O) and after 24 h (P - R). White arrows indicate regions with actin - lamin A/C colocalization (white). Scale bar is 1 μm.

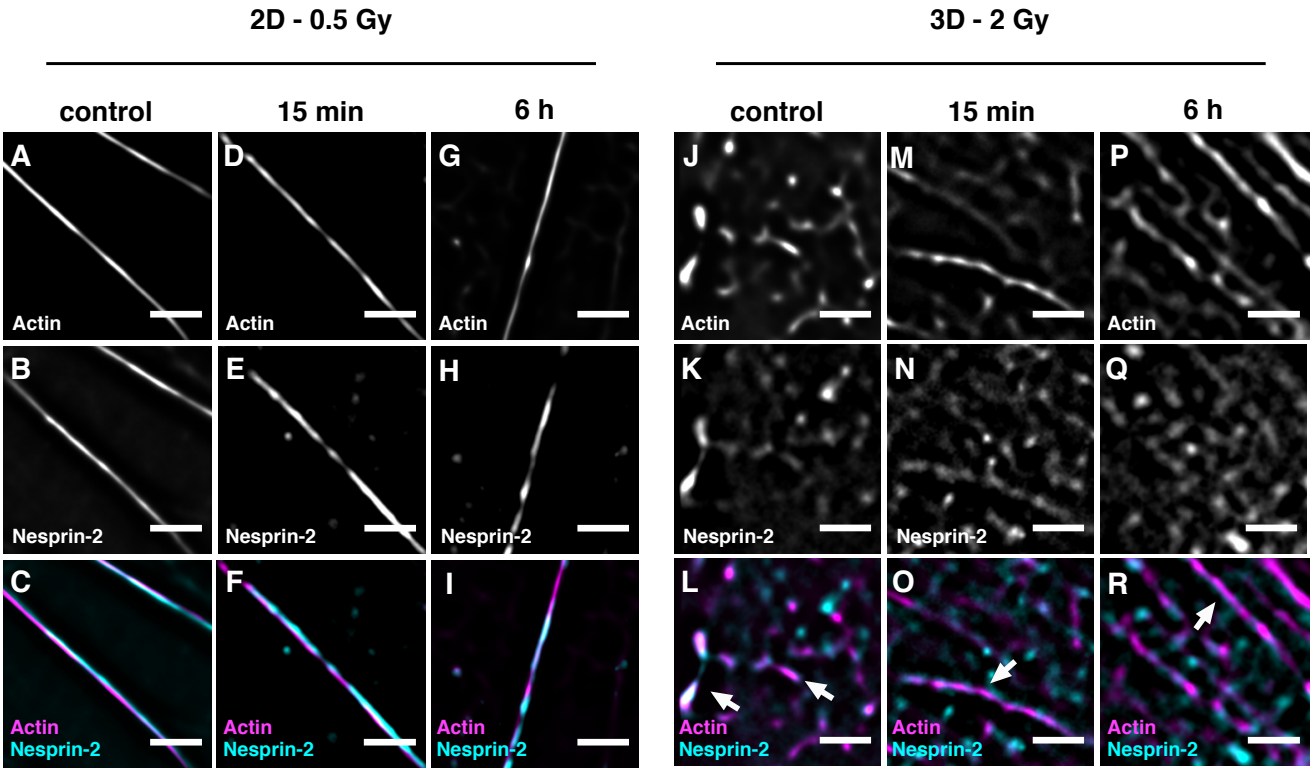

Figure 5.13: Low doses of IR do not affect the nesprin-2 - f-actin connection. Superresolution images of actin (A, D, G, J, M, P), nesprin-2 (B, E, H, K, N, Q, T) and the corresponding overlay (C, F, I, L, O, R, U - actin: magenta, nesprin-2: cyan) of 2D (A - I) and 3D (J - R) cultured cells. 2D cell were irradiated with 0.5 Gy and were fixed 15 min (D - F) and 6 h (G - I) after irradiation, also untreated control cells were fixed (A - C). (J - R) Corresponding results for 3D cells, irradiated with 2 Gy. White arrows indicate regions with actin - lamin A/C colocalization (white). Scale bar is 1 μm.

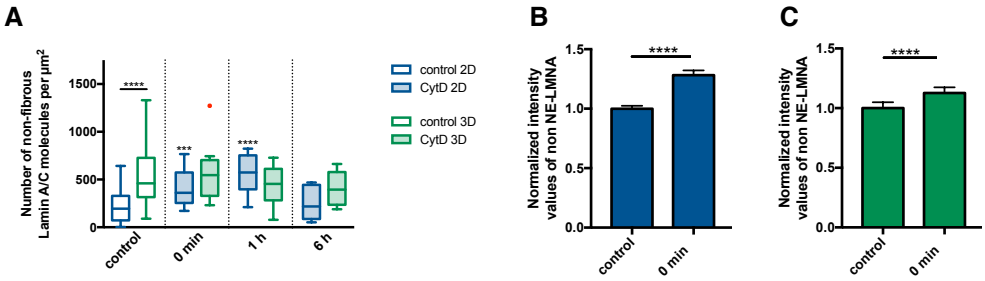

Figure 5.14: Actin polymerization inhibition only affects the nuclear lamina of 2D cells. Single molecule data analysis and line profile analysis of confocal images of lamin A/C immunostainings. (A) Box plots of the number of non f-actin located lamin A/C molecules of 2D and 3D cultured cells fixed directly after CytD treatment (0 min), after a recovery time of 1 h and 6 h, as well as untreated control cells. Statistical analysis was performed with an unpaired t-test and with an one-way ANOVA. For 2D cells N=2, n=20, for 3D cells N=2, n=10 (2D control: N=5, n=50, 3D control: N=3, n=30). (B - C) Line profile analysis of confocal images of 2D (B) and 3D (C) cells, plotted are normalized intensity values of intranuclear lamin A/C. Same treatment as described above. Statistical analysis was performed with an unpaired t-test. **$p \leq 0.01$ and ****$p \leq 0.0001$, N=2, n=20.

Chapter III

Lipid-rafts remain stable even after ionizing radiation induced disintegration of β1 integrin containing focal adhesions

6.1 Abstract

Objective: Cell adhesion with the extracellular matrix is facilitated by integrin adhesion receptors. Recently it was found that the plasma membrane (PM) located, nanoscale organization of integrins containing the $\beta 1$ subunit is responsible for a process termed cell-adhesion-mediated-radio-resistance (CAM-RR). Here, cells embedded in a 3D matrix are far more radioresistant in comparison to standard, monolayer-based 2D cultured cells. While ionizing radiation (IR) is known to have broad effects on PM located lipids and their organization in lipid-rafts, it is not clear whether the effects of IR on the nanoscale clustering of integrins are lipid-raft dependent.
Results: With the use of single molecule microscopy it could be shown that $\beta 1$ integrins and cholesterol lipid-rafts colocalize and that ionizing radiation, as an extrinsic stressor, causes the separation of $\beta 1$ integrins from their localization in cholesterol lipid rafts. Hence, the effects of IR on the clustering of $\beta 1$ integrins are lipid-raft independent.

6.2 Introduction

Radioresistance was found to be higher in cells cultured in presence of a 3D matrix, a process which has been termed cell-adhesion-mediated-radio-resistance (CAM-RR) [15, 16, 130]. Here, cells embedded in a 3D matrix are radioresistant if compared to standard, monolayer-based 2D cell cultures. Cell adhesion is facilitated by integrin receptors [131] and recently it was found that integrin $\beta 1$ clustering is a sensitive and robust indicator of radioresistance [41]. Cells cultured under standard (2D) conditions are not able to organize integrins into firm and stable clusters, but instead display a rather loose and dynamic cluster organization of the ECM (extracellular matrix) receptor. On the contrary, cells embedded in an ECM, exhibit a well maintained integrin organization. With the use of ionizing radiation, the unstable integrin organization of 2D cultured cells is severely disturbed by low doses of radiation, which do not have any effect on the well clustered organization of integrins in 3D cultured cells. Therefore it was possible to link the radioresistance of 3D cells with their ability to maintain stable clusters [41].
It is well accepted that IR has profound effects on the PM. Mainly lipid peroxidation, generation of ceramides and its organization in ceramide lipid rafts are well studied. Thereby, the generation of reactive oxygens (ROS) damages and modifies lipids directly with profound effects on lipid signaling, organization and dynamics [132, 112, 113]. Physical differences in lipids such as chain length, chain geometry and head group cause different membrane components not to be homogeneously distributed on the cell surface but rather to aggregate in domains. Specifically, sphingolipids and cholesterol aggregate in microdomains known as lipid rafts [80, 81]. Lipid rafts are highly dynamic structures (10 - 200 nm) that limit the free diffusive properties of biomembranes as proposed by Singer and Nicolson in their fluid mosaic model [133]. These micro structures are known to function as parts of signaling cascades or as platforms for membrane protein clustering and therefore for protein activity [40]. Proteins localize in lipid rafts either due to a direct interaction with the lipid head group or due to physical forces such as lateral pressure, charge interactions or the local curvature of the membrane [83]. It is known that integrins and cholesterol rich regions colocalize [134, 84].
With the use of ionizing radiation as an strong extrinsic manipulator of integrin clustering it is possible to interfere with the native co-cluster organization of cholesterol and integrin $\beta 1$. If lipid rafts are responsible for the observed effects on integrin clustering, it can be expected that (i) the cholesterol raft organization, as published for the integrin organization, is ECM dependent, and (ii) IR breaks cholesterol raft organization in concert with integrin cluster break down. Surprisingly, it was found that integrins disintegrate in a lipid raft independent manner. Even after high doses of IR cholesterol stays clustered, while $\beta 1$ integrins are separated from its raft localization.

6.3 Results and discussion

6.3.1 PM mobility and lipid raft organization are strongly affected by the cell culture condition

To investigate the mobility and nanoscale organization of the PM of cells in dependence of their culture conditions, an isoprenyl anchored membrane protein (CAAX-mCherry) as a reporter for the membrane's fluidity [135] and the clustering of cholesterol as a marker for lipid rafts were used and analyzed in 2D and 3D cultured cells.

For membrane mobility analysis, cells were transfected with CAAX-mCherry and FRAP (Fluorescence Recovery after Photobleaching) analysis were performed. The recovery curves reveal (Figure 6.1 A) that 3D cultured cells possess a higher membrane fluidity as fluorescence recovery occurred faster in comparison to 2D cultured cells. An exponential fit yields a halftime recovery value of 10.63 s and a mobile fraction of 88% for 3D cells. Corresponding analysis for 2D cells on the top membrane reveal a considerable higher value for the halftime recovery value (27.41 s) and a similar value for the mobile fraction of 83%. These results show that already the bare fluidity of the PM differs if cells are cultured under 2D or 3D conditions. Hence, as basically all signaling cascades relay on a dynamic (re)organization of the PM [136], the dynamics of PM located signaling in 2D and 3D cultured cells are bound to differ as well.

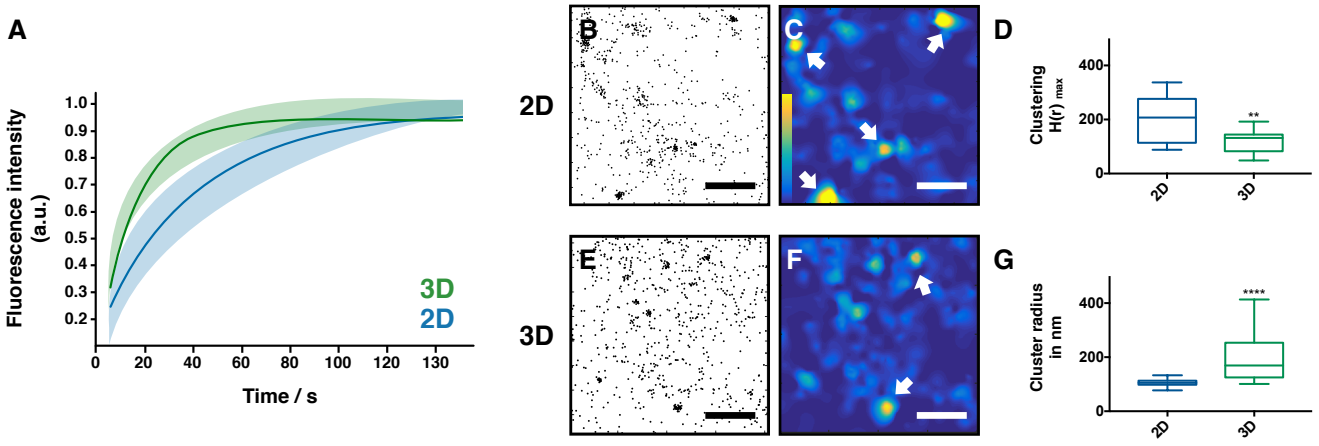

Figure 6.1: 2D vs. 3D cell culture conditions have a strong impact on the membrane mobility and cholesterol raft organization. (A) FRAP curves of CAAX-mCherry of 2D (blue, n=8) and 3D (green, n=9) cultured OV-MZ-6 cells. Plotted are exponential recovery fits and the standard derivations. This plot is adapted from the PhD Thesis of Dr. S. Bump [137]. (B - G) Single molecule data of cholesterol stainings from 2D and 3D MEF cells as well as corresponding cluster analysis. (B and E) Scatter plots show all detected cholesterol molecules, (C and F) corresponding heat maps visualize clustered (yellow) and unclustered (dark blue) regions, arrows indicate cholesterol rafts. Scale bar is 1 μm. Statistical analysis with the Ripley's K function reveals the clustering (D) and the cluster size (G). Statistical analysis was performed with a Mann-Whitney test. **p $\leq$ 0.01 and ****p $\leq$ 0.0001.

To further investigate if lipid rafts, often attributed as the organizers of PM located signaling [81], are affected by the different culture conditions, 2D and 3D cultured cells were stained with a cholesterol affine fluorescent probe (Dronpa-Θ4), imaged by single molecule localization microscopy and quantitatively assessed by a detailed cluster analysis (Figure 6.1, B - G). As it is, unfortunately, impossible to completely immobilize lipids via chemical fixation [138, 86], it was assured that the remaining mobility does not alter the cluster organization (Figure 6.4).

The effects of the cell culture condition on the cholesterol raft organization can directly be recognized by a visual inspection of the single molecule localization results. Each point in the scatter plot of Figure 6.1 (B and E) represents an individual detection of a cholesterol molecule. Both scatter plots reveal that cholesterol is organized in microdomains where a higher density of signals was detected. These domains, long known as sphingolipid-cholesterol lipid-rafts [139] vanish upon cholesterol depletion (Figure 6.5). To put the visual inspection on quantitative grounds, a Ripley's K function cluster analysis was performed [87, 88]. This function counts the number of signals that fall within a defined radius of each detected signal. By plotting this number versus the respective radii a distribution (H-plot) is yielded, whose first local maximum represents the most prominent cluster formation of the data set. The height of this maximum gives (i) a measure of the clustering (H(r) max) and (ii) its position the cluster radius (r max). For a better visualization of the single molecule localizations, 2D plots of the H(r) max values are represented as heatmaps to visualize clustered regions with a higher density of signals as yellow areas (Figure 6.1, C and F). The heat maps reveal that 2D cultured cells possess more cholesterol rafts with a higher degree of clustering (marked as yellow regions). Quantitative K function analysis underline these findings (Figure 6.1, D and G). 2D cultured cells possess a significantly (**$p \leq 0.01$) higher degree in clustering compared to 3D cultured cells and have a smaller radius (****$p \leq 0.0001$: 2D $\sim$ 100 nm, 3D $\sim$ 160 nm).
Taken together, not only the membrane mobility but also the organization of lipids into rafts are remarkably affected by the cell culture condition leading to the assumption that PM located signaling differs between 2D and 3D cultured cells. These results are well in line with the previous findings that not only integrin $\beta 1$ clustering, but also the number of its first activated downstream signaling partner pFAK (phosphorylated focal adhesion kinase) significantly differ between the culture conditions, telling that 2D cultured cells possess an impaired signaling efficiency [41]. At this point it can be concluded that the localization and organization of cholesterol rafts differs in dependence of the culture conditions.

6.3.2 Lipid-rafts do not change their cluster organization in response to high dose irradiation

To see whether the colocalization of integrin $\beta 1$ and cholesterol is maintained or lost after high dose irradiation, stainings for both micro organizations were performed. Co-stainings followed by single molecule localization analysis reveal a culture condition independent coclustering of cholesterol rafts and integrin $\beta 1$ clusters (Figure 6.2, A and I).
Previously, it was found that 2D cultured cells maintain a less well organized status of integrin $\beta 1$ into firm and stable clusters and said clusters to be easily disturbed even by low doses (2 Gy) of radiation. In contrast, the same IR dose turned out to be completely ineffective to affect the well clustered organization of integrins in 3D cultured cells. Hence, an irradiation with a high dose leads to a complete integrin cluster break down in 2D but only a partial disintegration in 3D cultured cells [41]. Now, if integrin cluster organization would mainly be determined by lipid rafts one would expect IR to cause a simultaneous disintegration of both. 2D cells fixed 15 min after an irradiation with 15 Gy lose their integrin clusters and total integrin signals, but the cholesterol raft organization remains unchanged (Figure 6.2 B) revealing that the integrin cluster break-down is a lipid raft unrelated effect. Heat maps support this finding (Figure 6.2, C - H). While the clustering of cholesterol remains unchanged, integrin clusters and signals are lost 15 min after irradiation and are only partly regenerated after 6 h.
In contrast to 2D cells, 3D cells not only maintain the clustered organization of $\beta 1$ integrins against much higher doses but also show a faster recovery. An irradiation with 15 Gy leads to a slight decrease in integrin clustering and therefore only to a reduction of integrin-cholesterol coclustering (Figure 6.3 J - P) 15 min after IR and to a complete recovery after 6 h. Equally, as reported for 2D cells, cholesterol rafts are not affected by a high dose irradiation with 15 Gy. Followed by visual inspection we used the Ripley's K function to generate H-plots to put our data on quantitative ground (Figure 6.3). The H-plots reveal that the cholesterol organization is unaffected by high dose irradiation in a cell culture independent manner. Our detailed cluster analysis reveals that also parameters, such as cholesterol raft density and number of

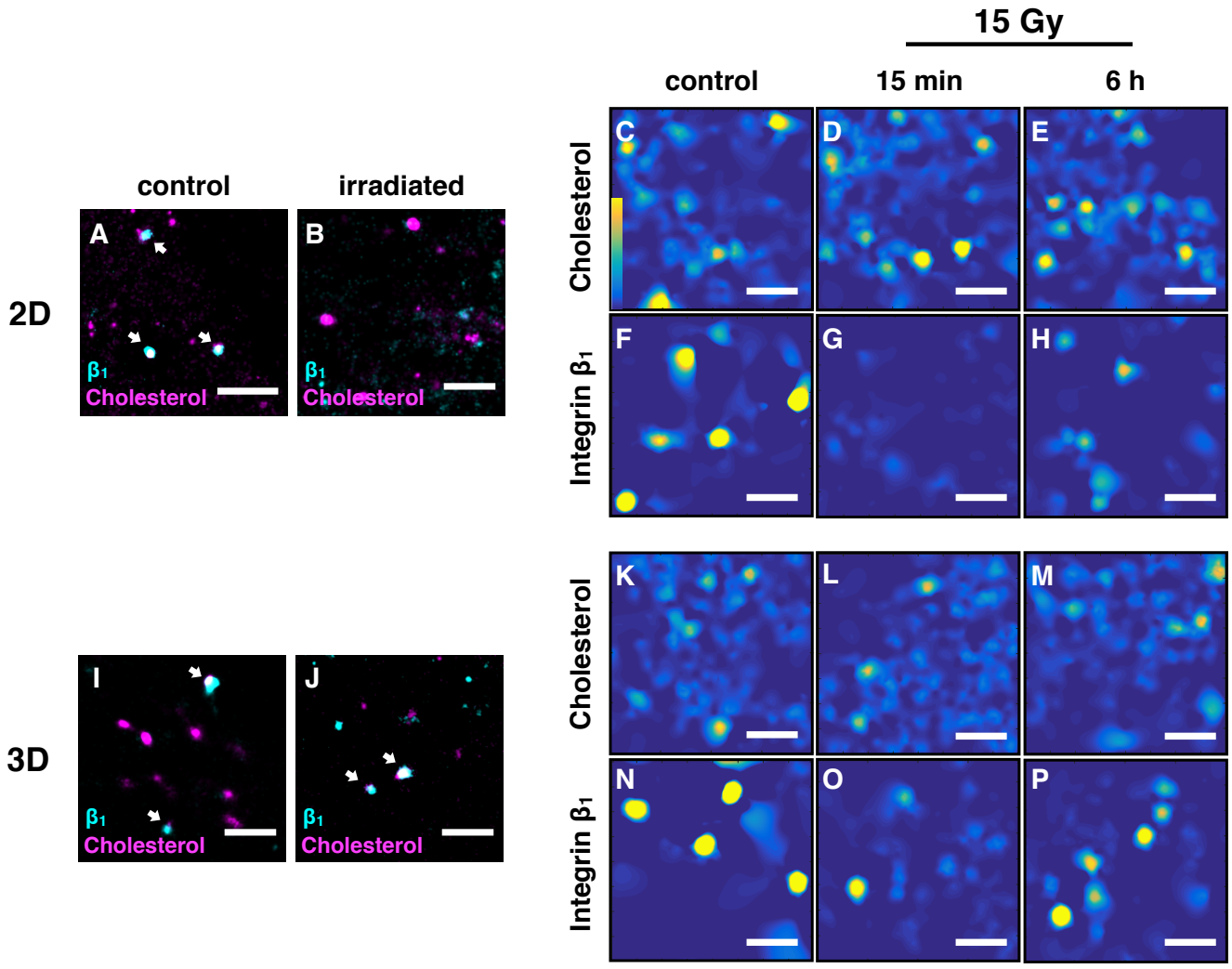

Figure 6.2: Effects of high dose irradiation on the integrin β1 - cholesterol raft colocalization of 2D and 3D cultured MEF cells. (A, B and I, J) Superresolution images of integrin β1 (cyan) and cholesterol (magenta) colocalizations of a 2D control cell (A), a 2D cell irradiated with 15 Gy (B), a 3D control cell (I) and a 3D cell irradiated with 15 Gy (J). Cells were fixed 15 min after irradiation. Scale bar is 2 μm. Arrows indicate regions with integrin β1 - cholesterol colocalization (white). (C - H) Heat maps visualize clustered (yellow) and unclustered (dark blue) regions of 2D cells stained for cholesterol (C - E) and integrin β1 (F - H). Shown are heat maps of controls (C and F), cells irradiated with 15 Gy and fixed after 15 min (D and G) and after 6 h (E - H). Scale bar is 1 μm. (K - P) Corresponding data for 3D cultured cells.

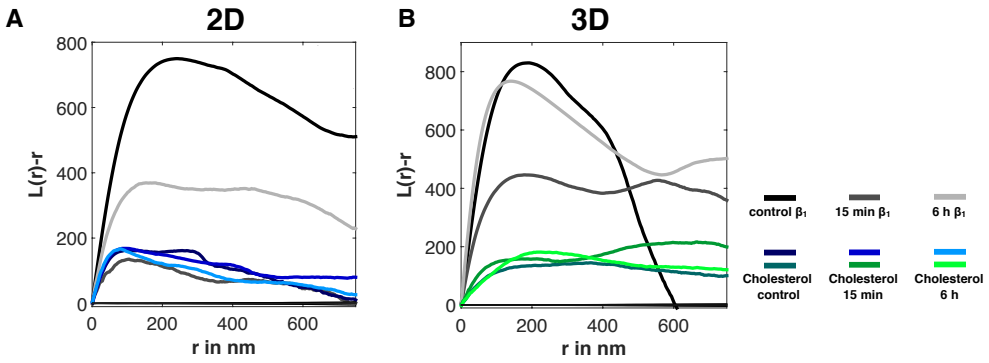

Figure 6.3: Effects of ionizing radiation on the integrin β1 and cholesterol microdomain organization of 2D and 3D cultured MEF cells. H-Plots of Ripley's K function analyzed datasets of integrin β1 and cholesterol microdomains from 2D (A) and 3D (B) cultured cells. The peak heights (H(r) = L(r)-r) represent the degree of clustering (H(r) max) and its position the most frequent cluster size (r in nm). H-plots show results for controls and cells irradiated with 15 Gy fixed 15 min and 6 h after IR. Color code: integrin β1 control (black), integrin β1 15 min after IR (dark gray), integrin β1 6 h after IR (light gray), 2D cholesterol control (dark blue), 2D cholesterol 15 min after IR (mid-blue), 2D cholesterol 6 h after IR (light blue), 3D cholesterol control (dark green), 3D cholesterol 15 min after IR (mid-green) and 3D cholesterol 6 h after IR (light green). Also, an analysis of 100 random distributions of localizations containing the same number of signals as the control are plotted (confidence interval, gray).

cholesterol microdomains do not change upon irradiation (Figure 6.6). These results clearly demonstrate that it is possible to separate a protein from its lipid raft localization implying that independent forces exist that lead to the co-organization of proteins and lipids in clusters.

6.3.3 Effects of IR on integrin β1 clustering are lipid raft independent

Taken together, it was found that

- membrane dynamics and cholesterol raft organization differ between 2D and 3D cultured cells
- the integrin-cholesterol raft colocalization is cell culture independent
- integrins can be separated from their lipid raft localization by an extracellular stressor
- cholesterol rafts remain surprisingly stable even after a sudden and complete disappearance of proteins they were colocalizing with

Even after high doses of IR cholesterol stays clustered while integrins decluster in response to this treatment and lose their association to lipid rafts, often referred to as „organizing platforms“ [80]. With this it was possible to show that the effects of IR on the integrin $\beta 1$ clustering are lipid raft independent. But these results also pose the question: Who organizes whom? - a well known question in the field of membrane research. The here presented data indicates that this question has to be answered with „neither is responsible for the organization of the other“. While integrins and cholesterol rafts clearly colocalize under unstressed conditions, treatment with IR showed that lipid rafts can not be responsible for the clustered organization of integrins. In other words, cholesterol does not pattern integrins. On the other hand, the distribution of integrins turned out not to be responsible for the presence of cholesterol rafts, as disintegration of the former did not effect the latter. Hence, patterning processes behind cholesterol and integrins appear to be independent or at least lack strong mutual influence. In conclusion, the generalized view of lipid rafts as an „organizing platform“ is questioned by the here presented data, as it was found that integrin and cholesterol clustering are independent and integrin clusters are not stabilized by their association to lipid rafts. With this, these findings are also not in line with the view that integrin-signaling stabilizes lipid rafts [140], as they remained stable in the absence of intact focal adhesions.

Acknowledgments

Many thanks to Dr. A. Miyawaki (RIKEN Brain Science Institute, Japan) for kindly providing the pET28/Dronpa-Θ-D4 and pET28/Dronpa-NT-Lys plasmids.

6.4 Material and Methods

6.4.1 Cell culture

MEF cells (mouse embryonic fibroblasts) were cultured in DMEM / Ham's F-12 (1:1) (Biochrom, Berlin, Germany) supplemented with 10% FCS (Sigma-Aldrich, St. Louis, Missouri, USA) and 1% NEAA (Biochrom, Berlin, Germany). OV-MZ-6 cells (human ovarian serous cystadenocarcinoma) were cultured in high glucose DMEM (Thermo Fischer Scientific, Waltham, Ma, USA) supplemented with 10 mM HEPES buffer (Thermo Fischer Scientific, Waltham, Ma, USA), 0.27 mM L-asparagine (Sigma-Aldrich, St. Louis, Missouri, USA) and 10% FCS. All cells were cultured in a humidified chamber at 37 °C and 5% CO_2. Cell cultures were prepared on round coverslips (Karl Hecht GmbH, Sondheim, Germany, NO 1.5, $\varnothing$ = 25 mm). The preparation of 3D cells was described in Babel et al. [41]. In brief, cells were cultured in 15 μl sized 1.5 mg/ml collagen I hydrogels (3 mg/ml rat-tail collagen I stock solution, Thermo Fischer Scientific, Waltham, Ma, USA) on APTS (3-Aminopropyl)triethoxysilane, Sigma-Aldrich, St. Louis, Missouri, USA) coated coverslips. 3D cells were incubated 4 to 5 days prior to use.

6.4.2 FRAP

FRAP experiments of OV-MZ-6 cells expressing CAAX-mCherry (pCDNA3.2) [9] were performed with the LEICA SP5II (Leica Microsystems, Mannheim, Germany) by using a 562 LASER. Five pre-bleach images were recorded with a frame interval of 38 ms, followed by bleaching with a zoomed in region of interest (ROI) for 10 frames with an interval of 38 ms. 60 Post-bleach images were acquired with a time resolution of 38 ms, followed by 30 post-bleach images recorded with a time resolution of 2 s and finally 15 post-bleach images with a frame interval of 5 s were recorded, resulting in 105 post-bleach images for 137.28 s after bleaching. FRAP recovery curves were then normalized and fitted to a single- exponential function as published previously [141].

6.4.3 Radiation

Cells were irradiated with an Isovolt 160 Titan E (GE Sensing & Inspection Technologies, Alzenau, Germany) x-ray source. Cells were irradiated with 15 Gy (voltage = 90 kV, current = 33.7 mA). Doses were delivered at a 30 cm source to probe distance with cell cultures placed on a 2 mm aluminum filtering plate with respect to the glass doubling factor [126].

6.4.4 Immunostainings

The following antibodies were used: anti CD 29 Alexa Fluor 647 conjugate (integrin β1, Biozol Diagnostica, Eching, Germany), anti phosphatidylserine Alexa Fluor 488 conjugate (Merck KGaA, Darmstadt, Germany), anti ceramide (Sigma-Aldrich, St. Louis, Missouri, USA) and anti mouse Alexa Fluor 488 conjugate (Thermo Fischer Scientific, Waltham, Ma, USA). All antibodies were diluted 1:10.000 for 2D and 1:5000 for 3D cells. Cells were fixed with 4% PFA (Carl Roth GmbH Karlsruhe, Germany) supplemented with 0.2% glutaraldehyde (Serva Electrophoresis, Heidelberg, Germany) in PBS (Sigma-Aldrich, St. Louis, Missouri, USA, pH 6.9) for 1h at 4 °C. Integrin β1 staining was described elsewhere [41]. For lipid stainings cells were incubated for 3 h / 37 °C in 3% BSA in PBS, followed by antibody staining for 1 h at 4 °C. For labeling the ceramide antibody, cells were blocked for 1 h / 37 °C in 1% BSA followed by secondary antibody staining (3 h /4 °C). After every fixation and staining step, cells were washed 3 times with PBS-T.

6.4.5 Lipid raft staining

pET28/Dronpa-Θ-D4 (stains cholesterol) and pET28/Dronpa-NT-Lys (stains sphingomyelin) plasmids were kindly provided by Dr. A. Miyawaki (RIKEN Brain Science Institute, Japan). Recombinant proteins were expressed in E.coli (BL 21) and purified using the Dynabeads His-tag isolation and pulldown kit (Thermo Fischer Scientific, Waltham, Ma, USA). MEF cells were incubated in HBSS buffer (Thermo Fischer Scientific, Waltham, Ma, USA) containing 16 ng/ml Dronpa-Θ-D4 or 60 ng/ml Dronpa-NT-Lys for 3 min on ice. Cells were washed quickly and were fixed with 4% PFA (Carl Roth GmbH Karlsruhe, Germany) supplemented with 0.2% glutaraldehyde (Serva Electrophoresis, Heidelberg, Germany) in PBS (Sigma-Aldrich, St. Louis, Missouri, USA, pH 6.9) for 1h at 4 °C.

6.4.6 Integrin - Lipid raft co-staining

MEF cells were stained with the anti CD 29 Alexa Fluor 647 antibody (30 min / 37 °C) in HBSS buffer followed by lipid raft staining and fixation.

6.4.7 Cholesterol depletion

MEF cells were incubated at 37 °C for 30 min in HBSS buffer supplemented with 10 mM of MβCD (Methyl-β-cyclodextrin, Sigma-Aldrich, St. Louis, Missouri, USA) followed by Dronpa-Θ-D4 staining and fixation.

6.4.8 Fixation control

To see whether a storage of Dronpa-Θ-D4 stained probes at 4 °C influences the cholesterol clustering, one probe was measured directly after fixation and one 24 h after fixation.

6.4.9 SMD measurements

All SMD measurements were performed with a custom-built instrument. A detailed description of the setup was published previously [41].

6.4.10 Image acquisition and data analysis

Editing of images was performed using Fiji (version: 1.51h) [15]. To analyze the effects of ionizing radiation on β1 integrins and cholesterol rafts, single molecule signals were detected and filtered using the ThunderStorm plugin for Fiji [16]. For the add-on cluster analysis custom written software in MATLAB R2014b was used.

6.4.11 Cluster analysis

To analyze our single molecule data we used the Ripley's K function. In brief, the result of this method is the so called H plot, where the degree of clustering (H(r) =L(r)-r) is plotted against a length scale. The maximum represents the most prominent cluster distribution. The height of the first local maximum (H(r)max) gives a measure of the degree of clustering and its position the radius of the most frequent clusters [87, 88, 89]. For statistical analysis confidence intervals of 68.27% were generated by simulating 100 random distributions with the same number of signals as a control data set. Pseudo colored heat

maps were created similar to Williamson et al. [142], binary cluster maps were created based on the publication of Owen et al. [90]. Binary cluster maps were used to determine the cluster density and the number of clusters per μm^2. A detailed description of our cluster analysis can be found in Babel et al. [41]. To remove duplicates, molecules that convert to the same position were removed within the distance of the uncertainty of each dataset.

6.4.12 Statistical analysis

Statistical analysis was performed with GraphPad Prism 7. For multiple comparisons, significances were analyzed with a Kruskal-Wallis test with a Dunn's multiple comparison post hoc test. For simple comparisons, significances were analyzed with a Mann-Whitney test. For all cases, $p \leq 0.05$ was considered significant (*), $p \leq 0.01$ very significant (**) and $p \leq 0.001$ extremely significant (***). Also $p \leq 0.0001$ (****) was noted. All presented box plots show as a central line the median, the top and bottom of each box are the first and third quartile, top and bottom line represent the maximum and minimum values. Outliers are colored in red.

6.5 Supplementary figures

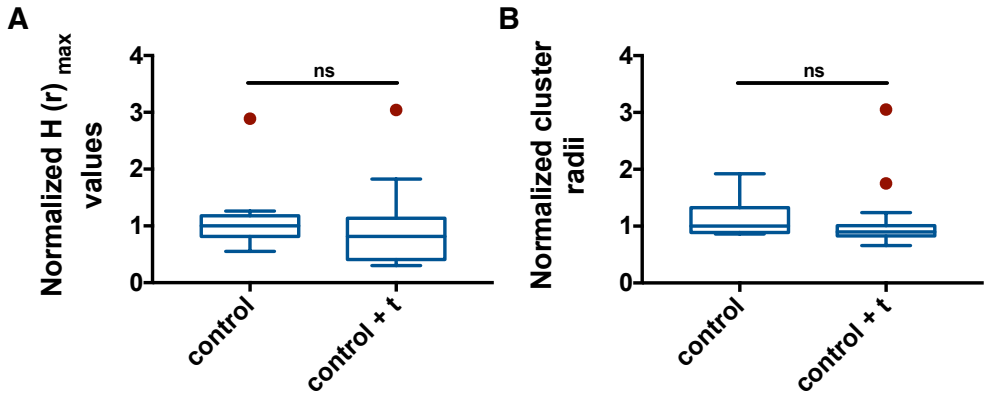

Figure 6.4: Time between fixation and probe measurement does not affect lipid raft organization. Box plots of normalized medians of H(r) max (A) and r max (B) obtained from Ripley's K function analyzed data sets. 2D cells were either measured directly after fixation (control) or after a storage time of 24 h (control + t). Statistical analysis was performed with a a Mann-Whitney test, no significance was detected (ns).

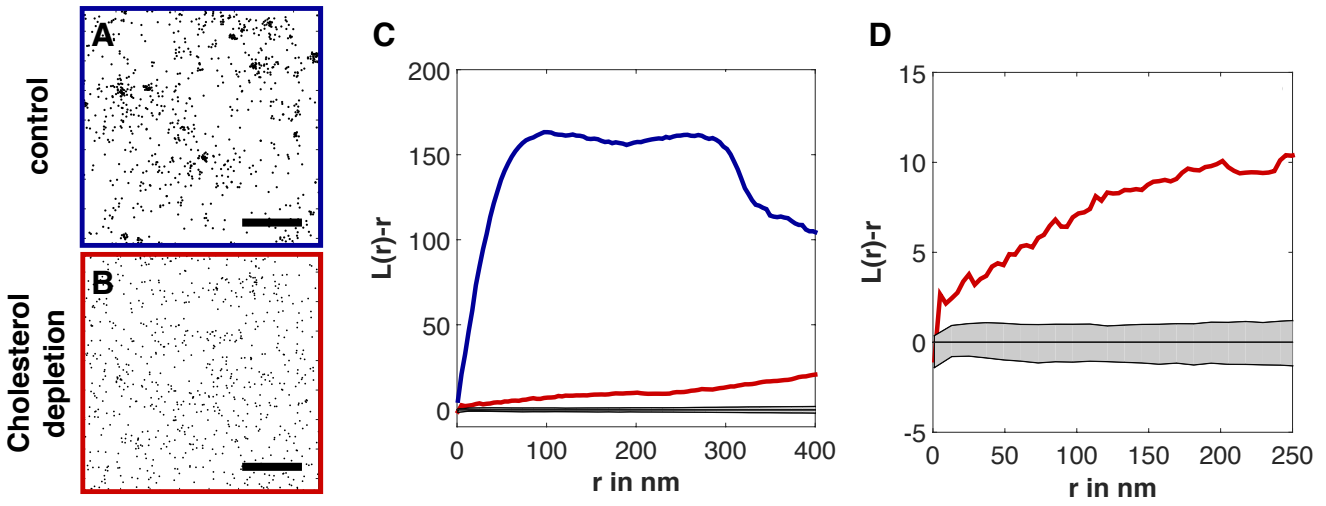

Figure 6.5: Cholesterol depletion leads to a loss of cholesterol microdomains. (A and B) Scatter plots of single molecule detections from cholesterol stained 2D cells. (A) Untreated control and (B) after cholesterol depletion, scale bar is 1 μm. (C) H-plots of the data from (A, blue) and (B, red) as well as an analysis of 100 random distributions of localizations containing the same number of signals as the control (confidence interval, gray). (D) Zoom-in of (C).

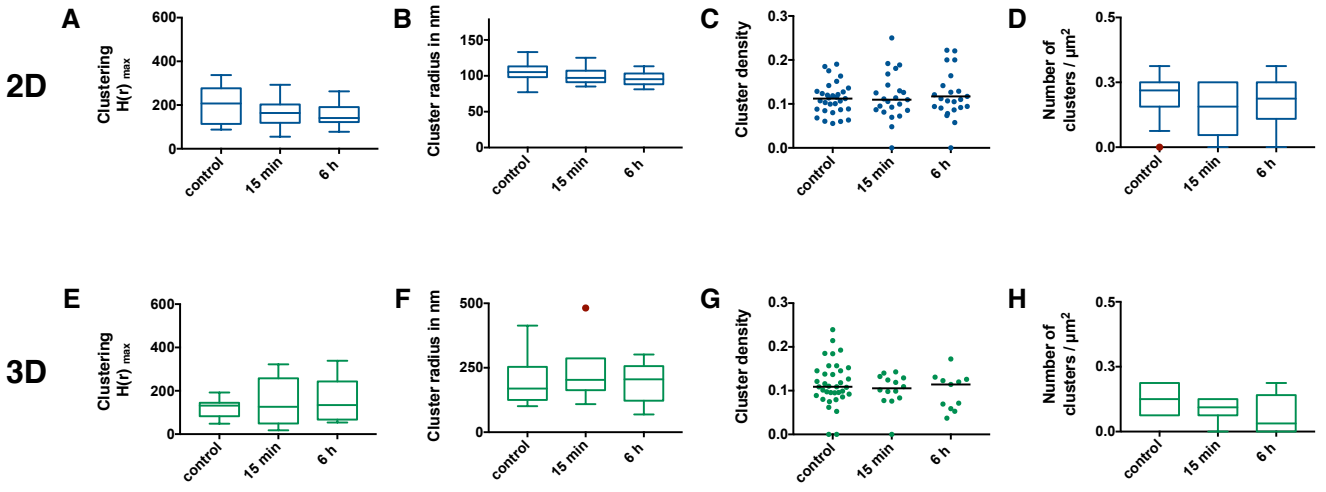

Figure 6.6: Detailed analysis of the effect of IR on various cholesterol raft parameters of 2D and 3D cultured cells. Box plots or scatter plots of the change of clustering (H(r) max), cluster radius (r in nm), cluster density and the number of clusters per μm^2 in response to a x-irradiation with 15 Gy. (A-D) Results for 2D cells. (E - H) Corresponding data of 3D cultured cells. Statistical analysis was performed with a Kruskal-Wallis test, no significances were detected.

7 General Discussion

The well known involvement of integrins in tumorgenesis (metastasis, angiogenesis) and cellular reactions towards anti-cancer treatment (drug- and radioresistance) makes them an important target in current tumor studies [22, 23]. Throughout this thesis, it was shown that:

I Integrin $\beta 1$ clustering is a target to induce radiosensitivity

II Lamin reorganization in response to integrin targeting is based on mechanosensing

III These processes are lipid-raft independent

IV 2D cultured cells are highly artificial and do not provide the means to investigate processes that depend on mechanobiological cues

These results could only be achieved with the combined use of:

I An *in vivo*-like 3D cell culture system

II Single molecule localization microscopy (SMLM)

This demonstrates that a combined approach of 3D cell cultures and SMLM should become a complementing part of preclinical screenings. With this, it would be possible to exploit the virtues of super resolution microscopy with the enhanced predictive value of 3D cultured cells.

7.1 SMD - the perfect tool for targeting the molecular phenotype of 3D cultured cells

Single molecule localization microscopy (SMLM) is a technology that allows for an accurate assessment of the localization of fluorescently labeled molecules. These techniques provide novel insights into sub-cellular processes and structures as they are able to resolve features below the diffraction limit [42].

SMLM as part of a preclinical screening can extend the assessment of the phenotype to the molecular dimension, a scale often carrying meaningful information in biological systems. This is a rigorous improvement if compared with traditional wide field fluorescence or confocal laser scanning microscopy (CLSM), which lack spatial resolution and only provide an average fluorescent signal of several molecules. A SMLM-based screen has the power to identify compounds that have a direct effect on the nanoscale (re-)organization and localization of proteins, i.e. processes that almost always start signaling cascades at the PM. As an example for this advantage, it was shown in this work that the well known effect of the integrin $\beta 1$ inhibitor AIIB2 to induce radiosensitivity [110] is based on its ability to reduce integrin clustering with the consequence of an impaired (nuclear)mechanosensing eventually leading to lamin reorganization [41].

The use of SMLM in a preclinical pipeline, however, would only make sense in combination with an *in vivo*-like cell culture system which exhibits a predictive value. 3D cell cultures (ECM-based or spheroid cell cultures) would overcome the limitations of monolayer 2D cultures (e.g. provide dimensionality or ECM binding sites) [56]. Both, high resolution microscopy and 3D cell cultures are, however, only slowly introduced in industrial pipelines, presumably due to problems regarding imaging and other methods established for 2D cultures.

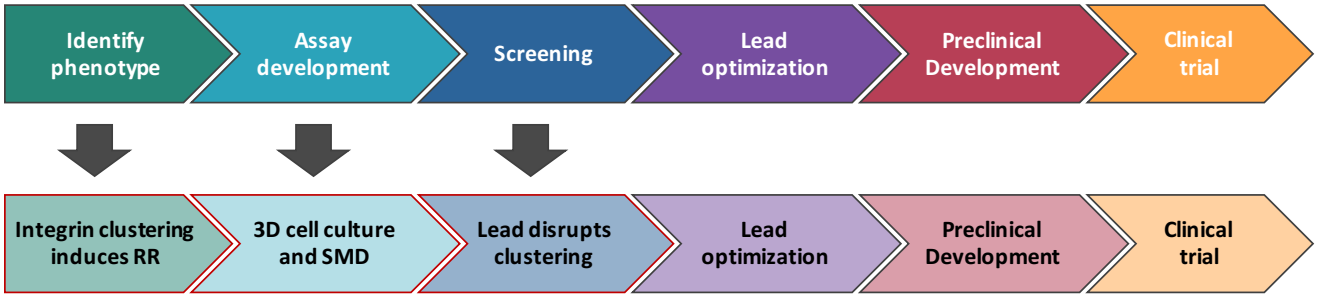

Figure 7.1: SMD and 3D cell cultures in preclinical screenings with the molecular phenotype as a target. The molecular phenotypic screening approach combines aspects of phenotypic and targeted-based screenings. With the use of SMD in a preclinical screening pipeline it would be possible to determine the molecular phenotype (e.g. integrin clustering is responsible for radio resistance (RR)) and in combination with an *in vivo*-like 3D cell culture system an appropriate assay could be developed to screen for lead molecules that for example, disrupt clustering and therefore induce radiosensitivity. These steps are followed by lead optimization, preclinical developments and finally, the clinical trial.

7.1.1 SMD and 3D cell cultures for preclinical molecular phenotype screenings

A screening based on the molecular phenotype would combine aspects of both, traditional phenotypic and targeted-based screenings. From the phenotypic approach it inherits the quality of assessing a cellular response — here the molecular distribution — from a treatment to which the targeted protein contributes but is not solely responsible. Rather, a multitude of factors are required to promote response (molecular reorganization) that eventually triggers downstream signaling. In other words, while investigating the organization of e.g. integrin $\beta 1$, this protein may either be the target itself (e.g. treatment with AIIB2), or, alternatively, the nanoscale organization of a downstream protein (e.g. lamin A/C) may serve as the molecular phenotypic read-out in response to the treatment of the integrin.

By combining advantages of these two approaches into a molecular phenotypic screening, it would be possible to identify (i) directly involved (i.e. integrin clustering) and more distantly related targets (i.e. lamin organization). Hence, alternative targets could be identified before lead structures [33, 34]. With this a library for a desired nanoscale effect could be screened against e.g. the protein clustering. By combining this approach with a classical, phenotypic screening it would enable to screen for unrelated targets, i.e. actin or lamin organization.

Therefore, a preclinical molecular phenotype screening starts with the (i) identification of the phenotype, and is followed by (ii) an appropriate assay development, (iii) compound library screening, (iv) lead structure optimization and (v) preclinical development, finally ending in (vi) the clinical trials. Thereby, the step between screening and lead optimization is a cycle of constant repetition (see Figure 7.1).

The molecular phenotype for (cell-adhesion-mediated) radioresistance identified in this thesis is the integrin $\beta 1$ clustering (direct target) or lamin distribution (indirect, distant target), see Figure 7.2. An appropriate assay would include an ECM-based 3D cell culture system and SMLM. At first sight, the target for the screening process would be the ability to interfere with integrin clustering so that a combined treatment with IR breaks integrin clustering and subsequently the mechanosensing system of the cells (see Figure 7.1). On a closer inspection, molecular phenotypic screenings could help to identify lead structures acting on *any* surface receptor that induces a desired effect within a cell, thereby obviating the need for cell penetrating compounds to address intracellular targets. To that end, a screen for such compounds acting on a molecular phenotype would follow the well recognized quality of traditional phenotypic screenings, in that precise molecular actions do not need to be known in order to reach an desired effect (see Figure 7.2).

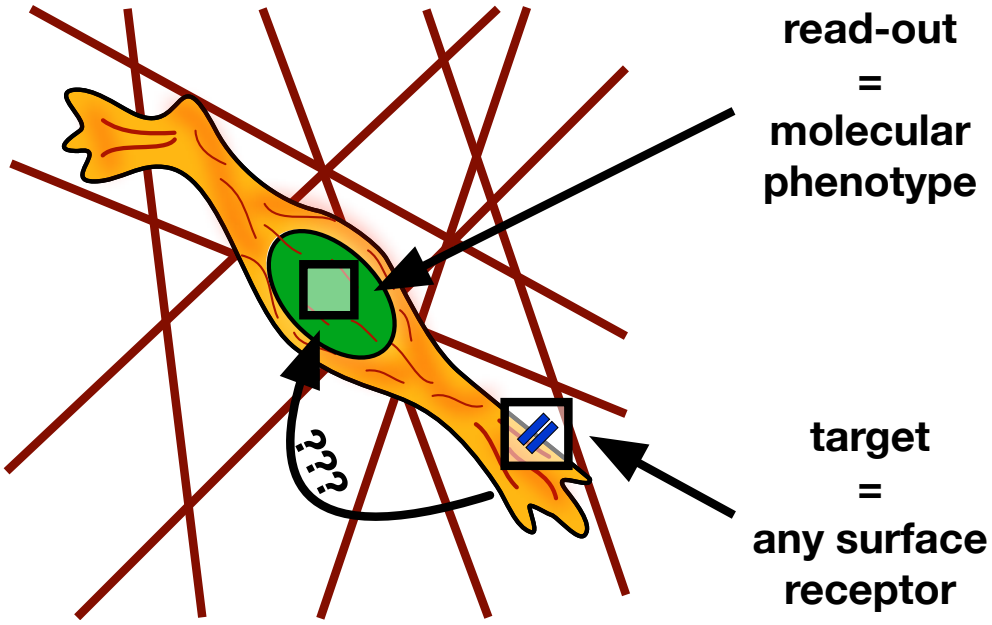

Figure 7.2: Molecular phenotype screening for directly involved or more distant targets. The molecular phenotypic screening could be used to identify lead structures acting on any surface receptor. The read out (the molecular phenotype) could be any intracellular target. The precise molecular interaction can remain unknown.

7.1.2 2D cell culture systems are highly artificial

Through this thesis and many other studies ([5, 6, 7, 51, 52, 53, 54, 55]), it should become clear that 2D cultured cells are highly artificial. Relevant for this study is the inability of 2D cultured cells to (i) probably organize integrin clusters, (ii) exhibit a functional integrin signaling and (iii) mechanosensing system as well as (iv) their significant differences in PM mobility and raft organization. The impaired ability of 2D cells, to maintain integrin clusters even in the absence of any treatments (other than the 2D culture condition itself) already points to a lower tolerance for additional stressors. Low doses of IR and AIIB2 treatment alone are sufficient to break the integrin-mechano system apart - making 2D cultured cell an over sensitive cell culture system.

Therefore, it is important to point out that the CAM-RR of 3D cultured cells is not an additional ability of these cells, rather 2D cells are inferior in so many ways that they are radiosensitive. Hence, the whole process should be rather termed planar-adhesion-mediated radiosensitivity **PAM-RS** and not CAM-RR.

Statement of own work

I have undertaken all experiments, data analysis and writing of the presented thesis and publication with exception of the following:

- Figure 2.1 was adapted from Lauer et al. ([42])
- Figure 2.4 A and B were provided by PD Dr. T. Meckel
- Section 2, 6 and 7 (without stated exceptions) are part of the publications stated in 3.

Chapter I: „Direct Evidence for Cell Adhesion-Mediated Radioresistance (CAM-RR) on the Level of Individual Integrin $\beta 1$ Clusters“

- Programming of the custom written MatLab software for cluster analysis was performed with: M. Grunewald, R. Lehn and T. Meckel
- Supplementary Figure 4 was prepared by M. Grunewald
- Critical revision and drafting of the manuscript was performed with L. Langhans and T. Meckel

Chapter II: „Radiosensitization by α-integrin $\beta 1$ (AIIB2) is based on integrin cluster breakdown and loss of nuclear mechanosensing“

- Adjustment of CytD concentration was done by I. Gregorz (Bachelor student, under my supervision)

Chapter III: „Lipid-rafts remain stable even after ionizing radiation induced disintegration of $\beta 1$ integrin containing focal adhesions?“

- About 50 % of the collected and analyzed data was done by L. Kruse (Bachelor student, under my supervision)
- Dr. S. Bump provided Figure 6.1 A

Danksagung

An dieser Stelle möchte ich mich bei all den Personen bedanken, die mich während meiner Zeit als Doktorandin begleitet und unterstützt haben:

Zuallererst bedanke ich mich bei **Herrn PD. Dr. Tobias Meckel** für die Möglichkeit an diesem Promotionsthema forschen zu dürfen, die Freiheit das Thema in die hier vorgestellte Richtung zu entwickeln und für die vielen Anregungen, die diese Arbeit erst möglich gemacht haben.

Ein großer Dank auch an **Herrn Prof. Dr. Gerhard Thiel** und seinem Interesse an dieser Arbeit und der Übernahme des Koreferats.

Danken möchte ich auch dem **GRK 1657** für die Finanzierung meiner Arbeit und ganz besonders den tollen Abenden im Klein-Walser-Tal.

Ein ganz großer Dank geht an **Herrn Dr. Markus Langhans** und seinem Enthusiasmus, immensen Wissens und seiner großartigen Hilfsbereitschaft. All das macht ihn zu einem tollen Mentor - ohne Markus wäre diese Arbeit nicht möglich gewesen und hätte auch nicht so viel Spaß gemacht.

Danken will ich auch meinen restlichen (Ex)büromitbewohnern: **Miriam, Robert, Marco, Alex und Wadim**. Ganz besonders für die vielen Liter Kaffee, der tollen Arbeitsatmosphäre und der ständigen Unterstützung bei allerlei wissenschaftlichen Rätseln und Problemen.

Vielen Dank auch an **Tine** für die tolle Zeit und ganz besonders den kurzen Pausen im botanischen Garten.

Den Studenten **Larissa und Isabell** will ich an dieser Stelle für die tolle Unterstützug im Labor danken. Viele der hier vorgestellten Ergebnisse wären ohne die Beiden nicht möglich gewesen.

Ein ganz besonderer Dank geht an **Barbara** und ihrer Hilfe bei allen administrativen Problemen. An dieser Stelle möchte ich auch **Mirja, Silvia H. und Silvia L.** für die tolle Unterstützung im Labor danken.

Doch der größte Dank geht an meinen Ehemann **Philipp**. Vielen Dank für all die Unterstützungen und Ermutigungen während meines Studiums und meiner Zeit als Doktorandin. Du bist der Beste Mann auf der ganzen Welt - ohne Dich wäre all das nicht möglich gewesen.

Conference Contributions

2016 Focus on Microscopy in Taipei in Taiwan
Talk
DAAD travel grant
Effects of ionizing radiation on the nanoscale distribution and organization of integrins measured in a 3D cell culture system

2015 EMBL Symposium: Seeing is Believing in Heidelberg
Flash-talk and Poster
Impact of the ECM on the nanoscale distribution and localization of integrins and lipid rafts

2015 European Biophysics Congress in Dresden
Poster
Effects of ionizing radiation on lipid rafts and integrins measured in a 3D cell culture system

2014 Annual Meeting of the Society for Biological Radiation Research in Tübingen
Poster
Travel grant
Effects of ionizing radiation on plasma membrane dynamics measured in a 3D cell culture system

CV

Personal details

	Laura Babel
Date of birth	01.10.1989
Born in	Frankfurt / Main

PhD Thesis

Since 08/2014	PhD student at the department of biology, TU Darmstadt
Research group	PD Dr. Tobias Meckel
Since 08/2014	Member of the equal opportunity team, GRK 1657
Since 11/2015	Member of SciMento

Education

10/2012 - 07/2014	M.Sc. Biomolecular Engineering (with honors) Department of chemistry, TU Darmstadt
10/2009 - 09/2012	B.Sc. Biomolecular Engineering
07/2009	Abitur (Higher school certificate) Max-Beckmann-Schule, Frankfurt / Main

Awards

03/2016	DAAD travel grant (Focus on Microscopy, Taiwan)
06/2015	Poster prize, GRK retreat
09/2014	Travel grant, Annual Meeting of the Society for Biological Radiation Research in Tübingen
07/2009	Karl-von-Frisch Abiturientenpreis Excellent achievements in the subject of biology
07/2009	GDCH-Preis Excellent achievements in the subject of chemistry
03/2009	2nd place at Jugend Forscht (subject: chemistry, state competition hesse)

Bibliography

[1] Leoni A Kunz-Schughart, James P Freyer, Ferdinand Hofstaedter, and Reinhard Ebner. The use of 3-D cultures for high-throughput screening: the multicellular spheroid model. *J. Biomol. Screen.*, 9(4):273–285, June 2004.

[2] Francesco Pampaloni, Emmanuel G Reynaud, and Ernst H K Stelzer. The third dimension bridges the gap between cell culture and live tissue. *Nat. Rev. Mol. Cell Biol.*, 8:839–845, 2007.

[3] Shilpa Sant, Matthew J Hancock, Joseph P Donnelly, Dharini Iyer, and Ali Khademhosseini. Biomimetic Gradient Hydrogels for Tissue Engineering. *Can. J. Chem. Eng.*, 88(6):899–911, December 2010.

[4] Jason W Nichol, Sandeep T Koshy, Hojae Bae, Chang M Hwang, Seda Yamanlar, and Ali Khademhosseini. Cell-laden microengineered gelatin methacrylate hydrogels. *Biomaterials*, 31(21):5536–5544, July 2010.

[5] Adam S Meshel, Qize Wei, Robert S Adelstein, and Michael P Sheetz. Basic mechanism of three-dimensional collagen fibre transport by fibroblasts. *Nat. Cell Biol.*, 7(2):157–164, February 2005.

[6] Sourabh Ghosh, Giulio C Spagnoli, Ivan Martin, Sabine Ploegert, Philippe Demougin, Michael Heberer, and Anca Reschner. Three-dimensional culture of melanoma cells profoundly affects gene expression profile: a high density oligonucleotide array study. *J. Cell. Physiol.*, 204(2):522–531, August 2005.

[7] Louisa C E Windus, Debra L Kiss, Tristan Glover, and Vicky M Avery. In vivo biomarker expression patterns are preserved in 3D cultures of Prostate Cancer. *Exp. Cell Res.*, 318(19):2507–2519, November 2012.

[8] Henning Karlsson, Mårten Fryknäs, Rolf Larsson, and Peter Nygren. Loss of cancer drug activity in colon cancer HCT-116 cells during spheroid formation in a new 3-D spheroid cell culture system. *Exp. Cell Res.*, 318(13):1577–1585, 1 August 2012.

[9] Anna C Luca, Sabrina Mersch, René Deenen, Stephan Schmidt, Isabelle Messner, Karl-Ludwig Schäfer, Stephan E Baldus, Wolfgang Huckenbeck, Roland P Piekorz, Wolfram T Knoefel, Andreas Krieg, and Nikolas H Stoecklein. Impact of the 3D microenvironment on phenotype, gene expression, and EGFR inhibition of colorectal cancer cell lines. *PLoS One*, 8(3):e59689, 26 March 2013.

[10] Elke Kaemmerer, Ferry P W Melchels, Boris M Holzapfel, Tobias Meckel, Dietmar W Hutmacher, and Daniela Loessner. Gelatine methacrylamide-based hydrogels: An alternative three-dimensional cancer cell culture system. *Acta Biomater.*, 10(6):2551–2562, June 2014.

[11] Melinda Larsen, Vira V Artym, J Angelo Green, and Kenneth M Yamada. The matrix reorganized: extracellular matrix remodeling and integrin signaling. *Curr. Opin. Cell Biol.*, 18(5):463–471, October 2006.

[12] Coert Margadant, Hanneke N Monsuur, Jim C Norman, and Arnoud Sonnenberg. Mechanisms of integrin activation and trafficking. *Curr. Opin. Cell Biol.*, September 2011.

[13] Markus Langhans, Wadim Weber, Laura Babel, Miriam Grunewald, and Tobias Meckel. The right motifs for plant cell adhesion: what makes an adhesive site? *Protoplasma*, 254(1):95–108, January 2017.

[14] Iris Eke and Nils Cordes. Radiobiology goes 3D: How ECM and cell morphology impact on cell survival after irradiation. *Radiother. Oncol.*, 99(3):271–278, June 2011.

[15] Zvi Fuks, Israel Vlodavsky, Michael Andreeff, Maureen Mclaughlin, and Adriana Naimovitz-friedman. Effects of Extracellular Matrix on the Response of Endothelial Cells to Radiation jn vitro. pages 725–731, 1992.

[16] Katja Storch. *Einfluss der Chromatinkondensation auf die zelluläre Strahlenempfindlichkeit unter dreidimensionalen Wachstumsbedingungen*. PhD thesis, 2010.

[17] Katja Storch and Nils Cordes. Focal adhesion-chromatin linkage controls tumor cell resistance to radio- and chemotherapy. *Chemother. Res. Pract.*, 2012:319287, January 2012.

[18] Iris Eke, Yvonne Deuse, Stephanie Hehlgans, Kristin Gurtner, Mechthild Krause, Michael Baumann, Anna Shevchenko, Veit Sandfort, and Nils Cordes. β 1 Integrin / FAK / cortactin signaling is essential for human head and neck cancer resistance to radiotherapy. 122(4):1529–1540, 2012.

[19] Stephanie Hehlgans, Michael Haase, and Nils Cordes. Signalling via integrins : Implications for cell survival and anticancer strategies. *Radiat. Res.*, 1775(1):163– 180, January 2007.

[20]

[21] Veit Sandfort, Iris Eke, and Nils Cordes. The role of the focal adhesion protein PINCH1 for the radiosensitivity of adhesion and suspension cell cultures. *PLoS One*, 5(9), January 2010.

[22] Patrick T Caswell, Suryakiran Vadrevu, and Jim C Norman. Integrins: masters and slaves of endocytic transport. *Nat. Rev. Mol. Cell Biol.*, 10(12):843–853, December 2009.

[23] W W Ma and A A Adjei. Novel agents on the horizon for cancer therapy. *CA Cancer J. Clin.*, 59(2):111–137, 2009.

[24] Leoni a Kunz-Schughart, James P Freyer, Ferdinand Hofstaedter, and Reinhard Ebner. The use of 3-D cultures for high-throughput screening: the multicellular spheroid model. *J. Biomol. Screen.*, 9(4):273–285, June 2004.

[25] Andrew Bullen. Microscopic imaging techniques for drug discovery. *Nat. Rev. Drug Discov.*, 7(1):54–67, January 2008.

[26] Jonathan D Humphries, Adam Byron, and Martin J Humphries. Integrin ligands at a glance. *J. Cell Sci.*, 119(Pt 19):3901–3903, October 2006.

[27] Z Fuks, I Vlodavsky, M Andreeff, M McLoughlin, and A Haimovitz-Friedman. Effects of extracellular matrix on the response of endothelial cells to radiation in vitro. *Eur. J. Cancer*, 28A(4-5):725–731, 1992.

[28] Milestones timeline. *Nature Milestones in Light Microscopy*, 2009.

[29] Milestones. *Nature Milestones in Light Microscopy*, 2009.

[30] M K Aalto, H Ronne, and S Keränen. Yeast syntaxins Sso1p and Sso2p belong to a family of related membrane proteins that function in vesicular transport. *EMBO J.*, 12(11):4095–4104, November 1993.

[31] Michael Boutros, Florian Heigwer, and Christina Laufer. Microscopy-Based High-Content screening. *Cell*, 163(6):1314–1325, 3 December 2015.

[32] David C Swinney. The value of translational biomarkers to phenotypic assays. *Front. Pharmacol.*, 5:171, 15 July 2014.

[33] John G Moffat, Joachim Rudolph, and David Bailey. Phenotypic screening in cancer drug discovery - past, present and future. *Nat. Rev. Drug Discov.*, 13(8):588–602, August 2014.

[34] Georg C Terstappen, Christina Schlüpen, Roberto Raggiaschi, and Giovanni Gaviraghi. Target deconvolution strategies in drug discovery. *Nat. Rev. Drug Discov.*, 6(11):891–903, November 2007.

[35] Wei Zheng, Natasha Thorne, and John C McKew. Phenotypic screens as a renewed approach for drug discovery. *Drug Discov. Today*, 18(21-22):1067–1073, November 2013.

[36] Yan Feng, Timothy J Mitchison, Andreas Bender, Daniel W Young, and John A Tallarico. Multi-parameter phenotypic profiling: using cellular effects to characterize small-molecule compounds. *Nat. Rev. Drug Discov.*, 8(7):567–578, July 2009.

[37] Emanuel Petricoin Lance Liotta. Molucular profiling of human cancer. *Nat. Genet.*, October 2016.

[38] Rainer Pepperkok and Jan Ellenberg. High-throughput fluorescence microscopy for systems biology. *Nat. Rev. Mol. Cell Biol.*, 7(9):690–696, September 2006.

[39] Jason R Swedlow. Innovation in biological microscopy: current status and future directions. *Bioessays*, 34(5):333–340, May 2012.

[40] Maria F Garcia-Parajo, Alessandra Cambi, Juan A Torreno-Pina, Nancy Thompson, and Ken Jacobson. Nanoclustering as a dominant feature of plasma membrane organization. *J. Cell Sci.*, 127(Pt 23):4995–5005, 1 December 2014.

[41] Laura Babel, Miriam Grunewald, Robert Lehn, Markus Langhans, and Tobias Meckel. Direct evidence for cell adhesion-mediated radioresistance (CAM-RR) on the level of individual integrin $\beta 1$ clusters. *Sci. Rep.*, 7(1):3393, 13 June 2017.

[42] Florian M Lauer, Elke Kaemmerer, and Tobias Meckel. Single molecule microscopy in 3D cell cultures and tissues. *Adv. Drug Deliv. Rev.*, 79-80:79–94, 15 December 2014.

[43] Claudio R Thoma, Miriam Zimmermann, Irina Agarkova, Jens M Kelm, and Wilhelm Krek. 3D cell culture systems modeling tumor growth determinants in cancer target discovery. *Adv. Drug Deliv. Rev.*, 69-70:29–41, April 2014.

[44] Christopher S Szot, Cara F Buchanan, Joseph W Freeman, and Marissa N Rylander. 3D in vitro bioengineered tumors based on collagen I hydrogels. *Biomaterials*, 32(31):7905–7912, November 2011.

[45] Christian Frantz, Kathleen M Stewart, and Valerie M Weaver. The extracellular matrix at a glance. *J. Cell Sci.*, 123(Pt 24):4195–4200, December 2010.

[46] Chris S Hughes, Lynne M Postovit, and Gilles a Lajoie. Matrigel: a complex protein mixture required for optimal growth of cell culture. *Proteomics*, 10(9):1886–1890, May 2010.

[47] Ulrich Hersel, Claudia Dahmen, and Horst Kessler. RGD modified polymers: biomaterials for stimulated cell adhesion and beyond. *Biomaterials*, 24(24):4385–4415, November 2003.

[48] Monica a Serban and Glenn D Prestwich. Modular extracellular matrices: solutions for the puzzle. *Methods*, 45(1):93–98, May 2008.

[49] Che B Hutson, D Ph, Jason W Nichol, Hug Aubin, Hojae Bae, and Ali Khademhosseini. Synthesis and Characterization of Tunable Poly (Ethylene Glycol): Gelatin Methacrylate. *Tissue Eng. Part A*, 17(13 and 14):1713–1723, 2011.

[50] Yu-San Liu, Shi-You Ding, and Michael E Himmel. Single-molecule tracking of carbohydrate-binding modules on cellulose using fluorescence microscopy. *Methods Mol. Biol.*, 908:129–140, January 2012.

[51] Oliver Zschenker, Thomas Streichert, Stephanie Hehlgans, and Nils Cordes. Genome-wide gene expression analysis in cancer cells reveals 3D growth to affect ECM and processes associated with cell adhesion but not DNA repair. *PLoS One*, 7(4):e34279, January 2012.

[52] Paraic A Kenny, Genee Y Lee, Connie A Myers, Richard M Neve, Jeremy R Semeiks, Paul T Spellman, Katrin Lorenz, Eva H Lee, Mary Helen Barcellos-Hoff, Ole W Petersen, Joe W Gray, and Mina J Bissell. The morphologies of breast cancer cell lines in three-dimensional assays correlate with their profiles of gene expression. *Mol. Oncol.*, 1(1):84–96, June 2007.

[53] Jill S Harunaga and Kenneth M Yamada. Cell-matrix adhesions in 3D. *Matrix Biol.*, 30(7-8):363–368, September 2011.

[54] Sara Geraldo, Anthony Simon, Nadia Elkhatib, Daniel Louvard, Luc Fetler, and Danijela M Vignjevic. Do cancer cells have distinct adhesions in 3D collagen matrices and in vivo? *Eur. J. Cell Biol.*, 91(11-12):930–937, November 2012.

[55] Krzysztof Wrzesinski, Adelina Rogowska-Wrzesinska, Rattiyaporn Kanlaya, Kamil Borkowski, Veit Schwämmle, Jie Dai, Kira Eyd Joensen, Katarzyna Wojdyla, Vasco Botelho Carvalho, and Stephen J Fey. The cultural divide: exponential growth in classical 2D and metabolic equilibrium in 3D environments. *PLoS One*, 9(9):e106973, 15 September 2014.

[56] Dietmar W Hutmacher, Daniela Loessner, Simone Rizzi, David L Kaplan, David J Mooney, and Judith A Clements. Can tissue engineering concepts advance tumor biology research? *Trends Biotechnol.*, 28(3):125–133, March 2010.

[57] D Hanahan and R A Weinberg. The hallmarks of cancer. *Cell*, 100(1):57–70, 7 January 2000.

[58] Douglas Hanahan and Robert A Weinberg. Hallmarks of cancer: the next generation. *Cell*, 144(5):646–674, 4 March 2011.

[59] Caitriona Holohan, Sandra Van Schaeybroeck, Daniel B Longley, and Patrick G Johnston. Cancer drug resistance: an evolving paradigm. *Nat. Rev. Cancer*, 13(10):714–726, October 2013.

[60] Jay S Desgrosellier and David a Cheresh. Integrins in cancer: biological implications and therapeutic opportunities. *Nat. Rev. Cancer*, 10(1):9–22, January 2010.

[61] Charles A Whittaker and Richard O Hynes. Essay Distribution and Evolution of von Willebrand / Integrin A Domains : Widely Dispersed Domains with Roles in Cell Adhesion and Elsewhere âŰą. *Mol. Biol. Cell*, 13(October):3369–3387, 2002.

[62] Pakorn Kanchanawong, Gleb Shtengel, Ana M Pasapera, Ericka B Ramko, Michael W Davidson, Harald F Hess, and Clare M Waterman. Nanoscale architecture of integrin-based cell adhesions. *Nature*, 468(7323):580–584, November 2010.

[63] E Ruoslahti. RGD and other recognition sequences for integrins. *Annu. Rev. Cell Dev. Biol.*, 12:697–715, January 1996.

[64] J P Xiong, T Stehle, B Diefenbach, R Zhang, R Dunker, D L Scott, A Joachimiak, S L Goodman, and M A Arnaout. Crystal structure of the extracellular segment of integrin alpha vbeta3. *Science*, 294(5541):339–345, 12 October 2001.

[65] Masamichi Nagae, Suyong Re, Emiko Mihara, Terukazu Nogi, Yuji Sugita, and Junichi Takagi. Crystal structure of $\alpha 5\beta 1$ integrin ectodomain: atomic details of the fibronectin receptor. *J. Cell Biol.*, 197(1):131–140, 2 April 2012.

[66] George M Whitesides. The origins and the future of microfluidics. *Nature*, 442(7101):368–373, July 2006.

[67] Jin-Min Nam, Yasuhito Onodera, Mina J Bissell, and Catherine C Park. Breast cancer cells in three-dimensional culture display an enhanced radioresponse after coordinate targeting of integrin $\alpha 5\beta 1$ and fibronectin. *Cancer Res.*, 70(13):5238–5248, 1 July 2010.

[68] Sanford J Shattil, Chungho Kim, and Mark H Ginsberg. The final steps of integrin activation : the end game. *EMBO J.*, 11(April):288–300, 2010.

[69] Junichi Takagi, Benjamin M Petre, Thomas Walz, and Timothy A Springer. Global conformational rearrangements in integrin extracellular domains in outside-in and inside-out signaling. *Cell*, 110(5):599–511, 6 September 2002.

[70] Katja Storch, Iris Eke, Kerstin Borgmann, Mechthild Krause, Christian Richter, Kerstin Becker, Evelin Schröck, and Nils Cordes. Three-dimensional cell growth confers radioresistance by chromatin density modification. *Cancer Res.*, 70(10):3925–3934, May 2010.

[71] Ronen Zaidel-Bar, Shalev Itzkovitz, Avi Ma'ayan, Ravi Iyengar, and Benjamin Geiger. Functional atlas of the integrin adhesome. *Nat. Cell Biol.*, 9(8):858–867, August 2007.

[72] Johanna Ivaska. Unanchoring integrins in focal adhesions. *Nat. Cell Biol.*, 14(10):981–983, October 2012.

[73] Olivier Rossier, Vivien Octeau, Jean-Baptiste Sibarita, Cécile Leduc, Béatrice Tessier, Deepak Nair, Volker Gatterdam, Olivier Destaing, Corinne Albigès-Rizo, Robert Tampé, Laurent Cognet, Daniel Choquet, Brahim Lounis, and Grégory Giannone. Integrins $\beta 1$ and $\beta 3$ exhibit distinct dynamic nanoscale organizations inside focal adhesions. *Nat. Cell Biol.*, 14(10):1057–1067, October 2012.

[74] Hari Shroff, Catherine G Galbraith, James A Galbraith, and Eric Betzig. Live-cell photoactivated localization microscopy of nanoscale adhesion dynamics. *Nat. Methods*, 5(5):417–423, May 2008.

[75] Stephanie I Fraley, Yunfeng Feng, Ranjini Krishnamurthy, Dong-Hwee Kim, Alfredo Celedon, Gregory D Longmore, and Denis Wirtz. A distinctive role for focal adhesion proteins in three-dimensional cell motility. *Nat. Cell Biol.*, 12(6):598–604, June 2010.

[76] Kristopher E Kubow and Alan Rick Horwitz. Reducing background fluorescence reveals adhesions in 3D matrices. *Nat. Cell Biol.*, 13(1):3–5; author reply 5–7, January 2011.

[77] Dana Bar-On, Ulrike Winter, Esther Nachliel, Menachem Gutman, Dirk Fasshauer, Thorsten Lang, and Uri Ashery. Imaging the assembly and disassembly kinetics of cis-SNARE complexes on native plasma membranes. *FEBS Lett.*, 582(23-24):3563–3568, October 2008.

[78] David J Williamson, Dylan M Owen, Jérémie Rossy, Astrid Magenau, Matthias Wehrmann, J Justin Gooding, and Katharina Gaus. Pre-existing clusters of the adaptor Lat do not participate in early T cell signaling events. *Nat. Immunol.*, 12(7):655–662, July 2011.

[79] Giovanni Sena, Zak Frentz, Kenneth D Birnbaum, and Stanislas Leibler. Quantitation of cellular dynamics in growing Arabidopsis roots with light sheet microscopy. *PLoS One*, 6(6):e21303, January 2011.

[80] Erdinc Sezgin, Ilya Levental, Satyajit Mayor, and Christian Eggeling. The mystery of membrane organization: composition, regulation and roles of lipid rafts. *Nat. Rev. Mol. Cell Biol.*, 18(6):361–374, June 2017.

[81] Daniel Lingwood and Kai Simons. Lipid rafts as a membrane-organizing principle. *Science*, 327(5961):46–50, January 2010.

[82] S J Singer and G L Nicolson. The Fluid Mosaic Model of the Structure of Cell Membranes. *Science*, 175(4023):720–731, February 1972.

[83] Garth L Nicolson. The Fluid—Mosaic model of membrane structure: Still relevant to understanding the structure, function and dynamics of biological membranes after more than 40 years. *Biochimica et Biophysica Acta (BBA) - Biomembranes*, 1838(6):1451–1466, 2014.

[84] Katharina Gaus, Soazig Le Lay, Nagaraj Balasubramanian, and Martin A Schwartz. Integrin-mediated adhesion regulates membrane order. *J. Cell Biol.*, 174(5):725–734, 28 August 2006.

[85] Makio Tokunaga, Naoko Imamoto, and Kumiko Sakata-sogawa. Highly inclined thin illumination enables clear single-molecule imaging in cells. *Nat. Methods*, 5(2):159–161, 2008.

[86] Kenji a K Tanaka, Kenichi G N Suzuki, Yuki M Shirai, Shusaku T Shibutani, Manami S H Miyahara, Hisae Tsuboi, Miyako Yahara, Akihiko Yoshimura, Satyajit Mayor, Takahiro K Fujiwara, and Akihiro Kusumi. Membrane molecules mobile even after chemical fixation. *Nat. Methods*, 7(11):865–866, November 2010.

[87] Philip M Dixon. RipleyâĂŹs K function. *Environmetrics*, 3(December):1796–1803, 2002.

[88] Peter Haase. Spatial pattern analysis in ecology based on Ripley âĂŹ s K -function : Introduction and methods of edge correction. *J. Veg. Sci.*, 6:575–582, 1995.

[89] Maria a Kiskowski, John F Hancock, and Anne K Kenworthy. On the use of Ripley's K-function and its derivatives to analyze domain size. *Biophys. J.*, 97(4):1095–1103, August 2009.

[90] Dylan M Owen, Carles Rentero, Jérémie Rossy, Astrid Magenau, David Williamson, Macarena Rodriguez, and Katharina Gaus. PALM imaging and cluster analysis of protein heterogeneity at the cell surface. *J. Biophotonics*, 3(7):446–454, July 2010.

[91] Liguo Wang and Fred J Sigworth. Structure of the BK potassium channel in a lipid membrane from electron cryomicroscopy. *Nature*, 461(7261):292–295, September 2009.

[92] Philipp Isermann and Jan Lammerding. Nuclear mechanics and mechanotransduction in health and disease. *Curr. Biol.*, 23(24):R1113–21, 16 December 2013.

[93] Katarina Wolf, Mariska Te Lindert, Marina Krause, Stephanie Alexander, Joost Te Riet, Amanda L Willis, Robert M Hoffman, Carl G Figdor, Stephen J Weiss, and Peter Friedl. Physical limits of cell migration: control by ECM space and nuclear deformation and tuning by proteolysis and traction force. *J. Cell Biol.*, 201(7):1069–1084, 24 June 2013.

[94] Colleen T Skau, Robert S Fischer, Pinar Gurel, Hawa Racine Thiam, Anthony Tubbs, Michelle A Baird, Michael W Davidson, Matthieu Piel, Gregory M Alushin, Andre Nussenzweig, Patricia S Steeg, and Clare M Waterman. FMN2 makes perinuclear actin to protect nuclei during confined migration and promote metastasis. *Cell*, 9 November 2016.

[95] Sangkyun Cho, Jerome Irianto, and Dennis E Discher. Mechanosensing by the nucleus: From pathways to scaling relationships. *J. Cell Biol.*, 216(2):305–315, February 2017.

[96] A J Maniotis, C S Chen, and D E Ingber. Demonstration of mechanical connections between integrins, cytoskeletal filaments, and nucleoplasm that stabilize nuclear structure. *Proc. Natl. Acad. Sci. U. S. A.*, 94(3):849–854, 4 February 1997.

[97] Hayri E Balcioglu, Hedde van Hoorn, Dominique M Donato, Thomas Schmidt, and Erik H J Danen. The integrin expression profile modulates orientation and dynamics of force transmission at cell-matrix adhesions. *J. Cell Sci.*, 128(7):1316–1326, 1 April 2015.

[98] G W Gant Luxton, Edgar R Gomes, Eric S Folker, Erin Vintinner, and Gregg G Gundersen. Linear arrays of nuclear envelope proteins harness retrograde actin flow for nuclear movement. *Science*, 329(5994):956–959, 20 August 2010.

[99] Joe Swift and Dennis E Discher. The nuclear lamina is mechano-responsive to ECM elasticity in mature tissue. *J. Cell Sci.*, 127(Pt 14):3005–3015, 15 July 2014.

[100] Joe Swift, Irena L Ivanovska, Amnon Buxboim, Takamasa Harada, P C Dave P Dingal, Joel Pinter, J David Pajerowski, Kyle R Spinler, Jae-Won Shin, Manorama Tewari, Florian Rehfeldt, David W Speicher, and Dennis E Discher. Nuclear lamin-a scales with tissue stiffness and enhances matrix-directed differentiation. *Science*, 341(6149):1240104, 30 August 2013.

[101] Alexandra P Navarro, Mary Ann Collins, and Eric S Folker. The nucleus is a conserved mechanosensation and mechanoresponse organelle. *Cytoskeleton*, 73(2):59–67, February 2016.

[102] G V Shivashankar. Mechanosignaling to the cell nucleus and gene regulation. *Annu. Rev. Biophys.*, 40:361–378, 2011.

[103] Aebi U, Cohn J, Buhle L, and Gerace L. The nuclear lamina is a meshwork of intermediate filaments. *Nature*, 323:560–564, 9 October 1986.

[104] Vicente Andrés and José M González. Role of a-type lamins in signaling, transcription, and chromatin organization. *J. Cell Biol.*, 187(7):945–957, 28 December 2009.

[105] Brian Burke and Colin L Stewart. The nuclear lamins: flexibility in function. *Nat. Rev. Mol. Cell Biol.*, 14(1):13–24, January 2013.

[106] Emad a Ahmed, Agnel Sfeir, Hiroyuki Takai, and Harry Scherthan. Ku70 and non-homologous end joining protect testicular cells from DNA damage. *J. Cell Sci.*, 126(Pt 14):3095–3104, July 2013.

[107] Carlos Mas-Moruno, Florian Rechenmacher, and Horst Kessler. Cilengitide: the first anti-angiogenic small molecule drug candidate design, synthesis and clinical evaluation. *Anticancer Agents Med. Chem.*, 10(10):753–768, December 2010.

[108] Roger Stupp, Monika E Hegi, Thierry Gorlia, Sara C Erridge, James Perry, Yong-Kil Hong, Kenneth D Aldape, Benoit Lhermitte, Torsten Pietsch, Danica Grujicic, Joachim Peter Steinbach, Wolfgang Wick, Rafał Tarnawski, Do-Hyun Nam, Peter Hau, Astrid Weyerbrock, Martin J B Taphoorn, Chiung-Chyi Shen, Nalini Rao, László Thurzo, Ulrich Herrlinger, Tejpal Gupta, Rolf-Dieter Kortmann, Krystyna Adamska, Catherine McBain, Alba A Brandes, Joerg Christian Tonn, Oliver Schnell, Thomas Wiegel, Chae-Yong Kim, Louis Burt Nabors, David A Reardon, Martin J van den Bent, Christine Hicking, Andriy Markivskyy, Martin Picard, Michael Weller, European Organisation for Research and Treatment of Cancer (EORTC), Canadian Brain Tumor Consortium, and CENTRIC study team. Cilengitide combined with standard treatment for patients with newly diagnosed glioblastoma with methylated MGMT promoter (CENTRIC EORTC 26071-22072 study): a multicentre, randomised, open-label, phase 3 trial. *Lancet Oncol.*, 15(10):1100–1108, September 2014.

[109] Catherine C Park, Hui J Zhang, Evelyn S Yao, Chong J Park, and Mina J Bissell. Beta1 integrin inhibition dramatically enhances radiotherapy efficacy in human breast cancer xenografts. *Cancer Res.*, 68(11):4398–4405, 1 June 2008.

[110] E Dickreuter, I Eke, M Krause, K Borgmann, M A van Vugt, and N Cordes. Targeting of β1 integrins impairs DNA repair for radiosensitization of head and neck cancer cells. *Oncogene*, 35(11):1353–1362, 17 March 2016.

[111] Isabelle Corre, Colin Niaudet, and Francois Paris. Plasma membrane signaling induced by ionizing radiation. *Mutat. Res.*, 704(1-3):61–67, 2010.

[112] Richard Kolesnick and Zvi Fuks. Radiation and ceramide-induced apoptosis. *Oncogene*, 22(37):5897–5906, September 2003.

[113] Massimo Aureli, Valentina Murdica, Nicoletta Loberto, Maura Samarani, Alessandro Prinetti, Rosaria Bassi, and Sandro Sonnino. Exploring the link between ceramide and ionizing radiation. *Glycoconj. J.*, 31(6-7):449–459, 2014.

[114] Johannes Kornhuber, Philipp Tripal, Martin Reichel, Christiane Mühle, Cosima Rhein, Markus Muehlbacher, Teja W Groemer, and Erich Gulbins. Functional inhibitors of acid sphingomyelinase (FIASMAS): A novel pharmacological group of drugs with broad clinical applications. *Cell. Physiol. Biochem.*, 26(1):9–20, 2010.

[115] Babak Oskouian and Julie D Saba. Cancer treatment strategies targeting sphingolipid metabolism. *Adv. Exp. Med. Biol.*, 688:185–205, 2010.

[116] Besim Ogretmen and Yusuf a Hannun. Biologically active sphingolipids in cancer pathogenesis and treatment. *Nat. Rev. Cancer*, 4(8):604–616, 2004.

[117] Jessica D Tytell Ning Wang and Donald E Ingber. Mechanotransduction at a distance: mechanically coupling the extracellular matrix with the nucleus. *NATuRE REVIEwS | Molecular cell Biology*, 10, 2009.

[118] I C Chang. Noncollinear acousto-optic filter with large angular aperture. *Appl. Phys. Lett.*, 25(7):370, 1974.

[119] Ian Gibbs-Seymour, Ewa Markiewicz, Simon Bekker-Jensen, Niels Mailand, and Christopher J Hutchison. Lamin A/C-dependent interaction with 53BP1 promotes cellular responses to DNA damage. *Aging Cell*, 14(2):162–169, April 2015.

[120] Franklin Mayca Pozo, Jinshan Tang, Kristen W Bonk, Ruth A Keri, Xinsheng Yao, and Youwei Zhang. Regulatory cross-talk determines the cellular levels of 53BP1 protein, a critical factor in DNA repair. *J. Biol. Chem.*, 292(14):5992–6003, 7 April 2017.

[121] Iris Eke, Yvonne Deuse, Stephanie Hehlgans, Kristin Gurtner, Mechthild Krause, Michael Baumann, Anna Shevchenko, Veit Sandfort, and Nils Cordes. β1 Integrin/FAK/cortactin signaling is essential for human head and neck cancer resistance to radiotherapy. *J. Clin. Invest.*, 122(4):1529–1540, April 2012.

[122] N Cordes and D van Beuningen. Cell adhesion to the extracellular matrix protein fibronectin modulates radiation-dependent G2 phase arrest involving integrin-linked kinase (ILK) and glycogen synthase kinase-3beta (GSK-3beta) in vitro. *Br. J. Cancer*, 88(9):1470–1479, May 2003.

[123] Tania V Humphrey, Dario T Bonetta, and Daphne R Goring. Sentinels at the wall: cell wall receptors and sensors. *New Phytol.*, 176(1):7–21, January 2007.

[124] Peter Kegel, Enriqueta Riballo, Martin Kühne, Penny a Jeggo, and Markus Löbrich. X-irradiation of cells on glass slides has a dose doubling impact. *DNA Repair*, 6(11):1692–1697, November 2007.

[125] Mark Bates, Bo Huang, Graham T Dempsey, and Xiaowei Zhuang. Multicolor super-resolution imaging with photo-switchable fluorescent probes. *Science*, 317(5845):1749–1753, 21 September 2007.

[126] Johannes Schindelin, Ignacio Arganda-Carreras, Erwin Frise, Verena Kaynig, Mark Longair, Tobias Pietzsch, Stephan Preibisch, Curtis Rueden, Stephan Saalfeld, Benjamin Schmid, Jean-Yves Tinevez, Daniel James White, Volker Hartenstein, Kevin Eliceiri, Pavel Tomancak, and Albert Cardona. Fiji: an open-source platform for biological-image analysis. *Nat. Methods*, 9(7):676–682, July 2012.

[127] Martin Ovesny, Pavel Křižek, Josef Borkovec, Zdeněk Svindrych, and Guy M Hagen. ThunderSTORM: a comprehensive ImageJ plugin for PALM and STORM data analysis and super-resolution imaging. *Bioinformatics*, pages 1–2, April 2014.

[128] Nils Gustafsson, Siân Culley, George Ashdown, Dylan M Owen, Pedro Matos Pereira, and Ricardo Henriques. Fast live-cell conventional fluorophore nanoscopy with ImageJ through super-resolution radial fluctuations. *Nat. Commun.*, 7:12471, 12 August 2016.

[129] P M Dixon. Ripley's K function. *Encyclopedia of environmetrics*, 2002.

[130] N Cordes, B Hansmeier, C Beinke, V Meineke, and D van Beuningen. Irradiation differentially affects substratum-dependent survival, adhesion, and invasion of glioblastoma cell lines. *Br. J. Cancer*, 89(11):2122–2132, December 2003.

[131] Iain D Campbell and Martin J Humphries. Integrin structure, activation, and interactions. *Cold Spring Harb. Perspect. Biol.*, 3(3), March 2011.

[132] Isabelle Corre, Colin Niaudet, and Francois Paris. Plasma membrane signaling induced by ionizing radiation. *Mutat. Res.*, 704(1-3):61–67, 2010.

[133] S J Singer and G L Nicolson. The fluid mosaic model of the structure of cell membranes. *Science*, 175(4023):720–731, February 1972.

[134] Roumen Pankov, Tania Markovska, Rusina Hazarosova, Peter Antonov, Lidia Ivanova, and Albena Momchilova. Cholesterol distribution in plasma membranes of beta1 integrin-expressing and beta1 integrin-deficient fibroblasts. *Arch. Biochem. Biophys.*, 442(2):160–168, 15 October 2005.

[135] Tobias Meckel, Stefan Semrau, Marcel J M Schaaf, and Thomas Schmidt. Robust assessment of protein complex formation in vivo via single-molecule intensity distributions of autofluorescent proteins. *J. Biomed. Opt.*, 16(7):076016, July 2011.

[136] Christian Eggeling. Super-resolution optical microscopy of lipid plasma membrane dynamics. *Essays Biochem.*, 57:69–80, 2015.

[137] Seven Bump. *Microscopic characterization of functionalized paper as a platform for 3D cell cultures*. PhD thesis, TU Darmstadt, 2015.

[138] Hideaki Mizuno, Mitsuhiro Abe, Peter Dedecker, Asami Makino, Susana Rocha, Yoshiko Ohno-Iwashita, Johan Hofkens, Toshihide Kobayashi, and Atsushi Miyawaki. Fluorescent probes for superresolution imaging of lipid domains on the plasma membrane. *Chem. Sci.*, 2(8):1548, 2011.

[139] K Simons and E Ikonen. Functional rafts in cell membranes. *Nature*, 387(6633):569–572, June 1997.

[140] Satyajit K Mitra and David D Schlaepfer. Integrin-regulated FAK-Src signaling in normal and cancer cells. *Curr. Opin. Cell Biol.*, 18(5):516–523, October 2006.

[141] Xuehua Xu, Tobias Meckel, Joseph A Brzostowski, Jianshe Yan, Martin Meier-Schellersheim, and Tian Jin. Coupling mechanism of a GPCR and a heterotrimeric G protein during chemoattractant gradient sensing in Dictyostelium. *Sci. Signal.*, 3(141):ra71, January 2010.

[142] David J Williamson, Dylan M Owen, Jérémie Rossy, Astrid Magenau, Matthias Wehrmann, J Justin Gooding, and Katharina Gaus. Pre-existing clusters of the adaptor Lat do not participate in early T cell signaling events. *Nat. Immunol.*, 12(7):655–662, 2011.

List of Figures